CHAPTER SIX

The path to continuous Bose-Einstein condensation

Chun-Chia Chen (陳俊嘉)[a,*,c], Shayne Bennetts[a,*], and Florian Schreck[a,b]

[a]Van der Waals-Zeeman Institute, Institute of Physics, University of Amsterdam, Amsterdam, The Netherlands
[b]QuSoft, Amsterdam, The Netherlands
*Corresponding authors: e-mail address: ContinuousBECReview@strontiumBEC.com

Contents

Abstract

Bose-Einstein condensates (BECs) have transformed quantum science and atomic physics. They are crucial for quantum simulation (Bloch et al., 2012) and sensing (Cronin et al., 2009; Bongs et al., 2019). However, despite long standing efforts quantum gas devices have until recently (Chen et al., 2022) remained restricted to pulsed operation by the need to execute cooling stages time-sequentially. This review discusses the many efforts made towards continuous-wave operation before focusing on our

[c] Present address: National Institute of Standards and Technology, 325 Broadway, Boulder, CO 80305, United States.

Advances in Atomic, Molecular, and Optical Physics, Volume 72
ISSN 1049-250X
https://doi.org/10.1016/bs.aamop.2023.04.004

group's approach to achieve continuous-wave Bose-Einstein condensation. Our proof-of-principle demonstration of continuous-wave Bose-Einstein condensation has limitations including low purity, coherence, and the lack of an out coupled atom laser beam. We therefore discuss alternative approaches to make such devices more robust and useful in the future. Finally, we will explore some of the applications that might benefit from the ability to create a continuous source of coherent matter-waves.

1. Introduction

The first demonstration of Bose-Einstein condensation in dilute gases (Anderson et al., 1995; Davis et al., 1995) and the subsequent demonstration of pulsed atom lasers (Mewes et al., 1997) took place already more than 25 years ago. Since then, the continuing absence of continuous-wave (CW) atom lasers and matter wave devices has become a conspicuous gap in the landscape of ultracold atoms. Despite the explosion in the number of studies, fundamental and applied, experiments using BECs and ultracold atoms have remained restricted to a pulsed paradigm of operation.

While the importance of CW optical lasers is clear, an obvious question is what advantages might be offered by a CW atom laser? Like their optical counterparts atom lasers offer numerous benefits when compared with thermal beams. For example, they have better beam quality and higher brightness (Robins et al., 2013). Coherence is another answer. Coherence is fundamental to applications like atom interferometry (Cronin et al., 2009; Bongs et al., 2019). Without CW operation the coherence of matter-waves remains limited to the atom number and lifetime of a single BEC (Baker et al., 2021). A CW BEC is an important step towards breaking this barrier. The coherence of a laser or matter-wave can be thought of roughly as the number of photons or atoms emitted consecutively into a beam with the same phase (Baker et al., 2021).

For a pulsed laser or matter-wave, coherence is fundamentally limited to less than the initial number of photons or atoms in the mode, N (Ketterle, 2002; Baker et al., 2021). By contrast, the coherence of a continuous source can be much larger than the initial number of photons or atoms in the laser or BEC itself. The coherence limit for a CW laser, the Schawlow-Townes limit was thought to be of order N^2 (Schawlow and Townes, 1958; Wiseman, 1999; Baker et al., 2021) though recent work has shown higher bounds may be possible (Baker et al., 2021; Liu et al., 2021). Reaching high coherence in practice requires overcoming many decoherence mechanisms, such as mean-field changes by atom number fluctuations and other fluctuating energy shifts.

On a practical level, perhaps the simplest example of where a continuous system might offer significant benefits is in addressing the impact of the Dick effect (Dick, 1987). The Dick effect limits all non-continuous measurements by aliasing high frequency noise into any measurement. For fields like atomtronics (Amico et al., 2022) and sensing (Cronin et al., 2009; Bongs et al., 2019) the lack of continuous gain has been particularly restrictive (Zozulya and Anderson, 2013; Caliga et al., 2017, 2016; Anderson, 2021). Atomtronics, like its more established contemporaries electronics and photonics, has long held a tantalizing yet so far largely unrealized place in technology. Within electronics and photonics the concept of active devices is foundational; the notion of coherent gain (Caliga et al., 2016) has been the cornerstone of much of their utility.

CW atom lasers promise a brand new set of laser-like tools for quantum sensing and devices. However, producing continuous amplification of an atomic matter wave that preserves its phase coherence necessitates meeting three key requirements (Bhongale and Holland, 2000). The first is a coherent gain mechanism that amplifies the matter-wave, the second is a continuous supply of ultracold atoms near quantum degeneracy and the third is a means of protecting the degenerate gas from resonant light. While several coherent gain mechanisms were demonstrated in the years following the first BECs (Miesner et al., 1998; Bhongale and Holland, 2000; Robins et al., 2008; Deng et al., 1999; Inouye et al., 1999b; Schneble et al., 2003a), in all these demonstrations the gain mechanism could not be sustained due to the lack of a continuous near-degenerate source of atoms. Tackling the second part of this problem required the development of new laser cooling approaches in which atoms are cooled in a series of sequential stages separated in space rather than time (Chikkatur et al., 2002; Williams et al., 1998; Lahaye et al., 2005; Bennetts et al., 2017; Chen et al., 2019b). Finally, a means to protect near degenerate atoms from the scattered resonant light necessary for laser cooling is needed. Several methods can be used to suppress rescattering of laser cooling photons (Bhongale and Holland, 2000; Cirac et al., 1996; Stellmer et al., 2013; Urvoy et al., 2019). Experimentally, a particularly straightforward approach for atomic systems with a narrow-line transition is to induce a light shift (Stellmer et al., 2013), the approach we employed to make a CW BEC.

In this review we will begin by describing some of the past approaches towards CW degenerate gases and discuss their achievements. Next we describe in detail the techniques that we developed culminating in our group's recent demonstration (Chen et al., 2022). Yet, much remains to be done

if we are to one day produce a CW atom laser that is a robust cornerstone of many atom-optics labs and quantum sensing devices the same way CW optical lasers are today. We therefore focus on describing some of the approaches that we believe offer opportunities to further improve the performance with the aim of inspiring future efforts. We conclude with a discussion of some of the applications where we believe this work and its key techniques might make an impact.

2. Early work

Laser cooling has been a crucial technique for manipulating atoms and played a significant role in the development of Bose-Einstein condensation (Anderson et al., 1995; Davis et al., 1995; Bradley et al., 1995; Schreck and Druten, 2021). Combining laser cooling with time sequential evaporative cooling has dominated approaches for achieving atomic BEC. However, methods that rely on controlled atom loss via time sequentially decreasing the trap depth and rethermalization prevent steady state operation and the realization of a CW atom laser. Thus, the question remained whether the quantum degenerate regime could be reached without evaporative cooling. One major obstacle to achieving Bose-Einstein condensation using laser cooling is the reabsorption of photons scattered during the cooling process. The recoil from the scattering of photons creates a repulsive force between atoms heating atoms that are already in the ground state. At higher densities heating becomes more pronounced making it difficult to achieve the required phase-space density increase needed to reach the critical BEC transition condition. This requires protecting the BEC from scattered resonant light. Finally, if one wants to produce a CW atom laser starting from a CW BEC, one needs a method for out coupling atoms.

2.1 High phase-space density platforms

The BEC phase transition occurs when the thermal de Broglie wavelength $\lambda_{\mathrm{dB}} = h/\sqrt{2\pi m k_B T}$, where h is Planck's constant, k_B is Boltzmann's constant, m is the atomic mass and T is the cloud temperature, reaches the same size as the inter-particle spacing (Ketterle, 2002). In a harmonic trap of mean trap frequency $\bar{\omega}$, this phase transition occurs at a critical temperature, $T_C = 0.94\frac{\hbar\bar{\omega}}{k_B}N^{1/3}$, where N is the total atom number. The resulting condensate fraction N_0/N is directly related to the temperature:

$\frac{N_0}{N} = 1 - (T/T_C)^3$. Experimentally, we tend to measure the peak phase-space density (PSD), which for a harmonic trap is $\rho = N\left(\frac{\hbar\bar{\omega}}{k_B T}\right)^3$. In such a trap the BEC phase transition corresponds to a peak PSD of $\rho = 1.2$. Cooling an atomic sample or beam from room temperature to quantum degeneracy requires a series of cooling steps that together boost the phase-space density to over 1.2. These steps can be distributed across time, space, or a combination of both. The first demonstration of a continuously existing degenerate source was in Chikkatur et al. (2002). This approach involved producing a series of independent condensates and transferring them periodically to refill a trap containing a BEC. While there was no phase relationship between the trapped condensate before and after each refilling event, and the trapped atom number fluctuated strongly, there was a continuously available reservoir of condensed atoms that could, in principle, be used to continuously output an atom laser beam. While this system demonstrated a path to produce a continuously existing sample of degenerate gas it was not a steady-state system. For this reason, work has continued looking for steady-state approaches able to reach degeneracy.

Achieving a steady-state system requires a spatially distributed cooling and trapping sequence. There are existing concepts in common use that employ this method. For example, atoms exiting a heated oven are typically followed by a series of spatially distributed cooling stages, such as transverse cooling and Zeeman slowing (Phillips and Metcalf, 1982) before being captured by a magneto-optical trap (MOT). Similar architectures use a 3D MOT to capture and cool the output from a 2D MOT (Dieckmann et al., 1998). These experimental architectures are able to reliably capture atoms and increase the phase-space density (PSD) by many orders of magnitude, however, they are limited by the final stage of the MOT. For a typical steady-state MOT using alkali atoms like Rb, the phase-space density achievable remains more than 6 orders of magnitude below the BEC phase transition condition (Radwell et al., 2013).

An apparent solution is to use evaporation to further improve phase-space densities beyond what is attainable using a MOT, the same as is used in time sequential cooling to produce a BEC. Some of the most spectacular efforts to create a steady-state source of high PSD atoms and continuous atom lasers have used evaporation to cool a beam of atoms propagating along a guide. Much of the pioneering work in this area was carried out by the group of David Guéry-Odelin in LKB from 1999 until 2008 (Lahaye et al., 2004; Cren et al., 2002; Lahaye et al., 2005; Roos et al., 2003c; Reinaudi et al., 2006a; Roos et al., 2003b; Lahaye and Guéry-Odelin, 2006,

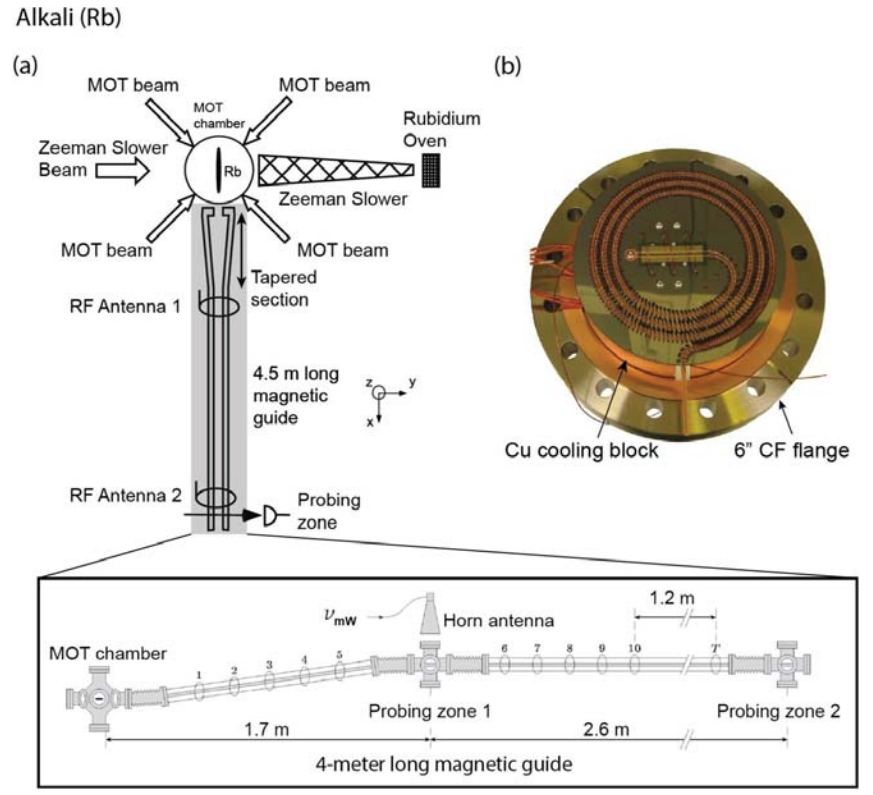

Figure 1 Rubidium (Rb) experiments aiming to realize a continuous atom laser. (a) From 1999 until 2008 the group of David Guéry-Odelin explored evaporatively cooling a magnetically guided rubidium beam along a 4.5 m path (reproduced with permission from Lahaye et al. (2004, 2005)). (b) The Raithel group developed a compact chip-based quadrupole magnetic guide for a rubidium beam designed to implement continuous distributed surface adsorption evaporative cooling (reproduced with permission from Power et al. (2012)).

2005; Roos et al., 2003a; Reinaudi et al., 2006b; Lahaye et al., 2003; Vermersch et al., 2011; Gattobigio et al., 2009; Couvert et al., 2008) with some ongoing numerical work since then. This experiment out coupled a steady-state beam of rubidium atoms from a MOT into a magnetic guide. By using a series of RF out coupling stages to induce evaporative cooling as they traversed a 4.5 m long magnetic guide Lahaye et al., demonstrated steady-state atomic beams with a PSD of 10^{-7} (Lahaye et al., 2005), a tenfold increase in the on-axis phase-space density. Their experiment is shown in Fig. 1(a). Despite achieving an increase in phase-space density, the cooling perfor-

mance in this approach fell far short of achieving degeneracy. Similar efforts were undertaken at Utrecht by the Vogels group (Kindt, 2011) and in the group of Georg Raithel, who constructed a compact 0.7 m long magnetic guide coiled on a silicon wafer as shown in Fig. 1(b) (Power et al., 2012; Teo and Raithel, 2001; Olson et al., 2006, 2014). However, these efforts did not result in any significant improvements in beam phase-space density. A similar effort (Mahnke et al., 2015) aimed at CW BEC using magnetically guided and evaporated ^{87}Rb atoms on an atom chip. This approach demonstrated a guided beam loading a magnetic reservoir with a PSD of 9×10^{-8}.

Further improvements have been explored by utilizing alkaline earth elements or other species. These elements offer improved phase-space densities through the use of both a strong transition to precool atoms and a weak transition, which provides a low Doppler cooling temperature (Schreck and Druten, 2021). Examples include bichromatic MOTs (Kawasaki et al., 2015; Lee et al., 2015; Grünert and Hemmerich, 2002) and narrow-line MOTs fed by an atomic source pre-cooled using a broad transition (Dörscher et al., 2013; Frisch et al., 2012). At present, the highest phase-space density continuous MOT results are achieved using the Sr 7.4 kHz narrow-line transition (Bennetts et al., 2017), which will be detailed in section 3.1. In addition, adding further steady-state trapping in a dipole trap and cooling stages to a MOT can further substantially increase the PSD.

A particularly interesting approach was pursued by the group of Axel Griesmaier and Tilman Pfau as shown in Fig. 2(a) (Griesmaier et al., 2009; Aghajani-Talesh et al., 2009; Falkenau et al., 2011, 2012; Volchkov et al., 2013; Rührig et al., 2015; Schneble et al., 2003b). In this work, they demonstrated a loading mechanism that used a conservative state-dependent potential in conjunction with optical pumping to continuously load a trap from a guided atomic beam (Falkenau et al., 2011). Their system, as shown in Fig. 2(a), didn't rely on a closed cycling transition, but instead made use of a Sisyphus cooling scheme. Griesmaier et al., achieved a significant improvement in the state-of-the-art steady-state phase-space density, reaching 4×10^{-4} for chromium loaded in a dipole trap (Volchkov et al., 2013). This work demonstrated the viability of loading atomic beams into dipole traps, in contrast to earlier work that focused on magnetic traps. Despite their relatively small trap depths and cross-sections, optical traps and guides offer higher trapping frequencies that are more favorable for evaporative cooling. Furthermore, this work highlighted that continu-

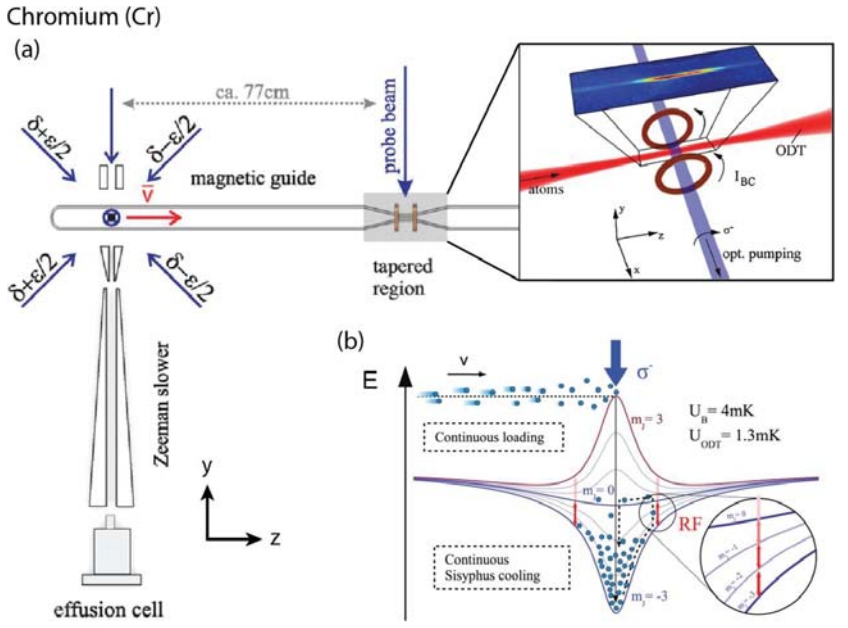

Figure 2 Chromium (Cr) experiment aiming to realize a continuous atom laser. (a) The chromium work lead by Axel Griesmaier and Tilman Pfau used a novel magnetic deceleration and loading scheme followed by a Sisyphus cooling scheme to demonstrate a steady-state phase-space density of 4×10^{-4}. Until our work Bennetts et al. (2017) this was the highest demonstrated steady-state phase-space density (reproduced with permission from Griesmaier et al. (2009); Falkenau et al. (2011)). (b) Novel loading and Sisyphus type cooling mechanism used in Volchkov et al. (2013) (reproduced with permission from Volchkov et al. (2013)).

ous atomic beam cooling and slowing at high PSD can be achieved using methods other than the radiation pressure force, such as using a Sisyphus type cooling mechanism. In this case, atoms are first slowed by a magnetic potential barrier at the top of which they are pumped from a low field seeking $m_F = +3$ to a high field seeking $m_F = -3$ state. This process may be continued in Sisyphus fashion by using RF to pump atoms with sufficient kinetic energy to reach the wings of the trap back to $m_F = 0$. They are then returned to the trap center by the dipole trap where they are optically pumped back to the high field seeking $m_F = -3$ state thus dissipating energy, see Fig. 2 (b). Removing the kinetic energy without the need of laser cooling is highly desirable especially at the last stage of a high PSD source where a sub-Doppler temperature at very high density is usually required.

While there have been relatively few machines specifically designed to target *continuous* high PSD sources, a variety of creative approaches have been developed to increase the PSD of magneto-optical traps (MOTs) using time-sequential cooling, which could be applied to continuous systems. Methods range from dark spots (Radwell et al., 2013; Yang et al., 2007), sub-Doppler cooling (Lett et al., 1988; Dalibard and Cohen-Tannoudji, 1989; Grier et al., 2013; Colzi et al., 2016; Rührig et al., 2015), cooling and trapping in the metastable state (Katori et al., 2001; Derevianko, 2001; Grünert and Hemmerich, 2002; Akatsuka et al., 2021; Riedmann et al., 2012; Hobson et al., 2020; Miyazawa et al., 2021), to sub-recoil cooling methods (Kasevich and Chu, 1992; Aspect et al., 1988; Hamann et al., 1998; Kerman et al., 2000; Han et al., 2000). Despite their exquisite performance, these techniques tend to suffer from small capture velocities. As a result for continuous architectures, atoms first need to be captured and pre-cooled, which necessitates the use of either a spatially distributed cooling sequence or multiple stages cooling atoms to different internal states like the metastable MOTs (Katori et al., 2001).

In our group we have focused on using the level structure of the alkaline-earth strontium, which is richer than that of alkali atoms. This offered opportunities not only for Doppler cooling using transitions with a lower Doppler cooling limit, but also potentially in the future sub-recoil cooling methods (Zhang et al., 2022) utilizing the $^1S_0 - {}^3P_0$ clock transition. Here we discuss strontium but these approaches apply to any element with narrow-line transitions like the alkaline earths but also rare earths like dysprosium. One important technique for achieving a high PSD high PSDs when cooling with narrow transitions is to support the atoms in an optical dipole (or magnetic) trap eliminating the need to scatter photons just to balance gravity. Lower intensities in turn reduce light assisted scattering and multiple scattering at high density. It also reduces power broadening of the narrow 7.5 kHz linewidth transition, further reducing temperature. The use of a magic wavelength optical dipole trap (Ido et al., 2000) also eliminates trap light shift inhomogeneities allowing narrow line cooling methods to approach their Doppler cooling limits. Together these effects boost the attainable PSD, allowing pulsed laser cooled systems in magic wavelength optical dipole traps to reach PSDs at the 0.1 level (Ido et al., 2000).

Our continuous high-PSD strontium source is shown in Fig. 3 (a) with a schematic shown in Fig. 3 (b). Its key features are spatially separated cooling stages with protection of the lower chamber from the 30 MHz linewidth blue $^1S_0 - {}^1P_1$ cooling light and a dipole trap guided atomic beam in the

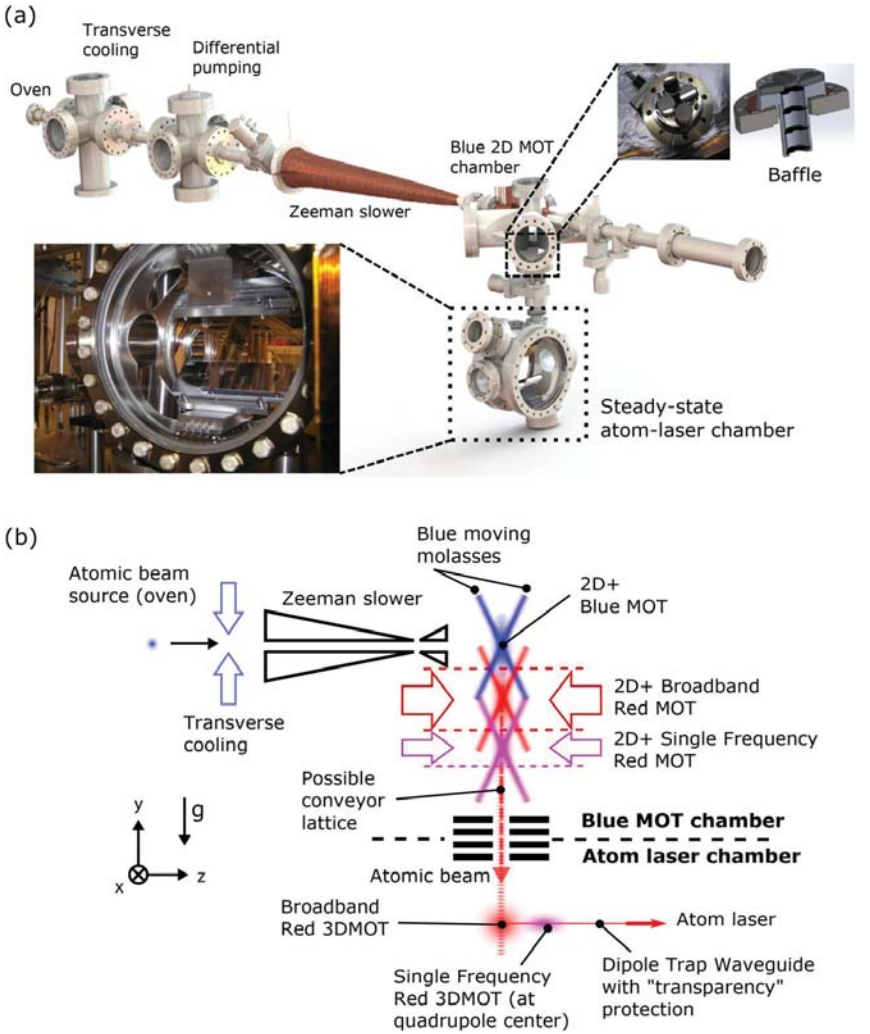

Figure 3 Amsterdam strontium continuous atom laser experiment. (a) In the strontium continuous atom laser machine developed by our group, different laser cooling steps are implemented sequentially in space (reproduced with permission from Bennetts et al. (2017); Bennetts (2019)). (b) The initial concept design for our continuous atom laser experiment was based on evaporation from a guided beam, this was somewhat different from the architecture with which we first demonstrated CW Bose Einstein condensation (reproduced with permission from Chen et al. (2019b)).

final chamber. This system benefits from the high capture velocity and the resulting high flux afforded from using an oven with Zeeman slower and transverse cooling all using the strong $^1S_0 - {}^1P_1$ laser cooling transition.

Simultaneously, high phase space densities are obtained from the guided atomic beam (Bennetts et al., 2017; Chen et al., 2019b) where the low Doppler cooling temperature allowed by the 7.5 kHz narrowline transition is combined with a dark spot and support against gravity. Together, these factors enabled new records in steady-state phase space densities both for MOTs (Bennetts et al., 2017) and for guided atomic beams (Chen et al., 2019b). Our continuous high-PSD source will be described in detail in section 3.1 and 3.2 with some of the many improvements possible described in section 4.

2.2 Protection: dark states and transparency mechanisms

In the previous section we reviewed the many varied architectures that have been explored in the effort to produce a steady-state "near degenerate" source. Whether pulsed or continuous, cooling to degeneracy almost always involves two separate stages, a first stage in which atoms are laser cooled to as high a PSD as is possible followed by an evaporation stage, which takes place in an environment free from resonant light. This is because high PSD samples are tremendously sensitive to resonant light, a fact that was realized very early in the race to achieve the first BEC (Sesko et al., 1991). In optically thick ultracold atomic gases, atoms reabsorb scattered photons leading to repulsion between atoms and recoil heating, which limits the achievable PSD. Since laser cooling performs most phase-space density enhancement for perhaps all species except hydrogen, creating steady-state sources of degenerate atoms is very challenging.

Steady-state solutions thus require a way to laser cool all the way to degeneracy or a way to protect evaporating atoms from resonant light. Here we shall discuss ways to protect high PSD samples from reabsorption in the presence of resonant light. Mitigating the reabsorption of photons is commonly achieved by engineering a dark state.[1] Cold atoms can accumulate in this state, which is decoupled from the atom - cooling light interaction, while hot atoms continue to be cooled by the laser light. Either potential or kinetic energy can be used to select those atoms in a dark state as illustrated in Fig. 4.

Early work on dark state laser cooling was focused mostly on demonstrating laser cooling to subrecoil temperatures. A review of laser cooling

[1] Some definitions of 'dark states' refer only to states that are dark due to quantum interference such as electromagnetically induced transparency (EIT). We will use a very broad definition of 'dark state' as any state that is decoupled from the atom-light interaction.

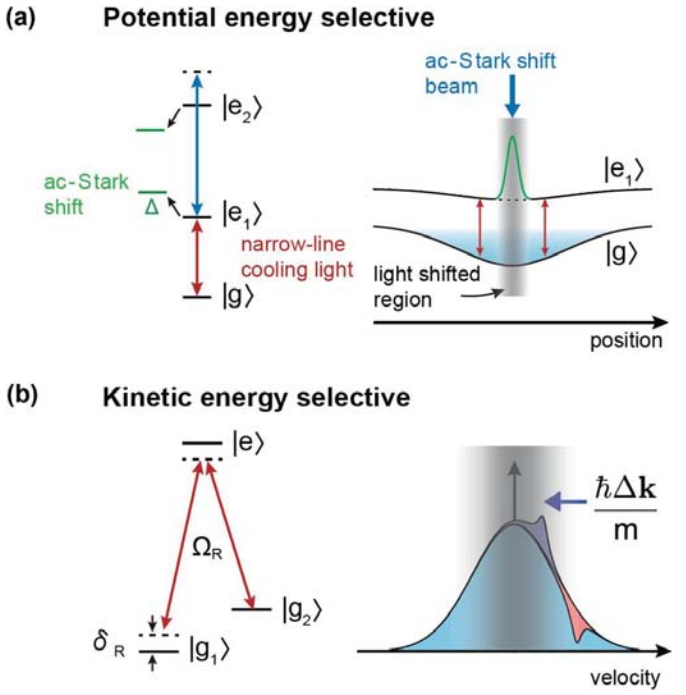

Figure 4 "Dark" states for selective excitation. (a) "Spatial" dark state. An ac-Stark shift beam overlapped with the trap creates a region where atoms are off-resonant to the laser cooling light due to the ac-Stark shift. (b) The Raman transition is resonant for atoms with a two-photon Doppler shift δ_R. Low energy atoms are "dark" to excitation due to Doppler shift (reproduced with permission from Urvoy et al. (2019)).

techniques can be found in Metcalf and van der Straten (1999); Schreck and Druten (2021). One such example is velocity selective coherent population trapping, VSCPT (Aspect et al., 1988). Here a zero-velocity dark state in momentum space is formed in systems like He with a closed three-level (Λ) configuration where destructive quantum interference suppresses excitation. A second similar example is Raman cooling (Kasevich and Chu, 1992). Velocity sensitive Raman pulses selectively excite atoms of a targeted velocity class. Cold atoms then accumulate in a low energy dark state. While such momentum dark states allow sub-recoil cooling, laser cooling to high phase-space densities requires cooling in a trap to maintain high density.

A number of proposals have explored spatially selective pumping mechanisms in a trap. In 1983 Pritchard described cyclic cooling (Pritchard, 1983), a scheme using the potential of a magnetic trap combined with an

RF change of state and optical repumping to cycle and extract energy only from atoms hot enough to reach the RF 'knife'.

In 1993 the Walraven group proposed using the optical density of a high phase-space density cloud itself to protect a cold dense core thus allowing an optical beam to selectively evaporate away hot atoms with the potential to achieve runaway evaporation (Setija et al., 1993). Also in 1993 the Ketterle group demonstrated the dark SPOT MOT (Ketterle et al., 1993), still one of the most widely used methods for reducing reabsorption and increasing phase-space density. This method reduces light reabsorption by shelving atoms in the center of the MOT in a dark state. Atoms that exit the dark region will be pumped out of the dark state and reenter the laser cooling cycle. In the same spirit, Morigi et al. (1998) proposed a "spatial" dark state by designing the laser profile to "position selectively" excite hot atoms to another internal state and then repump them back. These proposals focus on realizing the "position dark" state within an atom-plus-trap system, where atoms, once scattered into that dark state, are decoupled from the cooling radiation.

Another kind of "spatial dark state" was explored and used to demonstrate laser cooling to quantum degeneracy (Stellmer et al., 2013). This approach uses only laser cooling to remove entropy from the gas and is illustrated in Fig. 5. A dimple dipole trap enhances the density while atoms remain thermalized with those in a larger reservoir dipole trap. The enhanced phase-space density atoms within the dimple trap may then be ac-Stark shifted out of resonance rendering them transparent to laser cooling light, an approach similar to those proposed by the Zoller group (Dum et al., 1994; Taïeb et al., 1994). This works particularly effectively thanks to the extremely narrow 7.5 kHz linewidth cooling transition afforded by strontium. In this way, laser cooling only interacts with atoms energetic enough to escape beyond the ac-Stark shifted spatial "dark" region, the dimple trap, effectively realizing a spatially dependent laser cooling profile. In Stellmer et al. (2013) atoms within the dark region were ac-Stark shifted away from resonance by around 100Γ in addition to providing separation between laser cooled atoms scattering photons and the cold dense atoms in the dimple.

All these schemes create a spatially dependent and thus energy dependent excitation mechanism, which leaves cold atoms protected and dark to resonant light reducing reabsorption and allowing higher phase-space densities.

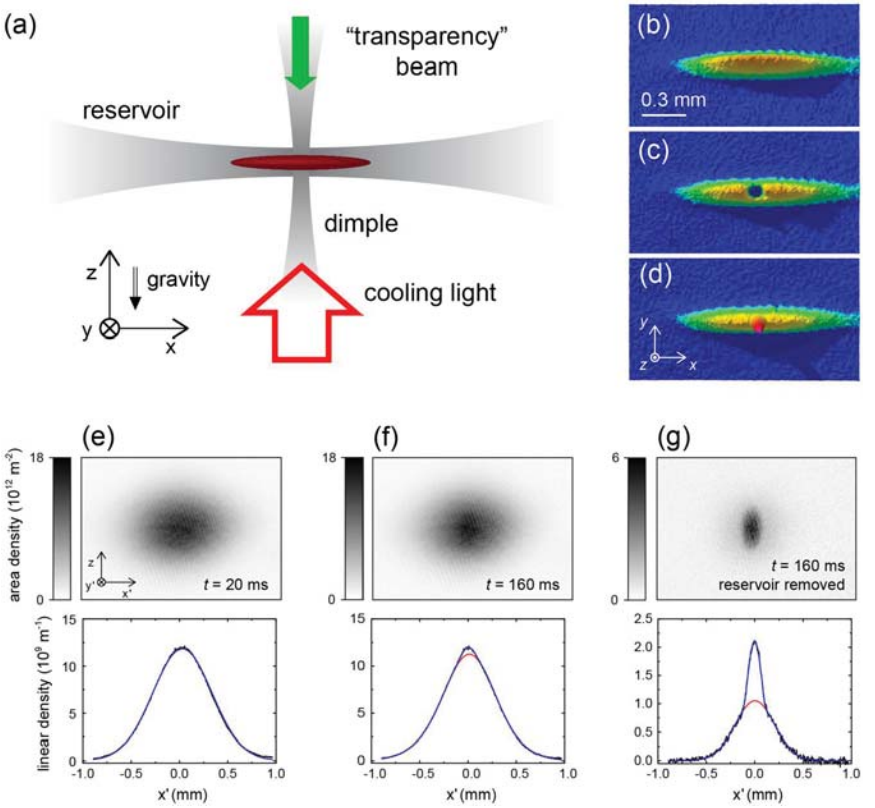

Figure 5 (Pulsed) Laser cooling to degeneracy. (a) The laser and dipole trap configuration. (b) Absorption image on the $^1S_0 - {}^3P_1$ transition of atoms loaded into the reservoir trap. (c) Absorption image on the $^1S_0 - {}^3P_1$ transition of atoms loaded into the reservoir trap with the transparency beam applied, which shifts a patch out of resonance imaging light. (d) Absorption image on the $^1S_0 - {}^3P_1$ transition of atoms loaded into the reservoir trap with the dimple (but not transparency) beam applied. (e, f) Formation of a BEC in 160 ms. (g) Improved visibility by 'blowing away' the reservoir. Figures reproduced with permission from Stellmer et al. (2013).

An alternative approach is possible in systems in which atoms are trapped where detrimental heating effects associated with reabsorption are reduced if the vibration frequency exceeds the optical pumping rate (Cirac et al., 1996; Castin et al., 1998). This is also known as the *festina lente* condition. In traps that have high trapping frequencies, such as lattices, further suppression is possible in the Lamb-Dicke regime, which for cold atoms corresponds to the condition $l_{\mathrm{HO}} \ll \Lambda/2\pi$, where l_{HO} is the harmonic oscillator length of the trap ground state and Λ the laser cooling wavelength.

Under this condition the vibrational trap level will most of the time remain unchanged when a spontaneous emission occurs. The Weiss group demonstrated the suppression of reabsorption heating using 1D (Winoto et al., 1999) and 3D lattices (Wolf et al., 2000).

In 1996 the Chu group demonstrated the power of Raman cooling on trapped sodium atoms by showing a phase-space density improvement of 250 times (Lee et al., 1996), reaching PSDs of 0.002. Soon after, Raman sideband cooling was demonstrated in 1D (Perrin et al., 1998) and 2D (Hamann et al., 1998) and in 1998 the Chu group reached a PSD of 1/180 using Raman sideband cooling in a 3D lattice (Vuletić et al., 1998). Over the following three years a series of papers from the Weiss and Chu groups demonstrated Raman sideband cooling and polarization gradient cooling in optical lattices often including toggling between 3D and 1D lattices to cycle between compression and cooling with ever increasing phase-space densities (DePue et al., 1999; Kerman et al., 2000; Han et al., 2001, 2000). This culminated in a PSD exceeding 1/30 (Han et al., 2000; DePue et al., 1999). The potential of these "visionary" approaches was vindicated some 17 years later when the Vuletic group demonstrated laser cooling to degeneracy using a combination of 3D Raman sideband cooling and 3D-1D lattice compression-cooling cycles (Hu et al., 2017) and then with Raman cooling in the *festina lente* regime of a dipole trap (Urvoy et al., 2019).

2.3 Matter-wave amplification

Compensating loss is essential to maintain any system in steady-state. In an optical laser, this is achieved by maintaining population inversion for example by optical pumping or electrical discharge. Bose-stimulated emission can then provide linear, phase preserving amplification, gain, which can maintain a continuous output. With feedback this enhances brightness, producing a coherent state with high order coherences, a laser. This simple stimulated emission process applies equally to matter-wave amplification. When the phase-space density in a trap exceeds the critical phase-space density, Bose-stimulated elastic scattering produces net matter-wave gain. When the gas is trapped, this results in the macroscopic population of the trap ground state, forming a Bose-Einstein condensate (Miesner et al., 1998). Similar to the optical case this process creates long range coherence (Ketterle and Miesner, 1997) and when combined with out coupling

a matter-wave in a coherent state, an atom laser.[2] Since the phase evolution of an atom laser is very sensitive to external fields there are inherently many decoherence mechanisms. Constructing practical atom lasers with high coherence will require extreme field stability, including external fields, such as dipole trap laser fields, and the condensate mean field. For example, a coherence time exceeding 1 s requires an atom number stability on the order of 0.1% and techniques such as feedback will likely be necessary to overcome such sources of noise (Kristensen et al., 2019; Thomsen and Wiseman, 2002).

Another approach involves creating two mode-matched condensates in different electronic states in which it is possible to pump or stimulate one condensate to Bose-stimulated scatter into the other and thus provide gain. This conceptually elegant approach was described by Santos et al. (2001); Cirac and Lewenstein (1996); Inouye et al. (1999b) and demonstrated by Robins et al. (2008). They showed condensate gain and output of an atom laser.

Stimulated gain is not the only mechanism for amplifying an optical wave or for that matter a matter-wave. Optical parametric amplification, where a nonlinear refractive index modulation leads to parametric gain, can also be used. When feedback is added to an optical parametric oscillator the output is in a coherent state just like a laser. Nevertheless, parametric gain does not increase brightness or overall coherence, it simply transfers brightness from a pump mode to a signal mode, which is thus amplified.

In matter-wave optics, collisions between atoms within an ultracold dense cloud contribute to an effective cubic nonlinear interaction term (Lenz et al., 1993; Zhang et al., 1994). Matter-wave four-wave mixing, phase conjugation, and atomic solitons were all predicted, but before the realization of BECs, phase-space densities were mostly too low for nonlinear atom optics experiments. With the realization of BECs parametric amplification using four-wave mixing became practical. In four-wave-mixing a nonlinear interaction allows three modes to mix amplifying a fourth mode at the expense of one of the "pump" modes (Moore and Meystre, 2001). Another way of looking at four-wave mixing is to consider

[2] There was initially some discussion (Kleppner, 1997; Michel et al., 1998) over the appropriateness of the term "atom laser". Kleppner argues in favor, pointing out that the atom field grows by stimulated scattering in analogy to growth by stimulated emission in an optical laser. Furthermore the coherence properties of an atom and optical laser are the same. Later Scully showed that the density matrix treatment for photons in a laser cavity also applies to the ground state of a BEC (Scully, 1999; Kocharovsky et al., 2000; Meystre, 2001).

two matter-waves forming a grating, which the pump condensate scatters off.

Early demonstrations of matter-wave amplification all began with a BEC and used parametric amplification. Many variations of four wave mixing have been demonstrated with varying combinations of optical and matter-wave modes. Inouye et al. (1999b) and Kozuma et al. (1999a) used one optical and two matter input waves to provide amplification for a third matter-wave while Deng et al. (1999) used three input matter-waves. Inouye et al. (1999a) used only one matter and one optical input wave in a superradiant Rayleigh scattering process to generate both a new optical field and matter-wave amplification. A similar configuration studied by Salzburger and Ritsch (2008) was proposed as a means to simultaneously produce a continuous-wave optical laser and atom laser. In the limit of intense optical pulses, cascaded stimulated Rayleigh scattering can generate multiple higher order momentum states (Schneble et al., 2003a) complicating matter-wave amplification. By suppressing superradiant Rayleigh scattering at high pump intensity Schneble et al. (2004) and Yoshikawa et al. (2004) demonstrated superradiant Raman scattering, where the change of internal state avoids cascading, resulting in a cleaner amplification process.

Shortly after these initial publications it was realized that these amplification effects do not in fact depend on Bose quantum statistics and should be observable in thermal or even fermionic systems (Moore and Meystre, 2001; Ketterle and Inouye, 2001b; Villain et al., 2001), a prediction realized in Wang et al. (2011) and Yoshikawa et al. (2004).[3]

From all the techniques for generating matter-wave amplification only Bose-stimulated scattering has demonstrated overall brightness and coherence enhancement as well as quasi-continuous operation. For this reason we focus on using Bose-stimulated scattering to provide gain for steady-state matter-wave devices.

2.4 Out coupling mechanisms

The concept of an atom laser is very similar to that of an optical laser. One begins with a single mode, coherent state resonating in a trap or cav-

[3] Ketterle and Inouye (2001b) noted that the requirement for amplification is that a system must be prepared in a cooperative state and that the amplification must take place within a time shorter than the system coherence time, set by the broadening of the source (Ketterle and Inouye, 2001b). Furthermore, in the case of fermions this amplification does not pile up atoms in a single quantum state, but rather in states that are in the same (or approximately the same) momentum state, but differing in other quantum numbers (Ketterle and Inouye, 2001a,b).

ity and a portion of the mode is out coupled into a travelling wave. It is a question of definition if a CW Bose-Einstein condensate without an output beam is already an atom laser. In any case, most applications one can imagine for an atom laser require out coupling a travelling wave. A wide variety of out coupling mechanisms have been explored, differing in achievable beam quality, flux, coherence, confinement etc. These include internal state-changing out couplers, such as RF and Raman out couplers, as well as internal state-preserving out couplers, which simply kick atoms out of a condensate, such as Bragg out couplers or even modelocked out couplers.

The first atom laser was demonstrated in 1997 by Ketterle's group (Mewes et al., 1997). It used a pulsed RF out coupler to change the state of atoms in a magnetically trapped BEC from a trapped to an untrapped state, see Fig. 6(a, b). Follow up measurements (Andrews et al., 1997) demonstrated the interference between two RF out coupled condensates. These measurements confirmed that these pulses of atoms formed a coherent matter-wave burst with a defined phase relative to the source BEC: an atom laser.

The first quasi-continuous out coupler (Bloch et al., 1999) again used RF coupling between trapped and untrapped magnetic sublevels, see Fig. 6(c). By making the bias field of their magnetic trap extremely stable the group of Esslinger was able to tune the out coupling location within the condensate by tuning the RF frequency, thereby improving effective linewidth and transverse beam quality. Nevertheless, significant interaction of the beam with the inhomogeneous density profile of the condensate distorted the beam, especially when out coupling on a broad spatial annulus. The beam quality of continuous RF out couplers was studied by the group of Aspect (Le Coq et al., 2001; Riou et al., 2006) as shown in Fig. 6(d). This work culminated in a guided quasicontinuous atom laser shown in Fig. 6(f) (Guerin et al., 2006). RF out couplers have also been used to demonstrate very high out coupling rates with the von Klitzing group showing fluxes of 4×10^7 atoms per second (Bolpasi et al., 2014) as shown in Fig. 6(e).

Raman out couplers can provide a solution to the interaction and beam quality problems found with RF out couplers. The advantages of Raman out couplers are firstly that optical beams can be focused tightly into a condensate, avoiding beam distortion from an inhomogeneous mean-field. Secondly, the Raman beams themselves can form a mode-matched dipole guide for the out coupled matter-wave beam. Thirdly, counter-propagating

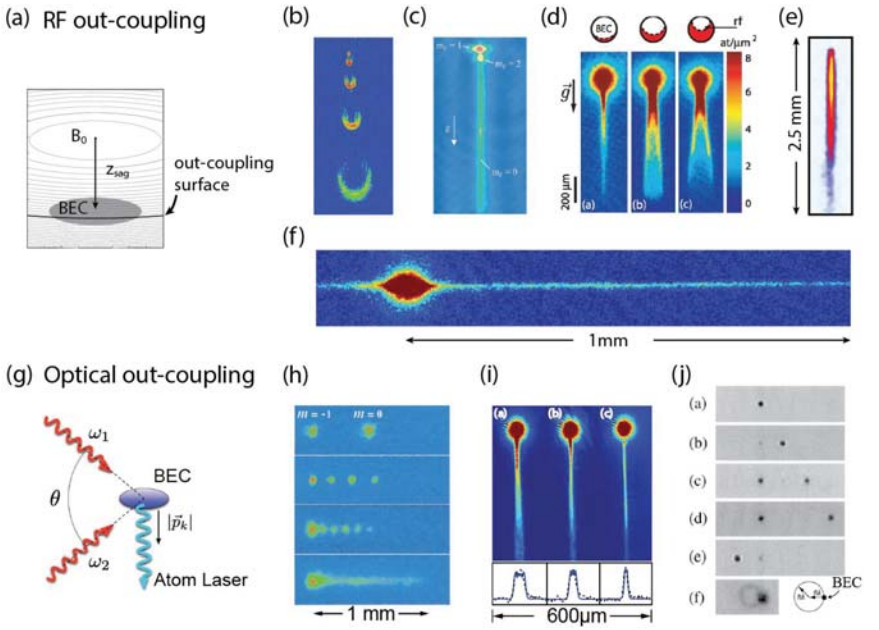

Figure 6 Gallery of experiments using different out coupling methods to realize a pulsed atom laser. RF out coupling: (a) In RF out coupled atom lasers, condensed atoms are resonantly transferred from a trapped to an untrapped magnetic state. This transfer occurs over a shell and therefore requires a very stable magnetic field to avoid poor atom laser beam quality (adapted from Bloch et al. (1999)). (b) The first demonstration of coherent atoms periodically out coupled from a condensate. Short pulses of RF radiation were used to couple Bose condensates to an untrapped hyperfine state (Mewes et al., 1997). (c) A collimated beam of atoms is continuously extracted from a Bose-Einstein condensate over 100 ms (Bloch et al., 1999). (d) Dependence of the atom laser beam quality with respect to the RF out coupling location relative to the BEC (Riou et al., 2006). (e) High flux quasi-continuous atom laser (Bolpasi et al., 2014). (f) Guided quasicontinuous atom laser (Guerin et al., 2006). **Optical out coupling**: (g) A two-photon Raman transition out coupling atoms from a trapped state to an untrapped state can be used to create an improved atom laser. The Raman optical beams can be focused to out couple at a well defined location, improving beam quality. The photon momentum kick also allows the out coupled beam to exit the condensate with minimal interaction. Figure reproduced with permission from Robins et al. (2013). A Bragg out coupler works similarly albeit without a state transfer. (h) A highly directional, quasi-continuous matter wave is extracted by coherent, stimulated Raman pulses (Hagley et al., 1999). (i) A Raman out coupled atom laser (Jeppesen et al., 2008). (j) A Bragg out coupled atom laser (Kozuma et al., 1999b). Figures reproduced with permission.

Raman beams impart a $2\hbar k$ momentum kick to the out coupled beam so that the atoms quickly exit the condensate, limiting beam distortion from

inhomogeneous interactions. Raman out coupling was first demonstrated by the Phillips group in 1999 (Hagley et al., 1999). In Hagley et al. (1999) a time orbiting potential trap was used to trap the BEC, necessitating the use of orbit synchronized Raman out coupling pulses. This led to a pulsed atom laser with a 20 kHz repetition frequency as shown in Fig. 6(h). A quasicontinuous Raman out coupler was demonstrated by the Close group in 2006 (Robins et al., 2006) as shown in Fig. 6(i) and a detailed comparison between RF and Raman out couplers is given in Debs et al. (2010).

Out coupling atoms by transferring them from a trapped low field seeking to an untrapped high field seeking magnetic state has worked well for alkali atoms. By contrast the bosonic isotopes of strontium have a single, non-magnetic ground state. For strontium it might be possible to excite condensed atoms to the metastable $^3P_0$ or $^3P_2$ states, but inelastic collision losses for these states is concerning, particularly at high densities. Another approach for very weak traps is to use a Bragg out coupler, much the same as a Raman out coupler except that only the momentum state, not the atom's internal state is changed.

Bragg out couplers use two laser beams that are usually counter-propagating. An atom absorbs a photon from one beam followed by stimulated emission into the second beam. This process is coherent (as long as off-resonant scattering is kept low by detuning the laser beams far enough from atomic transitions) and imparts a momentum of $2\,\hbar k$. Since the atomic state is unchanged, a Bragg-scattered atom will still feel the trap potential. The imparted momentum is used to push the atom out of the trap. The Phillips group demonstrated a pulsed Bragg out coupler in 1999 (Kozuma et al., 1999b) as shown in Fig. 6(j). In order to push atoms more effectively out of a trap one can use large momentum transfer (LMT) multi-photon Bragg pulses. Such pulses are commonly used as beam splitters for atom interferometers. Bragg transfers of $10\sim20\,\hbar k$ are relatively easy to achieve (McDonald et al., 2013; Müller et al., 2008) with momentum transfers of over $400\,\hbar k$ having been demonstrated (Wilkason et al., 2022).

While other more exotic out coupler schemes exist, such as modelocked out couplers (Anderson and Kasevich, 1998), these are perhaps less important for constructing continuous atom lasers. A review of atom lasers and their production including a more extensive description of out couplers can be found in Robins et al. (2013).

3. Continuous Bose-Einstein condensation

Our group's laser cooling to degeneracy experiment (Stellmer et al., 2013) overcame two restrictions that had constrained attempts to realize a CW degenerate gas. Firstly it was no longer necessary to turn off all laser cooling light at the BEC location to achieve BEC. Some small amount of light resonant with the 7.5 kHz narrow linewidth $^1S_0 - {}^3P_1$ cooling transition could be allowed. Secondly, forced evaporative cooling was unnecessary. This opened a path to move beyond the paradigm of time-sequential cooling to BEC: applying a sequence of laser cooling stages in spatially separated regions simultaneously. This path enables one to reduce the temperature of a gas by a factor of 10^9 to sub-μK while increasing the phase-space density by 10^{13}, resulting in a CW BEC.

To implement this path we needed a new machine that could deliver a continuous stream of atoms at high phase-space density to a region protected from resonant light. Protection of a BEC against the 30 MHz linewidth $^1S_0 - {}^1P_1$ blue transition photons is impractical using a transparency beam and required baffling. In addition, far greater levels of protection against light on the 7.5 kHz narrow linewidth $^1S_0 - {}^3P_1$ cooling transition were also required. The initial concept design for our continuous atom laser machine and the final CAD drawing of the vacuum system are shown in Fig. 3.

In this section, we will review the development of the technology that our group pursued over six years to eventually achieve CW Bose-Einstein condensation.

3.1 Steady-state 7.5 kHz narrow-line MOT with high PSD

The first challenge is to achieve a continuously operating MOT using only the 7.5 kHz narrow linewidth Sr intercombination line protected from photons on the 30 MHz blue $^1S_0 - {}^1P_1$ transition.

Our machine consists of a strontium oven source operating at up to 580 °C, producing a 10 mm diameter atomic beam collimated by ~5000 8 mm long 100 μm inner diameter 50 μm wall thickness microtubes (Bennetts, 2019). This atomic beam is transversally cooled in two axes over an 80 mm long cooling region before passing through two differential pumping tubes and a spin-flip Zeeman slower (Bennetts, 2019). Finally the atomic beam is captured by a 2D MOT operating on the $^1S_0 - {}^1P_1$ blue transition and using a permanent magnet array. The 30 mm $1/e^2$ diameter MOT beams capture and compress the incoming atoms, redirecting them

into a well confined vertical beam with a velocity around 4 $\mathrm{m\,s^{-1}}$ and a radial temperature on the order of 10 mK.

Our objective is to transfer these atoms to a separate chamber free from resonant $^1S_0 - {}^1P_1$ blue light on the 30 MHz $^1S_0 - {}^1P_1$ transition. To achieve this we must transversely cool the atomic beam from the 2D blue MOT. Several approaches are possible. We considered using either a MOT or a molasses on the red $^1S_0 - {}^3P_1$ transition. A MOT has the advantage of also compressing the beam but takes a much longer time to reach steady-state when compared with a molasses. This is because a 2D MOT begins by accelerating atoms in a beam towards the quadrupole center whereas a 2D molasses simply radially cools the beam. If the cooling lasers in a MOT are turned off before the system reaches steady-state the result can actually be transversal heating rather than cooling of the atomic beam. Furthermore, the magnetic field gradient to operate efficiently on the red $^1S_0 - {}^3P_1$ transition of strontium needs to be around 1 $\mathrm{G\,cm^{-1}}$ whereas the gradient required for an effective blue MOT is $\sim$ 30 $\mathrm{G\,cm^{-1}}$. This requires rapidly spatially varying the magnetic field gradient as the atomic beam passes from the 2D blue MOT cooling region to the 2D red MOT cooling region. While this is feasible using permanent magnets there is some risk of the magnetic field gradient changing sign in the transition region. Passing through negative field gradient regions would rapidly heat and disperse the atomic beam.

Our machine was designed to be able to operate using a red 2D MOT (Bennetts, 2019) to cool the atomic beam from the 2D blue MOT. To do this, our magnet array situated just 4.4 cm from the quadrupole axis generates a field which rapidly transitions from $\sim$ 30 $\mathrm{G\,cm^{-1}}$ needed for the 2D blue MOT to $\sim$ 2 $\mathrm{G\,cm^{-1}}$ needed in the 2D red MOT region. Red $^1S_0 - {}^3P_1$ transverse cooling is performed over a 50 mm long path overlapping with the bottom $\sim$ 5 mm of the 2D blue MOT. Nevertheless, we found experimentally that transfer efficiencies to the lower chamber were already high ($\sim$ 20%) using the much simpler and more robust molasses approach. Our molasses operates on the magnetically insensitive $^1S_0 - {}^3P_1$ ($m_J = 0$) 7.5 kHz linewidth transition. To frequency shift the magnetic $\sigma^{\pm}$ $^1S_0 - {}^3P_1$ transitions out of band and generate a strong π component in the red molasses region Helmholtz coils apply a vertical bias field of a few Gauss along the axis of the 2D MOTs. This bias field has little effect in the 2D blue MOT region compared with the 30 $\mathrm{G\,cm^{-1}}$ quadrupole field.

The resulting atomic beam has an estimated radial temperature of just 10 μK allowing efficient transfer through a set of four stacked 1-inch ab-

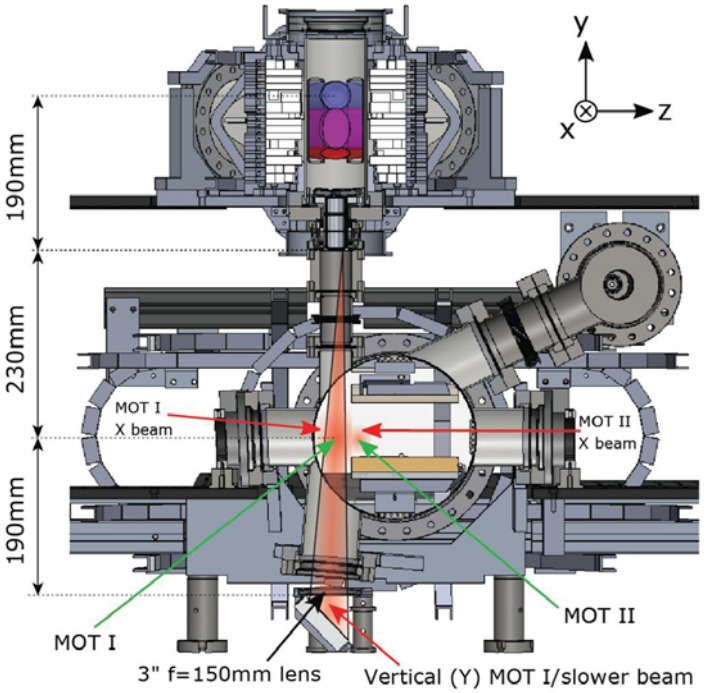

Figure 7 Steady state red MOT. A cross section of the main chamber of our apparatus illustrating the main laser cooling beams used to create the high PSD stead-state MOT. Atoms slowed by the Zeeman slower are captured by the permanent magnet 2D MOT in the top chamber. These atoms are then transversely cooled by a modulated red molasses before they fall to the lower chamber. An intense focused vertically propagating laser beam is used for a Zeeman slower (in combination with the magnetic field of the MOT), for a white light slower and for a MOT beam. This allows a steady-state red MOT at the location MOT I. To make a higher PSD steady-state MOT (MOT II) the MOT quadrupole magnetic field center can instead be placed to the right of the MOT I location and low intensity MOT beams targeting this location can be added.

sorptive neutral density filters (Thorlabs NE60A) acting as baffles against scattered blue $^1S_0 - {}^1P_1$ light from the 2D blue MOT. These each have an 8 mm diameter aperture to allow the atoms to pass. Finally, the atomic beam is slowed and captured by a 3D MOT operating on the 7.5 kHz transition.

There are several techniques needed to efficiently capture the atomic beam directly into a MOT using only the weak 7.5 kHz linewidth red $^1S_0 - {}^3P_1$ transition. We use a five-beam MOT as shown in Fig. 7 where gravity provides the restoring force from above. The beam coming from

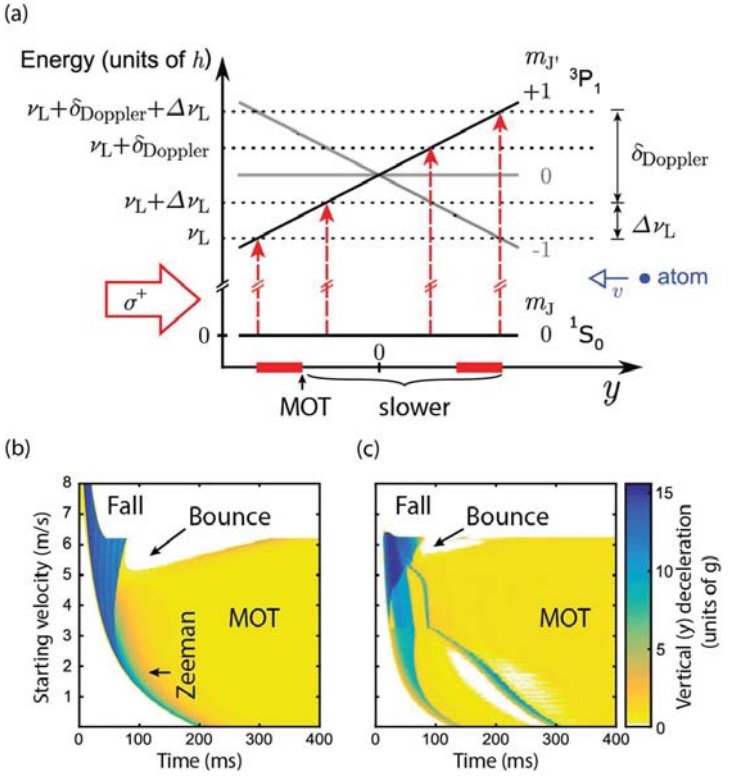

Figure 8 Working principle of the hybrid MOT+Zeeman slower. (a) Energy diagram of the $^1S_0$, m_J and the $^3P_1$, $m_{J'}$ states in dependence of y for $x = z = 0$, where the coordinate origin lays in the quadrupole field center. Axes are defined in Fig. 7. An atom with a specific velocity $|v| > 0$ along the y axis is addressed by the upward-propagating Red MOT I beam in a region delimited by the pair of red dashed arrows on the right. The range of this region is determined by the span of the laser frequency modulation $\Delta\nu_L$ and the magnetic field gradient. An atom with $v = 0$ is addressed in the region delimited by the pair of dashed arrows on the left. (b) y deceleration from scattering of photons on the red $^1S_0 - {}^3P_1$ transition (in units of earth acceleration g) as a function of the initial velocity of atoms 20 cm above the quadrupole field center, obtained by an idealized 1D calculation. Annotations indicate regions dominated by Zeeman type slowing or red MOT type trapping. Atoms eventually captured in the MOT exhibit a time-independent force (yellow region at $\sim 1g$). The white regions show decelerations smaller than $0.25g$. The "Bounce" and "Fall" regions are undesirable cases where atoms bounce off the MOT beam or the MOT beam is not able to capture the atoms and they fall through. (c) Equivalent deceleration data obtained by a full 3D Monte Carlo calculation with a realistic geometry. Figure reproduced with permission from Bennetts et al. (2017).

below slows and captures the atoms that enter from above using several techniques, which are illustrated in Fig. 8(a). It performs as a Zeeman slower, a white light slower (Zhu et al., 1991) and a MOT beam. This "hybrid" Zeeman slower-MOT beam consists of a high power (10 mW) beam, frequency broadened (modulated by 3 MHz) to address an even wider velocity range by acting as a white light slower. We also focus the vertical slowing beam as shown in Fig. 7. Focusing adds a radial restoring force, reducing the divergence of the atomic beam as it slows. We adjust the polarization of this beam to choose the strength of the MOT and Zeeman slower components (Bennetts et al., 2017).

Using the magnetic field of the MOT, atoms are slowed using the Zeeman slower principle, as illustrated in Fig. 8(a). We have a mostly linear magnetic field gradient and strong variation from an ideal Zeeman slower beam profile intensity so we do not follow the ideal constant deceleration Zeeman slowing trajectory. For this reason, a single frequency slower beam would not be robust or efficient. Frequency modulation of this beam allows "white light slowing", overcoming this difficulty. For atoms that are successfully slowed and reach the region below the quadrupole field center, δ_{Doppler} is small and atoms are resonant with the laser light as in a standard broadband narrow-line MOT (Katori et al., 1999).

The high power broadband beams needed for this hybrid setup limit the MOT PSD to $2.8(1.2) \times 10^{-6}$. This is low compared to what can be achieved with a pure narrow-line MOT geometry in a time-varying sequence (Katori et al., 1999). However it does satisfy our first experimental requirement, allowing us to spatially separate the blue $^1S_0 - {}^1P_1$ from the red $^1S_0 - {}^3P_1$ laser cooling stages. We use this architecture for the high phase-space density beam experiment explained in the next section and for the CW BEC experiment.

We also implemented an alternative MOT configuration (MOT II), located to the side of MOT I described above, see Fig. 7. Data for MOT II was collected with the parameters optimized for flux and atom number, MOT II(a) as well as optimized for phase-space density, MOT II(b). By creating a MOT out of line of sight from the top chamber and using very weak MOT beams, much higher phase-space densities (10^{-3}) were possible, a 100-fold improvement over previous steady-state MOTs (Bennetts et al., 2017). In Fig. 9, we highlight the progress of steady state PSD performance from previous architectures to MOT II. Attempts were also made to continuously load a dipole trap directly from MOT II as a potentially simpler path to a CW BEC. However, the near resonant light intensity needed to

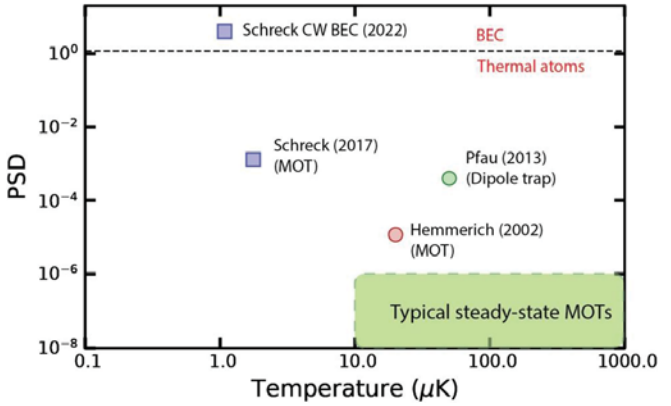

Figure 9 Progress in steady-state ultracold samples. Typical steady-state MOTs achieve phase-space densities below 1×10^{-6} and operate with temperatures above 10 μK. In 2002 the Hemmerich group demonstrated a calcium MOT cooling the $^3P_2$ metastable state using the $^3P_2$-$^3D_3$ transition with a PSD of 1.17×10^{-5} and a temperature of 20 μK (Grünert and Hemmerich, 2002). This was surpassed by the Pfau group in 2013 with chromium continuously loaded into a dipole trap (Falkenau et al., 2011; Volchkov et al., 2013). In 2017 our group demonstrated a strontium MOT with a PSD of 1×10^{-3} (Bennetts et al., 2017) and in 2022 a CW BEC using the same apparatus (Chen et al., 2022).

support the MOT atoms against gravity strongly heated atoms in the dipole trap making this approach unsuitable for a CW BEC (Bennetts, 2019).

A summary of the performance from these high phase-space density steady-state red MOTs is listed in Table 1. This data was obtained before inserting the dark spots into the MOT beams which was necessary to make the high PSD guided atomic beam described in section 3.2 and beyond. These dark spots reduced both the flux and PSD that could be obtained in MOT II. Later the blue $^1S_0 - {}^1P_1$ Zeeman slower power was increased from $\sim$ 64 mW to $\sim$ 172 mW, which increased the flux by a factor of five.

3.2 High phase-space density beam

Our steady-state MOT achieved a record high phase-space density of 10^{-3} (using ^{88}Sr).[4] However, the scattering rate needed to capture atoms and support them against gravity prevents phase-space densities from approaching degeneracy (Bennetts, 2019). For this reason, we next developed a dipole trap guided atomic beam that continuously transfers atoms from

[4] After increasing the Zeeman slower power from 64 mW to 172 mW the flux increased by a factor of five beyond the characterization discussed here.

Table 1 Characteristics of the three red MOT configurations for ^{84}Sr and ^{88}Sr. MOT II(a) used parameters optimized for flux and atom number whereas MOT II(b) used parameters optimized for phase-space density. All uncertainties are taken as $\pm 2\sigma$ from the fitted data. The parameters were optimized for ^{88}Sr, not ^{84}Sr. In some cases this resulted in a severe performance hit such as for the temperature for the z axis on the ^{84}Sr MOT. Axes are defined in Fig. 7. The MOT performances are sensitive to the parameters and need to be individually adjusted for each isotope to obtain optimal performance. Note that this data was obtained before inserting the dark spots into the MOT beams which were necessary to make the high PSD guided atomic beam described in section 3.2 and beyond. These dark spots reduced both the flux and PSD performance that could be obtained in MOT II. Further information can be found in Bennetts et al. (2017); Bennetts (2019); Chen (2019).

	^{88}Sr Red MOT I	^{88}Sr Red MOT II(a)	^{88}Sr Red MOT II(b)	^{84}Sr Red MOT I	^{84}Sr Red MOT II(a)	^{84}Sr Red MOT II(b)
Flux [atoms s^{-1}]	$5.1(7) \times 10^8$	$5.3(4) \times 10^7$	$5.3(9) \times 10^6$	4.85×10^6	$1.7(4) \times 10^6$	$4.7(15) \times 10^5$
Temperature x	-[a]	3.7(3) μK	2.01(6) μK	-[a]	-[b]	-[b]
Temperature y	20(5) μK	1.9(1) μK	1.42(3) μK	16(2) μK	2.3(3) μK	1.6(3) μK
Temperature z	26(7) μK	2.8(2) μK	1.91(9) μK	66(17) μK	8.4(12) μK	3.6(12) μK
Width σ_x	-[a]	385(4) μm	150(2) μm	-[a]	552(30) μm	351(4) μm
Width σ_y	725(61) μm	192(3) μm	88(1) μm	748(35) μm	245 μm	180(13) μm
Width σ_z	2086(41) μm	528(3) μm	247(3) μm	1571(49) μm	778(30) μm	386(11) μm
Atom number	$2.54(10) \times 10^9$	$1.71(5) \times 10^8$	$2.5(1) \times 10^7$	$6.69(8) \times 10^8$	$1.55(3) \times 10^8$	$5.9(2) \times 10^6$
Peak density [atoms cm^{-3}]	$5.1(7) \times 10^{10}$	$2.8(2) \times 10^{11}$	$4.8(4) \times 10^{11}$	$2.3(3) \times 10^{10}$	$9(1) \times 10^{10}$	$1.7(2) \times 10^{10}$
Peak PSD	$2.8(12) \times 10^{-6}$	$4(1) \times 10^{-4}$	$1.3(2) \times 10^{-3}$	$6.4(22) \times 10^{-7}$	$4.5(17) \times 10^{-5}$	$2.0(1) \times 10^{-5}$
$1/e$ lifetime	4.53(6) s	2.8(2) s	1.95(6) s	12.0 s	9.6 s	11.4 s

[a] At the location of Red MOT I no imaging system for the x axis was available so Red MOT I density and PSD calculations assume that temperature and width along x are the same as along z.

[b] Top view data was not recorded so the temperature for the x axis is assumed to be the same as for the z axis.

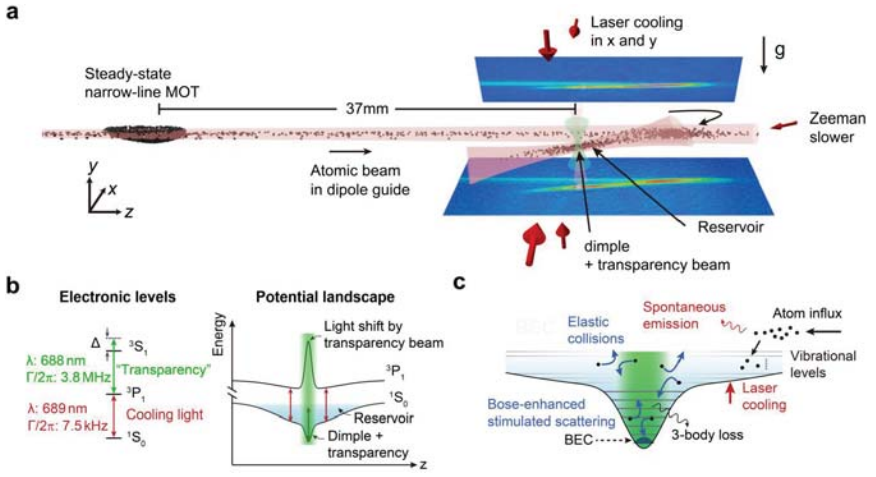

Figure 10 Architecture of the CW BEC apparatus. (a) ^{84}Sr atoms from a steady-state narrow-line magneto-optical trap (MOT) are continuously out coupled into a guide and loaded into a crossed-beam dipole trap that forms a large reservoir with a small, deep dimple. Atoms accumulate in the laser cooled reservoir and densely populate the dimple, where a BEC forms in steady state. (b) By off-resonantly addressing the $^3P_1 - {}^3S_1$ transition using a "transparency" laser beam, we produce a strong spatially varying light shift on the $^3P_1$ electronic state, rendering atoms locally transparent to laser cooling photons addressing the $^1S_0 - {}^3P_1$ transition. This enables condensation in the protected dimple region. (c) Schematic of the potential landscape from both reservoir and dimple trap, and of the dominant mechanisms leading to BEC atom gain and loss. Figures reproduced with permission from Chen et al. (2022).

the MOT to a second dipole trap reservoir 37 mm away, which is mostly shielded from resonant MOT light. This is illustrated in Fig. 10(a). By supporting atoms against gravity very small scattering rates allow cooling to much higher phase-space densities. In addition to the advantage of moving outside the high power MOT beams, transporting the atoms to a displaced dipole trap reservoir also eliminates line of sight with the upper chamber and its resonant blue $^1S_0 - {}^1P_1$ photons.

To implement this scheme we used a dipole trap guide collinear with the z axis MOT beams, where the axes are defined in Fig. 7. To form the guide we use 12 W of 1070 nm light focused just after the MOT center with the retro reflected beam focused near the reservoir. The displacement between the focal points allows us to propagate the atoms further with the limited power available. It also serves to flatten the dipole trap potential along the guide compared to a single beam with an equivalent waist size (Chen, 2019). We also carefully considered the use of a Bessel

beam (Schmid et al., 2006; Brzobohatý et al., 2008; Klostermann et al., 2022) but for the transport application decided against it for simplicity and to improve loading without the complication of having multiple traps. For guided evaporation the Bessel beam remains promising as we will describe in the outlook.

We launch atoms from the continuous red MOT down the guide with a 1.15 MHz broad, modulated, 20 nW blue detuned push beam on the $^1S_0 - {}^3P_1$ transition. As the atoms propagate along the guide they are radially cooled using weak cooling beams operating on the non-magnetic $^1S_0 - {}^3P_1$ transition.

To minimize the interaction with the co- and counter-propagating MOT beams we keep the MOT light at very low intensity along this axis. Additionally, the Zeeman shift due to the MOT's quadrupole magnetic field quickly shifts the atoms propagating in the beam out of resonance with the MOT light. Finally, we implement the Dark SPOT technique (Ketterle et al., 1993) and achieve an attenuation of the MOT light by a factor $30 \sim 40$ along the center of the transport guide. The dark SPOT was created by suspending a 0.6 mm diameter capillary in the MOT beams and imaging these "dark SPOT cylinders" to maximally eliminate MOT light from the region of the dipole guide. The darkness was ultimately limited by imperfections of the cylinder's surface and imaging, and by Poisson's spot from diffraction. More details on the experimental setup can be found in Chen et al. (2019b); Chen (2019); Bennetts (2019).

To describe the characterization of our high phase space density beam (Chen et al., 2019b) we begin with the flux of our beam. Assuming a Gaussian density distribution of the atoms in the radial direction, the beam flux Φ can be represented by

$$\begin{aligned}\Phi &= \int_0^\infty n_0 \exp\left(-\frac{r^2}{2\Delta r^2}\right) 2\pi r dr \bar{v}_z \\ &= 2\pi \Delta r^2 n_0 \bar{v}_z = \rho_L \bar{v}_z,\end{aligned} \tag{1}$$

where Δr the root-mean-squared transverse spatial extension, n_0 the peak density, ρ_L the linear density and $\bar{v}_z$ the mean longitudinal velocity. All these parameters can be directly measured in our experiment with the results presented in Table 2.

The flux density which is the flux per unit cross-section area is given by $\rho_\Phi = \Phi/\pi\Delta r^2$. This provides a better measure of the 'intensity' of a beam. However, for our purposes a low temperature is also important so a better

Table 2 Characteristics of the high phase-space density beam for ^{88}Sr and ^{84}Sr, measured 37 mm away from the MOT. The symbols and their expressions are detailed in the main text. All uncertainties are taken as the standard deviation from the fitted data. *The quantities $\bar{v}_z$ and Δv_z could not be measured for ^{84}Sr as the flux is not large enough. We assume the same values as for ^{88}Sr, scaled by the mass ratio. Further information can be found in Chen et al. (2019b).

Parameter	^{88}Sr beam	^{84}Sr beam
Axial temperature T_z (μK)	29(2)	29(2)
Radial temperature T_r (μK)	0.89(4)	2.0(1)
Axial velocity $\bar{v}_z$ (cm s^{-1})	8.4(4)	8.8(4)*
Axial Velocity spread Δv_z (cm s^{-1})	5.2(2)	5.3(2)*
Radial Velocity spread Δv_r (cm s^{-1})	0.92(2)	1.41(4)
Spatial spread Δr (μm)	23.3(4)	19.7(1.0)
Linear density ρ_L (m^{-1})	$3.88(8) \times 10^8$	$1.04(5) \times 10^7$
Peak density n_0 (m^{-3})	$1.14(4) \times 10^{17}$	$4.2(5) \times 10^{15}$
Flux Φ (s^{-1})	$3.25(14) \times 10^7$	$9.1(6) \times 10^5$
Flux density ρ_Φ (s^{-1} m^{-2})	$1.9(1) \times 10^{16}$	$7.4(9) \times 10^{13}$
Radial trapping frequency $\omega_r/2\pi$ (Hz)	185(10)	185(10)
Phase-space density ρ_{PSD}	$1.5(2) \times 10^{-4}$	$2.7(4) \times 10^{-6}$
Alternative PSD $\rho_{\mathrm{PSD,therm}}$	$1.3(2) \times 10^{-3}$	$7.1(1.2) \times 10^{-6}$
Collision rate Γ_{el} (s^{-1})	$3.5(2) \times 10^{-4}$	0.11(2)

measure of the beam performance is to measure the phase-space density in the moving frame which may be expressed as:

$$\begin{aligned} \rho_{\mathrm{PSD}} &= n_0 \lambda_{\mathrm{dB},r}^2 \lambda_{\mathrm{dB},z} \\ &= n_0 \left(\frac{h}{\sqrt{2\pi\, m k_B T_r}} \right)^2 \frac{h}{\sqrt{2\pi\, m k_B T_z}}. \end{aligned} \tag{2}$$

Here $\lambda_{\mathrm{dB},r}(\lambda_{\mathrm{dB},z})$ is the thermal de Broglie wavelength associated with the 1D temperature $T_r(T_z)$ in the radial(axial) direction. Since we observe that the velocities follow Gaussian distributions, these effective 1D temperatures are directly related to the measured root-mean-squared 1D velocity spreads by the relations $\Delta v_r = \sqrt{k_B T_r/m}$ and $\Delta v_z = \sqrt{k_B T_z/m}$.

There are two approaches in which we estimate the peak atom number density n_0. Firstly, we can use absorption imaging and fit a Gaussian profile to estimate the peak density. Alternatively, we may assume that the atom density inside the guide follows a Boltzmann distribution with radial temperature T_r. Using Eq. (1), the peak density in the thermalized case is then related to the linear density by $\rho_L = n_{0,\mathrm{therm}}\, 2\pi k_B T_r/m\omega_r^2$, and the

expression of the phase-space density of Eq. (2) can be written as

$$\begin{aligned}\rho_{\mathrm{PSD,therm}} &= n_{0,\mathrm{therm}}\,\lambda_{\mathrm{dB},r}^{2}\,\lambda_{\mathrm{dB},z} \\ &= \rho_L\left(\frac{\hbar\omega_r}{k_B T_r}\right)^2 \frac{h}{\sqrt{2\pi\, m k_B T_z}}.\end{aligned} \tag{3}$$

The temperatures T_r and T_z, the trapping frequency ω_r and the linear density ρ_L are directly accessible from the experimental data.

The final atomic beam property that we calculate is the elastic collision rate. In order to achieve efficient evaporation we would need a high elastic collision rate compared with the propagation time along a guide. The scattering lengths of the ^{88}Sr and ^{84}Sr isotopes are equal to $-1.4a_0$ and $122.7a_0$ respectively (Chen et al., 2019b). This results in much lower collision rates for ^{88}Sr despite its comparatively high density. Nevertheless, we see that neither isotope has sufficiently high collision rates that they present as viable candidates for evaporative cooling in our waveguide. A tighter beam waist (for example using a Bessel beam), higher flux (^{86}Sr has 10% natural abundance compared with 0.6% for ^{84}Sr) and higher scattering cross sections (^{86}Sr has $830a_0$) do however offer a compelling alternative for evaporatively cooling a beam to a continuous atom laser.

A number of other beam properties such as brilliance, brightness and velocity brightness are commonly used to characterize atomic beams for interferometry based precision measurement (Treutlein et al., 2001; Miossec et al., 2002; Riis et al., 1990; Chen and Riis, 2000) and to characterize atom lasers (Robins et al., 2013) and these are presented for our system in Chen et al. (2019b).

3.3 Loading a reservoir and dimple trap

Having transported atoms out of the steady-state MOT the next step is to slow them and load them into a dipole trap forming a reservoir of near degenerate atoms able to provide matter-wave gain. We begin by using a Zeeman slower to stop the 8.8(8) cm s^{-1} guided atomic beam. This Zeeman slower uses the MOT's magnetic quadrupole field and 4.5 nW of light at around I_{sat} on the $^1\mathrm{S}_0 - {}^3\mathrm{P}_1$ transition. A Gaussian beam focused to a 15 μm vertical and 110 μm horizontal $1/e^2$ waist radius forms a reservoir trap to collect these slowed atoms. The exact location and depth of this trap must be very carefully optimized to ensure a maximally flat potential landscape between the location where the Zeeman slowed atoms stop and the reservoir. A potential hill will prevent atoms from entering the reservoir

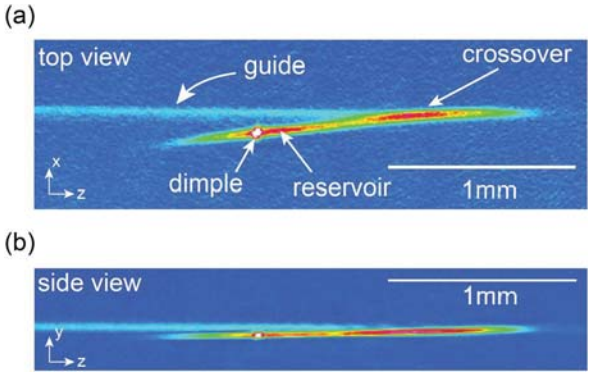

Figure 11 Atomic density distribution. Experimental in-situ absorption images of the atomic distribution in the CW BEC reservoir region. These images show the incoming guided atomic beam, which is slowed and trapped in the reservoir. Within the reservoir the dimple trap can be observed as a high density feature. (a) Top view. (b) Side view.

while a fall leads to excess energy and heating of the reservoir. In practice this is achieved by imaging the density of atoms in this crossover region and adjusting the height of the reservoir to maximize the uniformity of the atom density.

The reservoir beam is tilted slightly so that the additional dipole trap power of the guide beam is cancelled by a higher gravitational potential at the reservoir-guide crossing point as illustrated in Fig. 11(b). An additional 1070 nm beam passing close to the reservoir beam was used to tailor and deepen the reservoir around the location of the dimple trap to further improve loading. Typical profiles of the resulting atomic densities in the horizontal and vertical planes are shown in Fig. 11. Further details can be found in Bennetts (2019).

Within the reservoir, atoms continue to be cooled by a set of three weak ${}^1S_0 - {}^3P_1$ molasses beams, two from the sides and one vertically propagating upwards. These are the same beams that transversally cool the atomic beam. One final beam acting on the magnetic ${}^1S_0 - {}^3P_1$ transition and propagating along the reservoir counter to the Zeeman slower beam provides spatially limited slowing able to further reduce the temperature of the atoms entering the reservoir from the Zeeman slower. In this case the MOT magnetic field in combination with using a magnetic transition and a well controlled laser bandwidth allowed precise control of the location and extent of the applied slowing force.

The final element of our potential energy landscape is the dimple dipole trap (Pinkse et al., 1997; Stamper-Kurn et al., 1998). Conceptually, the

dimple trap is designed to enhance the atom density within the reservoir trap while maintaining an atomic temperature essentially in thermal equilibrium with atoms in the reservoir. It is thus essential that there be a high elastic collision rate between atoms in the dimple and reservoir.

One of the striking features observed in our results (Chen et al., 2022; Chen, 2019; Bennetts, 2019) is that the temperature along the z axis, the axis of the incoming atoms and the Zeeman slower beam, is significantly higher than the temperature along the other axes. This indicated the potential for significant gains by improving the z axis temperature. To try to exploit this potential we developed a Sisyphus cooling technique, the Sisyphus Optical Lattice Decelerator (SOLD) (Chen et al., 2019a). The concept of the SOLD is illustrated in Fig. 12. Essentially an optical lattice blue detuned by 30 GHz from the $^1S_0 - {}^3P_1$ transition is used to create a potential lattice for the $^3P_1$ state along the z axis. When laser cooling on the $^1S_0 - {}^3P_1$ transition is tuned to excite atoms at the bottom of this lattice, excited atoms typically roll up the walls of lattice sites before decaying, resulting in cooling along the lattice direction. Such a lattice was added along the reservoir with the aim of adding cooling in the problematic z direction. Although this technique was successfully demonstrated on its own, it was less effective in the CW BEC configuration and ultimately was not used in the final CW BEC experiment. Most likely this is because the ac-Stark shift from the SOLD lattice hinders the other laser cooling mechanisms. Variations on this scheme that use clock line Sisyphus cooling and do not interfere with cooling on the $^1S_0 - {}^3P_1$ will be discussed in section 4. Several additional cooling steps and improvements necessary to reach CW-BEC will be described in the next section but this remains an area offering significant potential for improvement.

3.4 BEC protection from near resonant light

The atoms in the reservoir trap have a lifetime of 7 s without laser cooling beams, a limit that arises mainly from collisions with the background gas of the vacuum chamber. While laser cooling beams are essential to load fresh atoms into the reservoir, they also lead to losses by light assisted collisions and photo-association as well as a reduction of density by multiple scattering. We use five techniques to minimize the exposure of atoms in the reservoir to unnecessary resonant light. (i) Blue light on the broad 30 MHz linewidth $^1S_0 - {}^1P_1$ transition is used only in the top chamber, which is separated by baffles to ensure there is no line of sight to the reservoir. (ii) The illumination of reservoir atoms by red $^1S_0 - {}^3P_1$ laser cooling light is

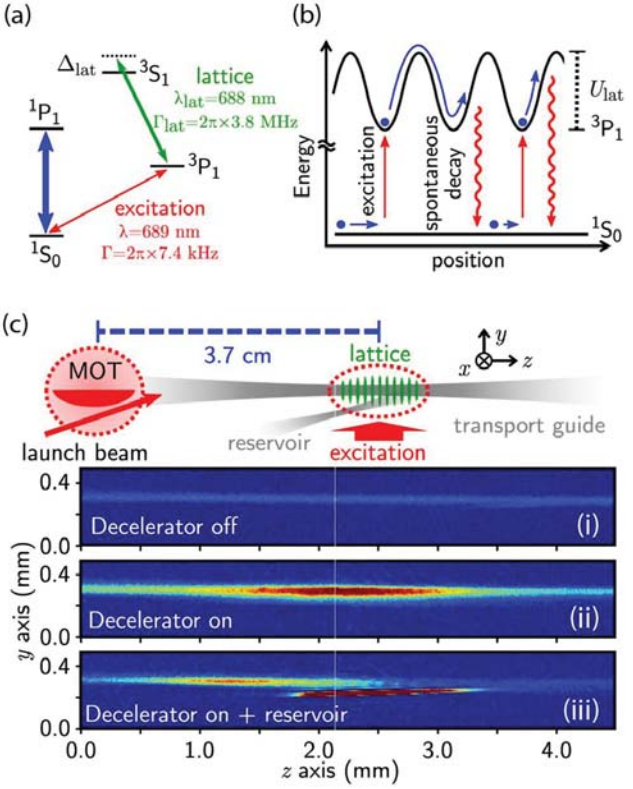

Figure 12 Sisyphus optical lattice decelerator. (a) Relevant electronic levels of strontium and the two transitions used for excitation and optical lattice creation, both necessary for the SOLD. (b) Schematic of two typical cooling cycles, from excitation to spontaneous decay. (c) Side view of the setup. (i)-(iii) Absorption imaging pictures of the atomic beam at the decelerator location: without lattice (i), with lattice (ii), and with lattice and reservoir (iii). Figures reproduced with permission from Chen et al. (2019a).

minimized. For this the 37 mm offset between the MOT and reservoir centers allows us to avoid any direct illumination from the x, y MOT beams on the reservoir, see Fig. 10(a). The axes are defined in Fig. 7. On the z axis, the influence of the MOT beams is greatly reduced by using a "dark cylinder", as described in Chen et al. (2019b). We also image 1 mm diameter steel balls placed within each of the z MOT beams onto the location of the reservoir, further reducing the z MOT light on the atoms. The Zeeman decelerator that stops the atomic beam is spatially separated from most of the reservoir. (iii) The cooling spectrum and intensity of each laser cooling beam entering the last vacuum chamber is optimized. By separately

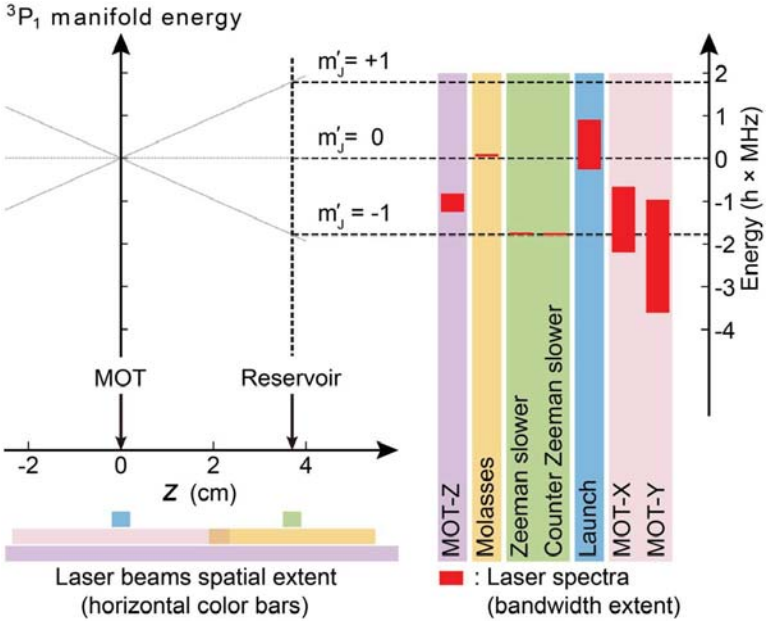

Figure 13 Suppressing photon reabsorption in the BEC by spatial and frequency selection. Spectra of narrow-linewidth cooling lasers, and their spatial extent. The right side represents the spectra of cooling lasers addressing the $^1S_0 - {}^3P_1$ transition (vertical red bars) with respect to the (relative) energy of the states in the $^3P_1$ manifold, shown on the left side. The energies of these m'_J states are given depending on the location along the *z* axis, and the horizontal black dashed lines represent their respective Zeeman shifts when atoms are located inside the reservoir. The horizontal color bars at the bottom left show the location and spatial extent of each laser beam. Figure reproduced with permission from Chen et al. (2022).

measuring their influence on the reservoir atom number, we optimize on a compromise between the lifetime of atoms and the loading flux as shown in Fig. 13. Where necessary, apertures were placed to avoid beams scattering off the chamber walls. (iv) The π polarization component of the molasses beams that illuminate the guided beam and the reservoir is maximized. This minimizes the effects of unwanted transitions. Unavoidably, beams along the y axis possess admixtures of σ^- and σ^+ polarization due to the orientation of the local magnetic field. (v) The spectrum of the light used to address the $^1S_0 - {}^3P_1$ cooling transition is purified. Our cooling light is produced by multiple injection-locked diode lasers beginning from a single external-cavity diode laser (ECDL). We reduce the linewidth of this ECDL to ~ 2 kHz by locking it onto a cavity with a finesse of ~ 15000, whose

spectrum has a full-width half maximum of ~ 100 kHz. By using the light transmitted through this cavity to injection lock a second diode laser, we can filter out the ECDL's amplified spontaneous emission and servo bumps. This filtering is critical to increase the atoms' lifetime inside the dimple by reducing resonant-photon scattering.

In addition to minimizing resonant light, a "transparency beam", introduced in Stellmer et al. (2013) is added to locally shift the $^1S_0 - {}^3P_1$ transition of the atoms in the dimple trap region. In this way, atoms in the dimple become off-resonant to the $^1S_0 - {}^3P_1$ laser cooling light. This is achieved by coupling light to the $^3P_1 - {}^3S_1$ transition, to induce a light shift on the $^3P_1$ state as illustrated in Fig. 14(a, b).

Due to the extreme sensitivity of the BEC to photon scattering, all sub-levels of the $^3P_1$ state must be shifted significantly. This requires using at least two of the three transition types $(\sigma^{\pm}, \pi)$ in this $J = 1 - J' = 1$ structure. However, when polarization components with the same frequency are combined, quantum interference between sub-levels always produces a dark state in the dressed $^3P_1$ manifold. The energy of this dark state can only be shifted between $\pm\Delta_{\text{Zeeman}}$, where Δ_{Zeeman} is the Zeeman shift of the $^3P_1$ $(m_J' = 1)$ state. This corresponds to $\Delta_{\text{Zeeman}} = 1.78$ MHz at the dimple location, giving a light shift that is insufficient to protect the BEC. Thus it is necessary to use different frequencies (1.4 GHz separation) for the different polarization components of the transparency beam. Due to the close 1.43 nm difference between the $^1S_0 - {}^3P_1$ cooling transition and the $^3P_1 - {}^3S_1$ transparency transition a series of dispersive prisms are used to spectrally filter the laser light of any unwanted components such as amplified spontaneous emission. The ac-Stark shifts achieved at the center of the transparency beam are shown in Fig. 14(b).

Our transparency protection beam shifts the $^1S_0 - {}^3P_1$ cooling transition lines to the blue. Due to the presence of a magnetic field at the reservoir trap the $^1S_0 - {}^3P_1 (m_j = -1)$ transition frequency crosses the free space $m_j = 0$ and $m_j = +1$ transition frequencies, see Fig. 14(b). As a result, for specific powers of the transparency beam these transitions are shifted into resonance rather than away from it. The Gaussian beam intensity profile of the transparency beam means that there is a spatial variation of the ac-Stark shift and always a (small) annulus where the transparency beam shifts the $^1S_0 - {}^3P_1$ $(m_j = -1)$ state onto resonance with the cooling light. This locally results in heating rather than protection. Experimentally, we minimize this unwanted heating by minimizing the polarization component of the molasses cooling beams that drives the $^1S_0 - {}^3P_1$ $(m_j = -1)$ transition.

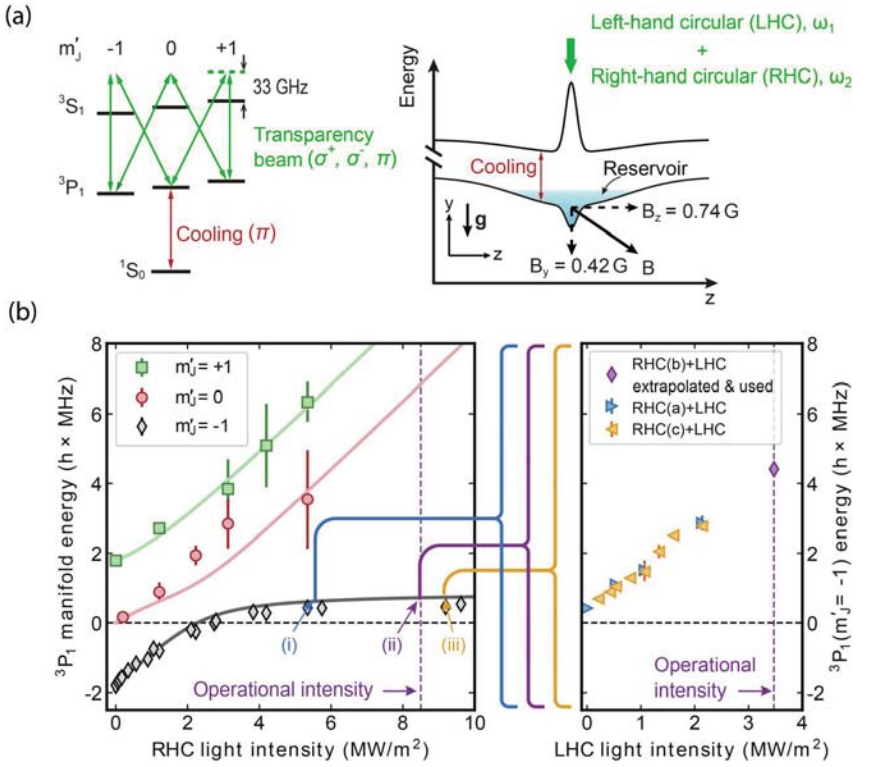

Figure 14 Suppressing photon reabsorption in the BEC using the transparency beam. (a) Light shift from the transparency beam. Transparency transition level scheme and schematic of the potential energy landscape of reservoir and dimple for the $^1S_0$ and $^3P_1$ states. Atoms are rendered insensitive to the laser cooling light by a single vertical "transparency" laser beam (green arrow), containing two frequency components, one for each circular polarization. (b) Transition energies to the three $m'_J = 0, \pm 1$ Zeeman sub-levels of the $^3P_1$ manifold, referenced to the transition at zero light intensity and magnetic field (black dashed line). The energy shifts are shown for a single right-hand circular (RHC) polarization (left) and with the addition of the left-hand circular (LHC) component (right). We show the solutions (solid lines) of the Schrödinger equation for the $^3P_1$ manifold coupled by a light field with single frequency component and RHC polarization. In this case, at high laser intensities, the energy of the state originating from $m'_J = -1$ saturates, corresponding to the presence of a dark state. (i, ii, iii) indicate three different operational intensities of the RHC light. For each of these the $m'_J = -1$ state light shift is characterized for varying LHC light intensity. The purple vertical dashed lines show the operating intensities of the LHC and RHC light fields used in the CW BEC experiment, and the purple diamond is extrapolated from the data. The error bars indicate estimates of the ranges in which the light shifted spectral lines lie. Figure reproduced with permission from Chen et al. (2022).

The architecture we have described here, shown in Fig. 10(a), was completed and first tested in late 2017 (Bennetts, 2019; Chen, 2019) and within a few months a steady-state ultracold gas with a phase-space density above one was demonstrated. Nevertheless several additional steps proved necessary to finally reach condensation. Of these, the key improvements were increasing the atomic flux and improving the polarization purity of the molasses cooling light, which was critical for reducing heating.

3.5 Continuous Bose-Einstein condensation

We have described all the elements necessary to produce continuous Bose-Einstein condensation. To prove achievement of our goal, we employ several techniques to observe and characterize the BEC. This proof is complicated by the immersion of the BEC in a significantly larger thermal cloud. Two key points have to be shown: that the BEC exists and that it persists indefinitely.

BEC existence is demonstrated using three methods. Firstly, we observe a bimodal distribution of the cloud after free expansion. Secondly, we show inversion of the anisotropy direction during free expansion and finally we show that an additional "BEC component" is needed to adequately fit the data after condensation.

Showing that the BEC persists indefinitely requires many independent experiments with varying hold times because our detection technique is destructive. We find that a BEC is always observed after a minimum time of 3.5 s, which is needed to load enough atoms into the dimple, form a BEC and reach steady-state. This is true over time scales much longer than all the lifetimes in the system. Here we shall describe the methods that we used to verify the presence of a steady-state BEC and the results we obtained.

A bimodal distribution: We analyze atomic cloud density images for $t_{\mathrm{hold}} = 2.2$ s and 3.2 s, immediately before and after the formation of a BEC, as shown in Fig. 15(a, b). These x-integrated absorption images are taken after switching off all laser beams and letting the cloud expand for 18 ms. Both images show broad distributions of thermal atoms that are horizontally extended, reflecting the spatial distribution of the gas before expansion. Interestingly, the image for the longer t_{hold} shows a small additional elliptical feature at the location of highest optical density, which is consistent with the presence of a BEC. The appearance of a BEC is clearly revealed in Fig. 15(c, d), showing y-integrated density distributions. For short t_{hold} only a broad,

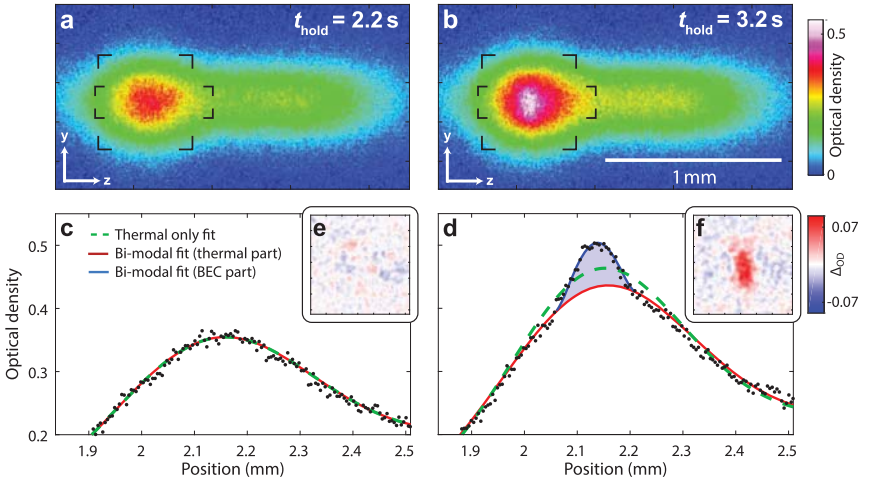

Figure 15 Detection of the CW BEC. (a, b) Absorption images of the atomic cloud before and after condensation. The atoms are imaged after an 18 ms time-of-flight expansion. (c, d) Optical density within the elongated rectangles marked by corners in (a) and (b), averaged along *y*. Fitted profiles using a thermal-only distribution (green dashed line) or a bi-modal distribution, consisting of a thermal (red line) and a Thomas-Fermi (blue line) component. The thermal-only fit fails to represent the condensed atoms in (d) (blue shaded area). (e, f) Corner-marked square region of absorption images (a) and (b) minus thermal parts of the bi-modal fits, showing the CW BEC. Figure reproduced with permission from Chen et al. (2022).

thermal distribution exists. However for long t_{hold} a bi-modal distribution appears, the hallmark of a BEC.

To quantify this observation the observed 2D density distribution after time of flight expansion can be fitted by an ensemble of four thermal components following Maxwell-Boltzmann distributions plus an additional Thomas-Fermi distribution when a BEC is present. Three independent 2D Gaussian functions fit the Maxwell-Boltzmann distributions representing atoms originating from the dimple, the reservoir, and the crossing between the guide and reservoir. Atoms originating from the guide are represented along the guide's axis by a sigmoid that tapers off due to the effect of the Zeeman slower, and in the radial direction by a Gaussian profile. When a BEC is present, it is necessary to add a Thomas-Fermi component to this fit function. The only additional free parameter used in the fit is the number of atoms in the BEC as the trapping frequencies are independently measured and the location of the BEC can be assumed to coincide with the dimple.

As shown in Fig. 15(c, d), excellent agreement was found by combining Thomas-Fermi (TF) with thermal Maxwell-Boltzmann distributions for long hold times while at short hold times before BEC formation, we find that a thermal fit alone is sufficient to describe the data. The atom numbers and temperatures of the thermal cloud in the various trap regions also provide a wealth of information for further understanding the system. Fig. 15(e, f) shows the data after removing the thermal fit component illustrating the presence of the BEC in (f). Its pronounced anisotropic shape is consistent with the expansion of a BEC from the dimple, whose trap frequency along the y axis is approximately double that along z, as shown in Fig. 15(e, f). With these fits we can plot both 2D fit residuals (Fig. 15(e, f)) and the integrated cross sections of the 2D fits with and without BEC components as shown in Fig. 15(c, d). Here the presence of a bimodal distribution can be clearly observed after BEC formation in Fig. 15(d). More information on the fitting can be found in the supplementary material of reference (Chen et al., 2022).

Aspect ratio inversion - anisotropy during time-of-flight: A Bose-Einstein condensate and a thermal gas expand very differently when released from a trap. A thermal gas expands isotropically, beginning with a shape reminiscent of the initial trap geometry and asymptotically approaching an isotropic shape for long times of flight. By contrast, the expansion of a BEC released from an anisotropic trap remains anisotropic, with the aspect ratio inverting for long times of flight (TOF). This originates from the BEC populating the ground state of an asymmetric trap which results in a corresponding asymmetry in the momentum space wavefunctions and thus higher rates of expansion in the more tightly confined axis. In most BECs (where there are interactions) this leads to a further asymmetric release of contact interaction mean-field energy, related to the asymmetric BEC density profile in the trap (Castin and Dum, 1996). Our trap has a trap frequency along the y axis that is approximately double that along z, leading to a correspondingly faster expansion and larger final cloud size along the y axis compared to the z axis (axes defined in Fig. 7).

The transpose-anisotropy centered at the location of the dimple trap provides an elegant method to efficiently detect the presence of a steady-state BEC. The transpose-anisotropy of the density distribution is defined by $n^T_{\mathrm{OD}}(y,z) = n^s_{\mathrm{OD}}(y,z) - n^s_{\mathrm{OD}}(z,y)$, where the origin of the coordinate system is at the density maximum. $n^s_{\mathrm{OD}}(y,z) = \left[n_{\mathrm{OD}}(y,z) + n_{\mathrm{OD}}(-y,-z)\right]/2$ is obtained from the optical density $n_{\mathrm{OD}}(y,z)$ through symmetrization by adding the same n_{OD} distribution

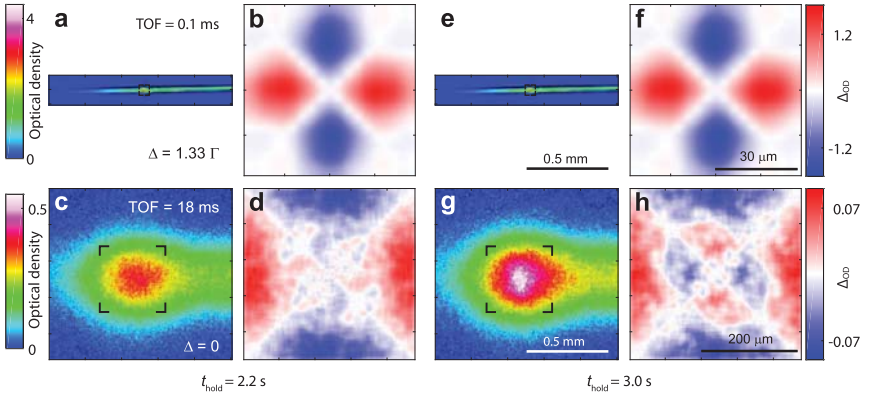

Figure 16 BEC anisotropy after time-of-flight. (a, e) Absorption images after short (0.1 ms) and (c, g) after long (18 ms) free-expansion time-of-flight (TOF), for (a, c) short ($t_{\mathrm{hold}} = 2.2$ s) and (e, g) long ($t_{\mathrm{hold}} = 3.0$ s) trap loading times. Pictures (a) and (e) were imaged with a detuning of $1.33\,\Gamma$ to avoid saturation. The regions of interest (corner-marked squares) centered around the density maximums are analyzed in panels (b, d, f, h), which show the transpose-anisotropy of the density distribution. This representation produces a cloverleaf pattern when the atomic cloud is anisotropic. (b, d) For short t_{hold} the cloverleaf pattern, which appears because of how the trap geometry initially shapes the thermal cloud, keeps a constant sign and diminishes during the expansion of a thermalized gas sample. (f, h) For long t_{hold} we observe at long expansion time (h) an additional smaller cloverleaf pattern of opposite sign, which is indicative of the presence of a BEC. Figure reproduced with permission from Chen et al. (2022).

rotated by 180 °. Transpose-anisotropies for short (0.1 ms) and long (18 ms) times of flight are shown in Fig. 16. For 0.1 ms TOF n_{OD} shows a marked anisotropy as indicated by a strong cloverleaf pattern. This initial anisotropy is solely due to the action of the trap geometry on the density distribution of the thermal gas, as the size of a potential BEC is below our imaging resolution. However for 18 ms TOF we see a difference between pictures for short (2.2 s) and long (3.0 s) hold time t_{hold}. For short t_{hold} the anisotropy is broad and simply a remnant of the initial cloud anisotropy. However for long t_{hold}, at which steady state is established, we see an additional smaller cloverleaf pattern with opposite anisotropy around the center of the picture. Both the existence and the sign of this pattern are consistent with the expansion of a BEC from a dimple with our trap frequencies.

The need for a 'BEC component' - statistical analysis: Adding additional fitting parameters can lead to overfitting. To rigorously determine whether including an additional Thomas-Fermi distribution provides a significantly better fit of the data, a statistical F-test can be used (Mil-

ton and Arnold, 2014). An F-test compares the difference in the residual sum of squares (RSS) between two models with the expected reduction in RSS gained from adding additional fitting parameters. For our analysis, we compared models with and without the additional degrees of freedom provided by adding an additional Thomas-Fermi distribution. For this F-test we isolate a region of interest (ROI) in the 18 ms time-of-flight image containing both thermal and BEC atoms. The test statistic is calculated as $F = \left[(RSS_1 - RSS_2)/(p_2 - p_1)\right] / \left[RSS_2/(n - p_2)\right]$ (Milton and Arnold, 2014), where p_i is the number of parameters in model i, n is the number of pixels in the ROI, and RSS_i is the residual sum of squares for model i. If the calculated F value is larger than the value from an F-distribution with degrees of freedom $(p_2 - p_1, n - p_2)$ at the desired level of significance, we may conclude that the model with more parameters fits better with that level of confidence. By plotting the achieved F-test significance against the fitted BEC atom number we can determine a threshold BEC atom number to claim the existence of a BEC with a desired confidence level. By applying this test we find that the BEC model fits better, with a confidence greater than 99.5 %, when the BEC atom number exceeds 2000. This sets our detection limit, above which a BEC exists.

Steady-state Bose Einstein Condensation: Once established, the BEC can be maintained in steady-state indefinitely with Bose-stimulated gain balancing losses. Since the observation of the BEC was inherently destructive we characterized the atomic cloud for different wait times t_{hold}, performing the same analysis as was used in Fig. 15 to fit and measure the number of condensed atoms. Fig. 17(a) shows representative density profiles during both the initial 5 s formation transient (a-f) and then in the presence of a stable BEC (f-j). Likewise, Fig. 17(b) shows the evolution and then stability of the BEC atom number and the peak phase-space density of the thermal gas in the dimple $\rho_D = N_D \left(\frac{\hbar^3 \omega_{Dx}\omega_{Dy}\omega_{Dz}}{k_B^3 T_D^3}\right)$, where N_D is the thermal atom number in the dimple and $\omega_{Di}/2\pi$ are the dimple trap frequencies. The peak PSD of the thermal gas provides a lower bound for the system peak PSD as it doesn't take the condensed fraction into account (Ketterle et al., 1999). The steady-state BEC was observed over times much longer than both the lifetime of a pure BEC ($1.5 - 3$ s) and the background-gas limited lifetime (7 s).

The atom number fluctuations in the BEC can be estimated from many independent observations. To analyze stability we collected ~ 200 measurements for $t_{\text{hold}} = 15$ s, significantly longer than both the lifetimes in

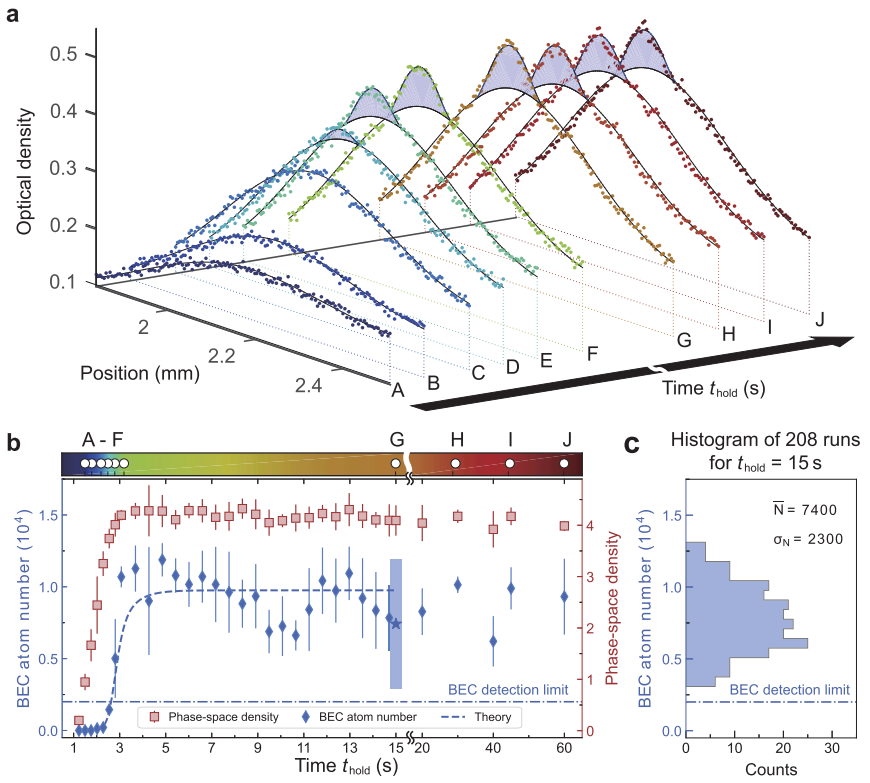

Figure 17 Formation and stability of the CW BEC. (a) Profiles as in Fig. 15(c,d) for various hold times (marked in (b)) first during the formation of the BEC (A: 1.5 s, B: 1.8 s, C: 2.2 s, D: 2.5 s, E: 2.8 s, F: 3.2 s), then during the steady state of the CW BEC (G: 15 s, H: 30 s, I: 45 s, J: 60 s). (b) Evolution of the BEC atom number and the dimple atom phase-space density ρ_D as a function of hold time t_{hold} after suddenly switching all laser beams on. The dashed blue line shows the result of the BEC evolution fitted to the data before 15 s using a rate-equation model (Chen et al., 2022). The error bars show the standard deviation from binning ~ 4 measurements for each time. (c) Histogram of the BEC atom number from 208 images for $t_{\text{hold}} = 15$ s, long after the establishment of steady state (blue star in (b)). No points fall below our BEC detection limit of 2000 atoms. The 95 % confidence interval ($4\sigma_N$) calculated from this data set is given in (b) at 15 s (blue rectangle). Figure reproduced with permission from Chen et al. (2022).

the system and the formation transient, see Fig. 17(c). We measure a BEC atom number of $\bar{N} = 7400(2300)$, with none of the points falling below our BEC detection threshold of 2000 atoms (Chen et al., 2022). This detection limit is more than $-2\sigma_N$ below the shot-to-shot BEC atom number fluctuations indicating that at all times after steady state is reached, a BEC exists.

Estimating the gain and loss from the BEC is important for practical applications such as producing a CW atom laser (Robins et al., 2008) and improving matterwave coherence. For this reason, we fit our BEC number evolution to a phenomenological rate-equation model. The full model is described in the supplementary material of Chen et al. (2022) but its essence is shown in Eq. (4).

$$\frac{\partial n_{\mathrm{BEC}}}{\partial t} = s_{\mathrm{in}} - s_{\mathrm{out}} - \gamma_{1\mathrm{b}} n_{\mathrm{BEC}} - \gamma_{3\mathrm{b}} \left[n_{\mathrm{BEC}}^3 + 6 n_{\mathrm{BEC}}^2 n_{\mathrm{th}} + 6 n_{\mathrm{BEC}} n_{\mathrm{th}}^2 \right]. \quad (4)$$

Here, $s_{\mathrm{in}} - s_{\mathrm{out}}$ is the flux scattered into the BEC, $\gamma_{1\mathrm{b}}$, $\gamma_{3\mathrm{b}}$ are the one- and three-body loss rate parameters and n_{BEC} and n_{th} are the local densities of the BEC and thermal atoms in the dimple. By fitting to transients in the measured parameters we estimate a steady-state gain of $2.4(5) \times 10^5\,\mathrm{atoms\,s^{-1}}$ into the BEC (Chen et al., 2022). A substantial fraction of this gain could conceivably be translated into an out coupled flux forming a CW atom laser. We also find that losses in the BEC at steady state are dominated by three-body recombinations with thermal atoms, due to the gas density exceeding $5 \times 10^{14}\,\mathrm{atoms\,cm^{-3}}$.

4. Next steps

The demonstration of CW Bose Einstein condensation (Chen et al., 2022) provides a long-awaited missing piece needed for the matter wave analogue of a CW laser: CW gain. However, much remains to be done to make this proof of principle demonstration robust for applications. In this section, we briefly outline several potential future experimental directions with prospects for achieving significant improvements.

The condensate fraction in our dimple trap is around 1%, a very small proportion considering the highly pure BECs typically used in experiments and a significant limitation in terms of coherence. The condensate purity is mainly limited by the high atomic temperature of $\sim 1.08(3)\,\mu$K in the dimple trap. As a result, we find that the density needed to reach degeneracy is so high that inelastic collisions result in high loss rates even for very small BECs (Chen et al., 2022). While the absence of an out coupling mechanism means that density will always rise until the three-body loss eventually balances gain, a much lower temperature of atoms in the dimple trap will produce much larger condensates with higher condensate purity. The reason for the relatively high dimple trap atom temperature is partly from using

a single laser beam to laser cool multiple sections of our steady state system, the transport guide, the crossover region and the reservoir, limiting us to a single global optimization. Furthermore, the ac-Stark shift variation across this potential landscape creates significant (>100 kHz) effective broadening. A significant improvement could be obtained by using a magic wavelength to create this potential landscape, particularly the reservoir and dimple traps (Ido et al., 2000). One might also be able to address this by painting a spatially optimized laser cooling profile using a galvanometer or similar device. However, even using optimized pulsed cooling sequences in a magic trap phase-space densities achievable using the $^1S_0 - {}^3P_1$ 7.5 kHz linewidth red $^1S_0 - {}^3P_1$ cooling transition of strontium have not exceeded 0.1 (Ido et al., 2000; Katori et al., 2001).

Cooling making use of the metastable clock states offers a promising alternative. For high phase-space density atoms in a dipole trap the ground state can be used as a dark state while selectively populating the metastable states with hot atoms. Here, the selectivity of the clock transition can be used to select atoms of high kinetic energy (using their Doppler shift). Furthermore, the selectivity of the clock line combined with the ac-Stark shift of the trap offers precise spatial selectivity over where in the trap the atoms may be excited to the metastable state. Since relatively few atoms are populated in the metastable states at any one time inelastic collisions can remain small. Clock and quenching transitions for $^3P_0$ which could be used to cool and return atoms to the ground state are illustrated in Fig. 18(c). Recently, laser cooling using such a clock transition (Fig. 18(c)) in ytterbium demonstrated quenched clock-line cooling to sub-recoil temperatures (Zhang et al., 2022). Similarly, sub-recoil temperatures have been achieved by adapting the SOLD technique (Chen et al., 2019a) to the $^3P_0 \rightarrow {}^3D_1$ transition of ytterbium (Chen et al., 2023). Using these cooling techniques could allow one to reach much lower temperatures and higher phase-space densities in the reservoir and dimple. Furthermore, it would allow protecting both the reservoir and dimple regions with a "transparency" beam while eliminating the small heating annulus described in section 3.4. Combined, these approaches could lower the temperature and thereby dramatically improve the condensate size and purity and hence the coherence of this system.

Cooling and trapping atoms in the metastable clock states provides yet another opportunity for simplifying our system. Since cooling lasers operating on the metastable states produce essentially no scattering for atoms in the ground state one can cool atoms in close proximity to a degenerate gas without any special protection. MOTs can be produced using atoms in the

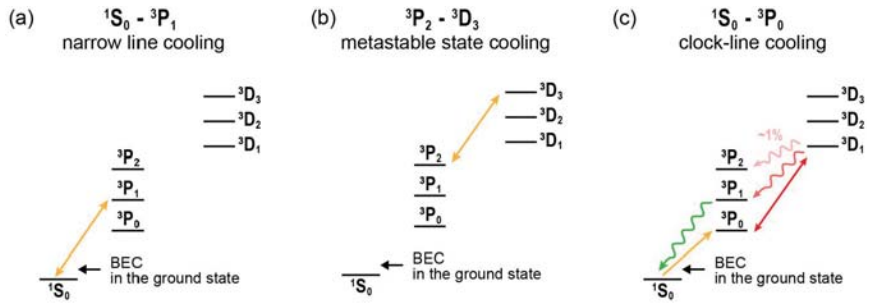

Figure 18 Comparison of different cooling schemes. (a) In our CW BEC work we relied on cooling using the 7.5 kHz linewidth $^1S_0 - {}^3P_1$ transition. (b) Cooling using the 57 kHz linewidth 2923 nm $^3P_2 - {}^3D_3$ cycling transition offers the possibility to produce a metastable MOT able to capture and cool atoms without interacting with a ground state BEC. (c) Quenched clock line cooling using the $^1S_0 - {}^3P_0$ clock transition. The selectivity of the $^1S_0 - {}^3P_0$ clock transition can be used to selectively populate $^3P_0$ with hot atoms. This allows the hot atoms to scatter photons on the $^3P_0 - {}^3D_1$ transition returning them to the ground state via $^3P_1$. Leaving cold atoms in the ground state undisturbed while executing a dark state cooling cycle should allow laser cooling to much higher phase-space densities. A similar configuration can be implemented using the $^3P_2$ state.

metastable states which have already been demonstrated in strontium (Hobson et al., 2020; Akatsuka et al., 2021), calcium (Grünert and Hemmerich, 2002), magnesium (Riedmann et al., 2012) and europium (Miyazawa et al., 2021). In the case of the europium work even the Zeeman slower used cooling transitions from the metastable state. These MOTs operate at low density allowing one to neglect any inelastic collisions between atoms in the metastable states.

In our experiment, we must use baffles and distance to separate the $^1S_0 - {}^1P_1$ blue and $^1S_0 - {}^3P_1$ red MOT laser cooling stages since both processes address ground state atoms. Furthermore, we separate the red MOT from the reservoir using distance and dark spots and we separate the reservoir and scattered red light from the degenerate gas using a "transparency" protection beam. While these approaches were effective it leads to a large, complex machine, which requires significant engineering effort.

Using a metastable MOT has the potential to dramatically simplify a machine such as ours (Katori et al., 2001; Derevianko, 2001; Grünert and Hemmerich, 2002; Akatsuka et al., 2021; Riedmann et al., 2012; Hobson et al., 2020; Miyazawa et al., 2021). For example, one could capture our Zeeman slowed atomic beam with a 3D blue MOT spatially overlapped with a 2D metastable MOT and a coaxial dipole guide. Using the 57 kHz

linewidth 2923 nm $^3P_2 - ^3D_3$ cycling transition (Akatsuka et al., 2021) shown in Fig. 18 (b), one could directly load a guided high phase-space density beam similar to ours (Chen et al., 2019b). With baffling between this beam source and a reservoir or evaporation region a single chamber could provide a complete platform for a CW BEC and atom laser.

Evaporation from a collisionally dense continuous guided beam within a protected guide offers a completely different approach to the architecture we have demonstrated (Lahaye et al., 2005; Power et al., 2012). We briefly reviewed some of the previous work on this type of architecture in section 2.1. Evaporatively cooling a guided beam to degeneracy would naturally produce an output beam, making the out coupling challenge trivial. A CW atom laser produced in this way may be more analogous to an amplified spontaneous emission (ASE) optical laser source than to a traditional laser. As a result, there are a number of interesting questions about the phase coherence of a CW atom laser produced in this manner. Improvements in coherence may be achieved by seeding this atom laser beam with the output from a CW BEC in much the same way we seed an amplifier.

Our experiment was also designed to explore these guided beam evaporation architectures. If one loaded our existing guided beam (Chen et al., 2019b) using ^{86}Sr (which our machine can do) one would increase the flux by around a factor of 20 compared to ^{84}Sr due to its higher abundance. Equally importantly, the elastic scattering length of ^{86}Sr is also higher by a factor of 6.7 times. Together this should place even the current guided beam in the collisionally dense regime where efficient evaporation is possible. While even this simple change may be sufficient to evaporate to degeneracy, when compared with our Gaussian dipole guide beam a Bessel beam (Brzobohatý et al., 2008; Schmid et al., 2006; Klostermann et al., 2022; Bennetts, 2019) offers a much improved guide geometry for two reasons. Firstly, a Bessel beam is non-diffracting meaning that it preserves its dimensions and shape as it propagates. This means that the tight waist of the central lobe of a Bessel beam may be maintained over many times the Rayleigh range of a similarly focused Gaussian shaped beam. As a result, high radial trapping frequencies and tight confinements can be maintained for much longer propagation distances compared with a Gaussian beam, ideal for evaporation. Secondly, unlike in a Gaussian beam where the reduction in trap depth is directly related to the divergence of the beam, the non-diffracting nature of a Bessel beam means that it preserves trap geometry as its depth tapers. This means that there is no corresponding reduction

in atomic beam density allowing Bessel beam guides to maintain the high collision rates needed for efficient evaporation.

Any guided beam evaporation architecture would inherently require protecting the length of the guide using an approach such as our transparency beam. While this is relatively easy it would also eliminate the transverse cooling of our guided beam that we rely on (Chen et al., 2019b). Once again, quenched clock line cooling may offer a solution. In ytterbium, fast ($\tau_{\text{cooling}} \sim 13$ ms), sub-recoil cooling has been demonstrated (Zhang et al., 2022), which would operate on a guided beam that is transparency protected. Using these approaches we believe an evaporatively cooled guided beam atom laser with high purity and high flux may be well within reach.

To study CW degenerate systems, continuous, non-destructive measurement techniques are needed. One such technique, Faraday imaging (Yamamoto et al., 2017), offers a straightforward solution with the sensitivity to image a system like ours. This may offer a window to study this open driven-dissipative quantum system (Chen et al., 2022). Open driven-dissipative systems such as this one are thought to show rich non-equilibrium many-body physics, such as purity oscillations (Haine et al., 2002), behaviors described by new critical exponents (Sieberer et al., 2013) and unusual quantum phases, especially in lower dimensions (He et al., 2017).

Finally, making a useful CW atom laser requires out coupling a matter-wave beam from a CW condensate. In our system a continuous matter-wave resonates, trapped deeply within our dimple trap. One approach to out couple from a BEC deep within a dimple trap might be to coherently transfer BEC atoms to an untrapped or weakly trapped metastable state. This could be done by appropriately choosing the dipole trap wavelength of the reservoir and dimple traps for example by choosing a wavelength close to a $^3P_0$ tune-out wavelength. A 3-photon Raman transition could then be used to coherently transfer atoms from the $^1S_0$ state to the $^3P_0$ clock state (Barker et al., 2016). When this is combined with the three photon momentum kick from the Raman transfer an atomic beam could be out coupled into free space.

5. Applications

Our CW BEC is a proof of principle demonstration showing that continuous matter-wave devices are now within reach. Nevertheless, much

work remains to be able to out couple an atom laser as well as to improve the flux, purity and coherence of CW atom lasers. For continuous operation many applications would require much higher fluxes in order to maintain the signal to noise ratios relied upon in pulsed operation. Here we will briefly visit some of the potential applications of CW atom lasers and the sources we developed to drive them.

Continuous operation offers advantages for sensing as it eliminates dead-time and can deliver higher bandwidths than pulsed operation (Essen and Parry, 1955; Keith et al., 1991; Kwolek et al., 2020; Savoie et al., 2018). At the same time, using the high phase-space density and unique coherence properties of Bose-Einstein condensates can improve sensitivity (Hardman et al., 2014; Müntinga et al., 2013; Cronin et al., 2009; Bongs et al., 2019; Lachmann et al., 2021; Aguilera et al., 2014; Hartwig et al., 2015). Combining these advantages, a CW atom laser beam out coupled from a CW condensate could be ideal for many quantum sensing applications (Ketterle, 2002; Robins et al., 2013; Spreeuw et al., 1995; Holland et al., 1996).

For these reasons continuous atom interferometers based on CW atom lasers may offer advantages for gravimetry (Peters et al., 1999; Stray et al., 2022), inertial sensors (Canuel et al., 2006; Stockton et al., 2011; Nelson et al., 2020) and magnetometry (Hardman et al., 2016) as well as more extreme interferometry applications like gravitational-wave detection (Yu and Tinto, 2011; Graham et al., 2013; Abe et al., 2021; Canuel et al., 2018; Badurina et al., 2020) and tests of Einstein's equivalence principle (Aguilera et al., 2014; Hartwig et al., 2015). For similar reasons atomic clocks would benefit from continuous operation and therefore from continuous sources although the requirement for the coherence of an atom laser is less clear. Continuous clocks could benefit applications ranging from dark-matter and dark-energy searches (Wcisłlo et al., 2018; Safronova et al., 2018; Safronova, 2019) to explorations in geodesy (Lisdat et al., 2016; Grotti et al., 2018; Takamoto et al., 2020).

More speculatively, the analogies between optical lasers and atom lasers are extensive. Our CW BEC has demonstrated a continuous source of matter-wave gain making continuous active devices that can maintain coherence possible. It is hard to imagine electronics or photonics achieving the impact they have today without access to gain. In the same way access to a continuous source of coherent gain may provide a key to unlock the potential of atomtronics (Amico et al., 2022). We hope that with continued work to make robust sources of continuous gain new atomtronic devices might be realized.

In the near term there are many applications that do not necessarily require the brightness and coherence of a CW atom laser but that do require continuous high flux and high phase-space density beams. Some continuous atom interferometers have been demonstrated using thermal beams (Kwolek and Black, 2022; Xue et al., 2015; Gustavson et al., 1997; Durfee et al., 2006; Riehle et al., 1992) and a number of proposals and realizations of continuous optical clocks are based on the interrogation of continuous beams (Katori, 2021; Olson et al., 2019). The high bandwidths of continuous clocks like beam clocks offer further advantages in terms of reduced requirements on the reference cavity performance (Katori, 2021). Within our group we have focused on using the beam sources developed as part of this work to drive active optical clocks and dead time free passive optical lattice clocks.

Dead-time free quantum sensors could benefit from using continuous high flux sources. A high phase-space density beam like the one used to replenish our CW BEC can also be used to sequentially load a series of optical lattice clocks to allow dead time free clock operation. Dead time free clocks can essentially eliminate Dick noise and enable very high precision with averaging times that are much shorter than were previously possible (Schioppo et al., 2017; Oelker et al., 2019; Katori, 2021). Dead time free measurement and control of the probe laser improves the Allan deviation as $1/\tau$ for an averaging time τ until the quantum projection noise limit is reached rather than the traditional $1/\sqrt{\tau}$ scaling (Schioppo et al., 2017). Furthermore, simultaneous operation of multiple clocks can be used to extend laser coherence and interrogation time to also reduce the quantum projection noise limit (Schioppo et al., 2017). Similar advantages might be possible by using our continuous sources to simultaneously operate multiple atom interferometers (Kwolek and Black, 2022). On a practical level the signal to noise or flux is also critical to sensor performance. The fluxes we obtain loading our steady state red MOT of 5×10^8 ^{88}Sr atoms/s (Bennetts et al., 2017) and from our high phase space density beam of 3×10^7 ^{88}Sr atoms/s (Chen et al., 2019b) are comparable with the brightest sources available. While a pulsed system which integrates this flux and then makes a low duty cycle measurement can obtain much higher instantaneous signal to noise ratios, there is simply a trade off between signal to noise and bandwidth. A continuous source offers the advantage of leaving the choice between bandwidth and signal to noise to the user. For our CW BEC an out coupler is still required for most applications but if something close to the estimated gain of 2.4×10^5 ^{84}Sr atoms/s could be realized in an out

coupled beam this would already be competitive with most pulsed BEC machines. As discussed in the previous section there are many opportunities for improvement.

Continuous active optical clocks (Chen, 2009; Meiser et al., 2009) offer an exciting alternative to conventional optical lattice clocks (Takamoto et al., 2005; Ludlow et al., 2015). An active optical clock consists of an atomic sample making use of superradiance to continuously emit light directly on a clock transition within a "bad cavity", that is, a cavity with a linewidth much broader than the gain linewidth. By beating the active optical clock output with a narrow linewidth laser an error signal can be obtained to lock this narrow linewidth laser to the superradiant clock output. Provided the narrow linewidth laser has a linewidth smaller than the locking bandwidth the coherence of the superradiant clock can be transferred. Since the output of the active clock is continuous, feedback bandwidths into the kilohertz range are possible (depending on the superradiant output power and required signal to noise ratio) (Bennetts et al., 2021). This offers great advantages over the hertz or sub-hertz regime that current state-of-the-art optical lattice clocks are limited to. Finally, by operating deep within the bad cavity regime this approach allows the suppression of cavity noise in an active optical clock by around six orders of magnitude (Cline et al., 2022; Norcia, 2017; Cline, 2021). Initial experiments designed to produce continuous active optical clocks are aiming for stability better than 7×10^{-18} when integrated over 1 s (Cline, 2021) although this could be further improved with higher atomic flux. By contrast, conventional optical lattice clocks require extremely narrow (mHz) linewidth reference cavities in order to stabilize their interrogation lasers. These high coherence times are needed to cope with the extremely low feedback bandwidths available from atomic sample interrogation. The need for such stable reference cavities creates particular challenges for fielding optical clocks in real world environments, which might be mitigated by active optical clocks. For sensing applications the continuous output and corresponding high bandwidths from an active optical clock creates new opportunities for high bandwidth precision sensing of gravity, magnetic fields, acceleration and more.

Although pulsed superradiant lasers on the strontium mHz clock transition have been demonstrated (Norcia et al., 2016; Norcia, 2017), a clock requires a continuous output (Cline et al., 2022; Bennetts et al., 2021; Cline, 2021). The challenge to reaching threshold in a continuous superradiant clock using a millihertz clock transition is coupling a high flux ($>1 \times 10^5$ atoms/s) of microkelvin cold excited state atoms into a high

(4×10^4) finesse optical cavity where they can be maintained for a long (1 s) period of time (Cline et al., 2022; Bennetts et al., 2021). While thermal beams have been proposed to pump continuous superradiant clocks on kilohertz linewidth transitions (Liu et al., 2020) something similar to the high flux continuous source needed to pump the continuous atom laser is essential to pump an active optical clock using a millihertz clock transition. The use of higher brightness atom laser sources to pump a superradiant laser offers further potential to reach the superradiant threshold with lower fluxes albeit with less output power and a resulting lower clock feedback bandwidth.

One final area of promise is the potential of continuous sources to aid in producing very large scale qubit factories for neutral atom quantum computers. Recent advances in quantum computing using neutral atoms have been immense (Kaufman and Ni, 2021), characterized by the qubit number, flexibility in connectivity (Bluvstein et al., 2022; Graham et al., 2022) and fast-improving gate fidelities (Levine et al., 2019; Madjarov et al., 2020). Although there are promising platforms for large arrays of atomic qubits (Park et al., 2022; Huft et al., 2022), traditional single-step trap loading remains susceptible to stochastic loading (Schlosser et al., 2001), which inevitably leads to defects in the array and requires additional sorting steps to initialize a large system. In recent years, improvements have been made by implementing more advanced cooling methods (Grünzweig et al., 2010; Lester et al., 2015; Brown et al., 2019) or by utilizing alkaline-earth metal species (Jenkins et al., 2022). While these advancements have led to a significant increase in loading probabilities, as the array size increases, the number of sorting steps required to achieve a defect-free system also increases.

The methods described in this review aimed at creating continuous-wave degenerate gases can also be used to create quantum degenerate samples on sub-second timescales (Stellmer et al., 2013; Hu et al., 2017; Vendeiro et al., 2022). These developments could make schemes competitive that prepare near defect-free arrays with uniform site occupation from low-entropy Mott-insulator states (Bloch et al., 2012; Greiner et al., 2002; Knight et al., 2003; Peil et al., 2003; Greif et al., 2016; Bloch and Greiner, 2022). Commercial microscope objectives are already capable of resolving individual lattice sites for site manipulation and readout. When combined with a reconfigurable tweezer for removing defects and atom transport, this offers a promising path towards creating next-generation large-array qubit registers. By utilizing a high repetition rate degenerate source or a continuous degenerate beam, a CW atom laser, it may be possible to load near

defect-free arrays at a rate of mega-qubits per second (Pause et al., 2023). Using a conventional tweezer approach is much more difficult to scale since the power requirements and sorting time needed to produce defect free arrays both scale linearly with site number and the traps need to be much deeper to load hot atoms from a MOT. Loading arrays from degenerate gases, combined with the long lifetimes achievable in a cryogenic environment (Schymik et al., 2021), could enable the creation of previously unattainable long-lived, very large-scale atomic qubit arrays.

6. In summary

Our demonstration of CW Bose-Einstein condensation provides a new, hitherto missing piece of atom optics, enabling the construction of continuous coherent-matter-wave devices. In this review we have described some of the many ideas and techniques developed over the past three decades upon which this work was built and without which this outcome could not have been possible. While CW Bose-Einstein condensation has now been shown, much work remains in order to turn this proof of principle experiment into a robust tool that can be used in real world applications. Some next steps are proposed that might significantly improve the purity and coherence of the condensate, simplify the machine and enable out coupling a useful CW atom laser beam. We also outlined some of the near and medium term applications where this work may have significant impact. With continued development we anticipate continuous degenerate ultracold atomic sources will become a powerful tool for future quantum technology applications.

Acknowledgments

We wish to recognize the immense and critical contribution that has been made to this work by Benjamin Pasquiou. From project conception to our final achievement of a CW BEC, Benjamin Pasquiou played an essential role. We also thank Benjamin Pasquiou for his careful reading of this manuscript and his insightful comments. We thank Rodrigo González Escudero and Jiří Minář for their important roles in achieving CW BEC and interpreting the results. We would also like to thank Baxter Weihe, Sheng Zhou, Sumit Sarkar and Junyu He for their support during the writing of this manuscript and for their helpful comments. We would like to thank Hélène Perrin for carefully reading the manuscript and providing insightful comments and helpful feedback. We thank the NWO for funding through Vici grant No. 680-47-619 and the European Research Council (ERC) for funding under Project No. 615117 QuantStro. This project has received funding from the European Union's Horizon 2020 research and innovation programme under grant

agreement No 820404 (iqClock project). S.B. and F.S. have received funding from the European Union's Horizon Europe research and innovation programme under grant agreement No 101080166 (AQuRA project) and were supported by the Dutch Ministry of Economic Affairs and Climate Policy (EZK), as part of the Quantum Delta NL programme. C.-C.C. thanks support from the MOE Technologies Incubation Scholarship from the Taiwan Ministry of Education.

References

Abe, M., Adamson, P., Borcean, M., Bortoletto, D., Bridges, K., Carman, S.P., Chattopadhyay, S., Coleman, J., Curfman, N.M., DeRose, K., Deshpande, T., Dimopoulos, S., Foot, C.J., Frisch, J.C., Garber, B.E., Geer, S., Gibson, V., Glick, J., Graham, P.W., Hahn, S.R., Harnik, R., Hawkins, L., Hindley, S., Hogan, J.M., Jiang, Y., Kasevich, M.A., Kellett, R.J., Kiburg, M., Kovachy, T., Lykken, J.D., March-Russell, J., Mitchell, J., Murphy, M., Nantel, M., Nobrega, L.E., Plunkett, R.K., Rajendran, S., Rudolph, J., Sachdeva, N., Safdari, M., Santucci, J.K., Schwartzman, A.G., Shipsey, I., Swan, H., Valerio, L.R., Vasonis, A., Wang, Y., Wilkason, T., 2021. Matter-wave atomic gradiometer interferometric sensor (MAGIS-100). Quantum Science and Technology 6 (4), 044003. https://doi.org/10.1088/2058-9565/abf719.

Aghajani-Talesh, A., Falkenau, M., Griesmaier, A., Pfau, T., 2009. A proposal for continuous loading of an optical dipole trap with magnetically guided ultra-cold atoms. Journal of Physics. B, Atomic, Molecular and Optical Physics 42 (24), 245302. https://doi.org/10.1088/0953-4075/42/24/245302.

Aguilera, D.N., Ahlers, H., Battelier, B., Bawamia, A., Bertoldi, A., Bondarescu, R., Bongs, K., Bouyer, P., Braxmaier, C., Cacciapuoti, L., Chaloner, C., Chwalla, M., Ertmer, W., Franz, M., Gaaloul, N., Gehler, M., Gerardi, D., Gesa, L., Gürlebeck, N., Hartwig, J., Hauth, M., Hellmig, O., Herr, W., Herrmann, S., Heske, A., Hinton, A., Ireland, P., Jetzer, P., Johann, U., Krutzik, M., Kubelka, A., Lämmerzahl, C., Landragin, A., Lloro, I., Massonnet, D., Mateos, I., Milke, A., Nofrarias, M., Oswald, M., Peters, A., Posso-Trujillo, K., Rasel, E., Rocco, E., Roura, A., Rudolph, J., Schleich, W., Schubert, C., Schuldt, T., Seidel, S., Sengstock, K., Sopuerta, C.F., Sorrentino, F., Summers, D., Tino, G.M., Trenkel, C., Uzunoglu, N., von Klitzing, W., Walser, R., Wendrich, T., Wenzlawski, A., Weßels, P., Wicht, A., Wille, E., Williams, M., Windpassinger, P., Zahzam, N., 2014. STE-QUEST—test of the universality of free fall using cold atom interferometry. Classical and Quantum Gravity 31 (11), 115010. https://doi.org/10.1088/0264-9381/31/11/115010.

Akatsuka, T., Hashiguchi, K., Takahashi, T., Ohmae, N., Takamoto, M., Katori, H., 2021. Three-stage laser cooling of Sr atoms using the $5s5p^3P_2$ metastable state below Doppler temperatures. Physical Review A 103, 023331. https://doi.org/10.1103/PhysRevA.103.023331. https://link.aps.org/doi/10.1103/PhysRevA.103.023331.

Amico, L., Anderson, D., Boshier, M., Brantut, J.-P., Kwek, L.-C., Minguzzi, A., von Klitzing, W., 2022. Colloquium: atomtronic circuits: from many-body physics to quantum technologies. Reviews of Modern Physics 94, 041001. https://doi.org/10.1103/RevModPhys.94.041001. https://link.aps.org/doi/10.1103/RevModPhys.94.041001.

Anderson, B.P., Kasevich, M.A., 1998. Macroscopic quantum interference from atomic tunnel arrays. Science 282 (5394), 1686–1689. https://doi.org/10.1126/science.282.5394.1686. https://www.science.org/doi/abs/10.1126/science.282.5394.1686.

Anderson, D.Z., 2021. Matter waves, single-mode excitations of the matter-wave field, and the atomtronic transistor oscillator. Physical Review A 104, 033311. https://doi.org/10.1103/PhysRevA.104.033311. https://link.aps.org/doi/10.1103/PhysRevA.104.033311.

Anderson, M.H., Ensher, J.R., Matthews, M.R., Wieman, C.E., Cornell, E.A., 1995. Observation of Bose-Einstein Condensation in a dilute atomic vapor. Science 269 (5221), 198–201. https://doi.org/10.1126/science.269.5221.198. https://www.science.org/doi/abs/10.1126/science.269.5221.198.

Andrews, M.R., Townsend, C.G., Miesner, H.-J., Durfee, D.S., Kurn, D.M., Ketterle, W., 1997. Observation of interference between two Bose Condensates. Science 275 (5300), 637–641. https://doi.org/10.1126/science.275.5300.637. https://www.science.org/doi/abs/10.1126/science.275.5300.637.

Aspect, A., Arimondo, E., Kaiser, R., Vansteenkiste, N., Cohen-Tannoudji, C., 1988. Laser cooling below the one-photon recoil energy by velocity-selective coherent population trapping. Physical Review Letters 61, 826–829. https://doi.org/10.1103/PhysRevLett.61.826. https://link.aps.org/doi/10.1103/PhysRevLett.61.826.

Badurina, L., Bentine, E., Blas, D., Bongs, K., Bortoletto, D., Bowcock, T., Bridges, K., Bowden, W., Buchmueller, O., Burrage, C., Coleman, J., Elertas, G., Ellis, J., Foot, C., Gibson, V., Haehnelt, M., Harte, T., Hedges, S., Hobson, R., Holynski, M., Jones, T., Langlois, M., Lellouch, S., Lewicki, M., Maiolino, R., Majewski, P., Malik, S., March-Russell, J., McCabe, C., Newbold, D., Sauer, B., Schneider, U., Shipsey, I., Singh, Y., Uchida, M., Valenzuela, T., van der Grinten, M., Vaskonen, V., Vossebeld, J., Weatherill, D., Wilmut, I., 2020. Aion: an atom interferometer observatory and network. Journal of Cosmology and Astroparticle Physics 2020 (05), 011. https://doi.org/10.1088/1475-7516/2020/05/011.

Baker, T.J., Saadatmand, S.N., Berry, D.W., Wiseman, H.M., 2021. The Heisenberg limit for laser coherence. Nature Physics (ISSN 1745-2481) 17 (2), 179–183. https://doi.org/10.1038/s41567-020-01049-3.

Barker, D.S., Pisenti, N.C., Reschovsky, B.J., Campbell, G.K., 2016. Three-photon process for producing a degenerate gas of metastable alkaline-earth-metal atoms. Physical Review A 93, 053417. https://doi.org/10.1103/PhysRevA.93.053417. https://link.aps.org/doi/10.1103/PhysRevA.93.053417.

Bennetts, S., Bober, M., Zhou, S., Witkowski, M., Kazakov, G., Witkowski, M., Zawada, M., Schreck, F., 2021. iqClock Deliverable 5.3: design of a superradiant optical clock on the $^1S_0 - ^3P_0$ "mHz" transition. https://drive.google.com/file/d/1Vzt4esDCx_qStPYDA4zKtlhwA7pR6jQi/view?usp=sharing.

Bennetts, S., Chen, C.-C., Pasquiou, B., Schreck, F., 2017. Steady-state magneto-optical trap with 100-fold improved phase-space density. Physical Review Letters 119, 223202. https://doi.org/10.1103/PhysRevLett.119.223202. https://link.aps.org/doi/10.1103/PhysRevLett.119.223202.

Bennetts, S.P., 2019. 1000 times closer to a continuous atom laser: Steady-state strontium with unity phase-space density. PhD thesis. Institute of Physics, University of Amsterdam. http://www.strontiumbec.com/StrontiumLab/Theses/Shayne_Bennetts_PhD_thesis.pdf.

Bhongale, S., Holland, M., 2000. Loading a continuous-wave atom laser by optical pumping techniques. Physical Review A 62, 043604. https://doi.org/10.1103/PhysRevA.62.043604. https://link.aps.org/doi/10.1103/PhysRevA.62.043604.

Bloch, I., Greiner, M., 2022. The superfluid-to-Mott insulator transition and the birth of experimental quantum simulation. Nature Reviews Physics (ISSN 2522-5820) 4 (12), 739–740. https://doi.org/10.1038/s42254-022-00520-9.

Bloch, I., Hänsch, T.W., Esslinger, T., 1999. Atom laser with a CW output coupler. Physical Review Letters 82, 3008–3011. https://doi.org/10.1103/PhysRevLett.82.3008. https://link.aps.org/doi/10.1103/PhysRevLett.82.3008.

Bloch, I., Dalibard, J., Nascimbène, S., 2012. Quantum simulations with ultracold quantum gases. Nature Physics (ISSN 1745-2481) 8 (4), 267–276. https://doi.org/10.1038/nphys2259.

Bluvstein, D., Levine, H., Semeghini, G., Wang, T.T., Ebadi, S., Kalinowski, M., Keesling, A., Maskara, N., Pichler, H., Greiner, M., Vuletić, V., Lukin, M.D., 2022. A quantum processor based on coherent transport of entangled atom arrays. Nature (ISSN 1476-4687) 604 (7906), 451–456. https://doi.org/10.1038/s41586-022-04592-6.

Bolpasi, V., Efremidis, N.K., Morrissey, M.J., Condylis, P.C., Sahagun, D., Baker, M., von Klitzing, W., 2014. An ultra-bright atom laser. New Journal of Physics 16 (3), 033036. https://doi.org/10.1088/1367-2630/16/3/033036.

Bongs, K., Holynski, M., Vovrosh, J., Bouyer, P., Condon, G., Rasel, E., Schubert, C., Schleich, W.P., Roura, A., 2019. Taking atom interferometric quantum sensors from the laboratory to real-world applications. Nature Reviews Physics (ISSN 2522-5820) 1 (12), 731–739. https://doi.org/10.1038/s42254-019-0117-4.

Bradley, C.C., Sackett, C.A., Tollett, J.J., Hulet, R.G., 1995. Evidence of Bose-Einstein Condensation in an atomic gas with attractive interactions. Physical Review Letters 75, 1687–1690. https://doi.org/10.1103/PhysRevLett.75.1687. https://link.aps.org/doi/10.1103/PhysRevLett.75.1687.

Brown, M.O., Thiele, T., Kiehl, C., Hsu, T.-W., Regal, C.A., 2019. Gray-molasses optical-tweezer loading: controlling collisions for scaling atom-array assembly. Physical Review X 9, 011057. https://doi.org/10.1103/PhysRevX.9.011057. https://link.aps.org/doi/10.1103/PhysRevX.9.011057.

Brzobohatý, O., Čižmár, T., Zemánek, P., 2008. High quality quasi-Bessel beam generated by round-tip axicon. Optics Express 16 (17), 12688–12700. https://doi.org/10.1364/OE.16.012688. https://opg.optica.org/oe/abstract.cfm?URI=oe-16-17-12688.

Caliga, S.C., Straatsma, C.J.E., Zozulya, A.A., Anderson, D.Z., 2016. Principles of an atomtronic transistor. New Journal of Physics 18 (1), 015012. https://doi.org/10.1088/1367-2630/18/1/015012.

Caliga, S.C., Straatsma, C.J.E., Anderson, D.Z., 2017. Experimental demonstration of an atomtronic battery. New Journal of Physics 19 (1), 013036. https://doi.org/10.1088/1367-2630/aa56d8.

Canuel, B., Leduc, F., Holleville, D., Gauguet, A., Fils, J., Virdis, A., Clairon, A., Dimarcq, N., Bordé, C.J., Landragin, A., Bouyer, P., 2006. Six-axis inertial sensor using cold-atom interferometry. Physical Review Letters 97, 010402. https://doi.org/10.1103/PhysRevLett.97.010402. https://link.aps.org/doi/10.1103/PhysRevLett.97.010402.

Canuel, B., Bertoldi, A., Amand, L., Pozzo di Borgo, E., Chantrait, T., Danquigny, C., Dovale Álvarez, M., Fang, B., Freise, A., Geiger, R., Gillot, J., Henry, S., Hinderer, J., Holleville, D., Junca, J., Lefèvre, G., Merzougui, M., Mielec, N., Monfret, T., Pelisson, S., Prevedelli, M., Reynaud, S., Riou, I., Rogister, Y., Rosat, S., Cormier, E., Landragin, A., Chaibi, W., Gaffet, S., Bouyer, P., 2018. Exploring gravity with the MIGA large scale atom interferometer. Scientific Reports (ISSN 2045-2322) 8 (1), 14064. https://doi.org/10.1038/s41598-018-32165-z.

Castin, Y., Dum, R., 1996. Bose-Einstein Condensates in time dependent traps. Physical Review Letters 77, 5315–5319. https://doi.org/10.1103/PhysRevLett.77.5315. https://link.aps.org/doi/10.1103/PhysRevLett.77.5315.

Castin, Y., Cirac, J.I., Lewenstein, M., 1998. Reabsorption of light by trapped atoms. Physical Review Letters 80, 5305–5308. https://doi.org/10.1103/PhysRevLett.80.5305. https://link.aps.org/doi/10.1103/PhysRevLett.80.5305.

Chen, C.-C., 2019. An atomic marble run to unity phase-space density. PhD thesis. Institute of Physics, University of Amsterdam. http://www.strontiumbec.com/StrontiumLab/Theses/Chun-Chia_Chen_PhD_thesis.pdf.

Chen, C.-C., Siegel, J., Hunt, B.D., Grogan, T., Hassan, Y.S., Beloy, K., Gibble, K., Brown, R.C., Ludlow, A.D., 2023. Clock-line mediated Sisyphus Cooling. In preparation.

Chen, C.-C., Bennetts, S., González Escudero, R., Schreck, F., Pasquiou, B., 2019a. Sisyphus optical lattice decelerator. Physical Review A 100, 023401.

https://doi.org/10.1103/PhysRevA.100.023401. https://link.aps.org/doi/10.1103/PhysRevA.100.023401.

Chen, C.-C., Bennetts, S., Escudero, R.G., Pasquiou, B., Schreck, F., 2019b. Continuous guided strontium beam with high phase-space density. Physical Review Applied 12, 044014. https://doi.org/10.1103/PhysRevApplied.12.044014. https://link.aps.org/doi/10.1103/PhysRevApplied.12.044014.

Chen, C.-C., González Escudero, R., Minář, J., Pasquiou, B., Bennetts, S., Schreck, F., 2022. Continuous Bose–Einstein condensation. Nature (ISSN 1476-4687) 606 (7915), 683–687. https://doi.org/10.1038/s41586-022-04731-z.

Chen, H., Riis, E., 2000. Cold atomic beam from a rubidium funnel. Applied Physics B (ISSN 1432-0649) 70 (5), 665–670. https://doi.org/10.1007/s003400050878.

Chen, J., 2009. Active optical clock. Chinese Science Bulletin (ISSN 1861-9541) 54 (3), 348–352. https://doi.org/10.1007/s11434-009-0073-y.

Chikkatur, A.P., Shin, Y., Leanhardt, A.E., Kielpinski, D., Tsikata, E., Gustavson, T.L., Pritchard, D.E., Ketterle, W., 2002. A continuous source of Bose-Einstein Condensed atoms. Science 296 (5576), 2193–2195. https://doi.org/10.1126/science.296.5576.2193. https://www.science.org/doi/abs/10.1126/science.296.5576.2193.

Cirac, J.I., Lewenstein, M., 1996. Pumping atoms into a Bose-Einstein condensate in the boson-accumulation regime. Physical Review A 53, 2466–2476. https://doi.org/10.1103/PhysRevA.53.2466. https://link.aps.org/doi/10.1103/PhysRevA.53.2466.

Cirac, J.I., Lewenstein, M., Zoller, P., 1996. Collective laser cooling of trapped atoms. Europhysics Letters 35 (9), 647. https://doi.org/10.1209/epl/i1996-00165-4.

Cline, J.R.K., 2021. Continuous Collective Strong Coupling Between Atoms and a High Finesse Cavity on a Forbidden Optical Transition. PhD thesis. University of Colorado. https://scholar.colorado.edu/concern/graduate_thesis_or_dissertations/8623hz92d.

Cline, J.R.K., Schäfer, V.M., Niu, Z., Young, D.J., Yoon, T.H., Thompson, J.K., 2022. Continuous collective strong coupling between atoms and a high finesse optical cavity. arXiv:2211.00158. https://doi.org/10.48550/arXiv.2211.00158.

Colzi, G., Durastante, G., Fava, E., Serafini, S., Lamporesi, G., Ferrari, G., 2016. Sub-Doppler cooling of sodium atoms in gray molasses. Physical Review A 93, 023421. https://doi.org/10.1103/PhysRevA.93.023421. https://link.aps.org/doi/10.1103/PhysRevA.93.023421.

Couvert, A., Kawalec, T., Reinaudi, G., Guéry-Odelin, D., 2008. Optimal transport of ultracold atoms in the non-adiabatic regime. Europhysics Letters 83 (1), 13001. https://doi.org/10.1209/0295-5075/83/13001.

Cren, P., Roos, C.F., Aclan, A., Dalibard, J., Guéry-Odelin, D., 2002. Loading of a cold atomic beam into a magnetic guide. The European Physical Journal. D, Atomic, Molecular, Optical and Plasma Physics (ISSN 1434-6079) 20 (1), 107–116. https://doi.org/10.1140/epjd/e2002-00106-3.

Cronin, A.D., Schmiedmayer, J., Pritchard, D.E., 2009. Optics and interferometry with atoms and molecules. Reviews of Modern Physics 81, 1051–1129. https://doi.org/10.1103/RevModPhys.81.1051. https://link.aps.org/doi/10.1103/RevModPhys.81.1051.

Dalibard, J., Cohen-Tannoudji, C., 1989. Laser cooling below the Doppler limit by polarization gradients: simple theoretical models. Journal of the Optical Society of America. B, Optical Physics 6 (11), 2023–2045. https://doi.org/10.1364/JOSAB.6.002023. https://opg.optica.org/josab/abstract.cfm?URI=josab-6-11-2023.

Davis, K.B., Mewes, M.O., Andrews, M.R., van Druten, N.J., Durfee, D.S., Kurn, D.M., Ketterle, W., 1995. Bose-Einstein Condensation in a gas of sodium atoms. Physical Review Letters 75, 3969–3973. https://doi.org/10.1103/PhysRevLett.75.3969. https://link.aps.org/doi/10.1103/PhysRevLett.75.3969.

Debs, J.E., Döring, D., Altin, P.A., Figl, C., Dugué, J., Jeppesen, M., Schultz, J.T., Robins, N.P., Close, J.D., 2010. Experimental comparison of Raman and rf outcouplers for high-flux atom lasers. Physical Review A 81, 013618. https://doi.org/10.1103/PhysRevA.81.013618. https://link.aps.org/doi/10.1103/PhysRevA.81.013618.

Deng, L., Hagley, E.W., Wen, J., Trippenbach, M., Band, Y., Julienne, P.S., Simsarian, J.E., Helmerson, K., Rolston, S.L., Phillips, W.D., 1999. Four-wave mixing with matter waves. Nature (ISSN 1476-4687) 398 (6724), 218–220. https://doi.org/10.1038/18395.

DePue, M.T., McCormick, C., Winoto, S.L., Oliver, S., Weiss, D.S., 1999. Unity occupation of sites in a 3D optical lattice. Physical Review Letters 82, 2262–2265. https://doi.org/10.1103/PhysRevLett.82.2262. https://link.aps.org/doi/10.1103/PhysRevLett.82.2262.

Derevianko, A., 2001. Feasibility of cooling and trapping metastable alkaline-earth atoms. Physical Review Letters 87, 023002. https://doi.org/10.1103/PhysRevLett.87.023002. https://link.aps.org/doi/10.1103/PhysRevLett.87.023002.

Dick, G.J., 1987. Local oscillator induced instabilities in trapped ion frequency standards. In: Proceedings of the 19th Annual Precise Time and Time Interval Systems and Applications. https://apps.dtic.mil/dtic/tr/fulltext/u2/a502386.pdf.

Dieckmann, K., Spreeuw, R.J.C., Weidemüller, M., Walraven, J.T.M., 1998. Two-dimensional magneto-optical trap as a source of slow atoms. Physical Review A 58, 3891–3895. https://doi.org/10.1103/PhysRevA.58.3891. https://link.aps.org/doi/10.1103/PhysRevA.58.3891.

Dörscher, S., Thobe, A., Hundt, B., Kochanke, A., Targat, R.L., Windpassinger, P., Becker, C., Sengstock, K., 2013. Creation of quantum-degenerate gases of ytterbium in a compact 2D-/3D-magneto-optical trap setup. Review of Scientific Instruments 84 (4), 043109. https://doi.org/10.1063/1.4802682.

Dum, R., Marte, P., Pellizzari, T., Zoller, P., 1994. Laser cooling to a single quantum state in a trap. Physical Review Letters 73, 2829–2832. https://doi.org/10.1103/PhysRevLett.73.2829. https://link.aps.org/doi/10.1103/PhysRevLett.73.2829.

Durfee, D.S., Shaham, Y.K., Kasevich, M.A., 2006. Long-term stability of an area-reversible atom-interferometer Sagnac gyroscope. Physical Review Letters 97, 240801. https://doi.org/10.1103/PhysRevLett.97.240801. https://link.aps.org/doi/10.1103/PhysRevLett.97.240801.

Essen, L., Parry, J.V.L., 1955. An atomic standard of frequency and time interval: a cæsium resonator. Nature (ISSN 1476-4687) 176 (4476), 280–282. https://doi.org/10.1038/176280a0.

Falkenau, M., Volchkov, V.V., Rührig, J., Griesmaier, A., Pfau, T., 2011. Continuous loading of a conservative potential trap from an atomic beam. Physical Review Letters 106, 163002. https://doi.org/10.1103/PhysRevLett.106.163002. https://link.aps.org/doi/10.1103/PhysRevLett.106.163002.

Falkenau, M., Volchkov, V.V., Rührig, J., Gorniaczyk, H., Griesmaier, A., 2012. Evaporation-limited loading of an atomic trap. Physical Review A 85, 023412. https://doi.org/10.1103/PhysRevA.85.023412. https://link.aps.org/doi/10.1103/PhysRevA.85.023412.

Frisch, A., Aikawa, K., Mark, M., Rietzler, A., Schindler, J., Zupanič, E., Grimm, R., Ferlaino, F., 2012. Narrow-line magneto-optical trap for erbium. Physical Review A 85, 051401. https://doi.org/10.1103/PhysRevA.85.051401. https://link.aps.org/doi/10.1103/PhysRevA.85.051401.

Gattobigio, G.L., Couvert, A., Jeppesen, M., Mathevet, R., Guéry-Odelin, D., 2009. Multimode-to-monomode guided-atom lasers: an entropic analysis. Physical Review A 80, 041605. https://doi.org/10.1103/PhysRevA.80.041605. https://link.aps.org/doi/10.1103/PhysRevA.80.041605.

Graham, P.W., Hogan, J.M., Kasevich, M.A., Rajendran, S., 2013. New method for gravitational wave detection with atomic sensors. Physical Review Letters 110, 171102. https://doi.org/10.1103/PhysRevLett.110.171102. https://link.aps.org/doi/10.1103/PhysRevLett.110.171102.

Graham, T.M., Song, Y., Scott, J., Poole, C., Phuttitarn, L., Jooya, K., Eichler, P., Jiang, X., Marra, A., Grinkemeyer, B., Kwon, M., Ebert, M., Cherek, J., Lichtman, M.T., Gillette, M., Gilbert, J., Bowman, D., Ballance, T., Campbell, C., Dahl, E.D., Crawford, O., Blunt, N.S., Rogers, B., Noel, T., Saffman, M., 2022. Multi-qubit entanglement and algorithms on a neutral-atom quantum computer. Nature (ISSN 1476-4687) 604 (7906), 457–462. https://doi.org/10.1038/s41586-022-04603-6.

Greif, D., Parsons, M.F., Mazurenko, A., Chiu, C.S., Blatt, S., Huber, F., Ji, G., Greiner, M., 2016. Site-resolved imaging of a fermionic Mott insulator. Science 351 (6276), 953–957. https://doi.org/10.1126/science.aad9041. https://www.science.org/doi/abs/10.1126/science.aad9041.

Greiner, M., Mandel, O., Esslinger, T., Hänsch, T.W., Bloch, I., 2002. Quantum phase transition from a superfluid to a Mott insulator in a gas of ultracold atoms. Nature (ISSN 1476-4687) 415 (6867), 39–44. https://doi.org/10.1038/415039a.

Grier, A.T., Ferrier-Barbut, I., Rem, B.S., Delehaye, M., Khaykovich, L., Chevy, F., Salomon, C., 2013. Λ-enhanced sub-Doppler cooling of lithium atoms in D_1 gray molasses. Physical Review A 87, 063411. https://doi.org/10.1103/PhysRevA.87.063411. https://link.aps.org/doi/10.1103/PhysRevA.87.063411.

Griesmaier, A., Aghajani-Talesh, A., Falkenau, M., Sebastian, J., Greiner, A., Pfau, T., 2009. A high flux of ultra-cold chromium atoms in a magnetic guide. Journal of Physics. B, Atomic, Molecular and Optical Physics 42 (14), 145306. https://doi.org/10.1088/0953-4075/42/14/145306.

Grotti, J., Koller, S., Vogt, S., Häfner, S., Sterr, U., Lisdat, C., Denker, H., Voigt, C., Timmen, L., Rolland, A., Baynes, F.N., Margolis, H.S., Zampaolo, M., Thoumany, P., Pizzocaro, M., Rauf, B., Bregolin, F., Tampellini, A., Barbieri, P., Zucco, M., Costanzo, G.A., Clivati, C., Levi, F., Calonico, D., 2018. Geodesy and metrology with a transportable optical clock. Nature Physics (ISSN 1745-2481) 14 (5), 437–441. https://doi.org/10.1038/s41567-017-0042-3.

Grünert, J., Hemmerich, A., 2002. Sub-Doppler magneto-optical trap for calcium. Physical Review A 65, 041401. https://doi.org/10.1103/PhysRevA.65.041401. https://link.aps.org/doi/10.1103/PhysRevA.65.041401.

Grünzweig, T., Hilliard, A., McGovern, M., Andersen, M.F., 2010. Near-deterministic preparation of a single atom in an optical microtrap. Nature Physics (ISSN 1745-2481) 6 (12), 951–954. https://doi.org/10.1038/nphys1778.

Guerin, W., Riou, J.-F., Gaebler, J.P., Josse, V., Bouyer, P., Aspect, A., 2006. Guided quasi-continuous atom laser. Physical Review Letters 97, 200402. https://doi.org/10.1103/PhysRevLett.97.200402. https://link.aps.org/doi/10.1103/PhysRevLett.97.200402.

Gustavson, T.L., Bouyer, P., Kasevich, M.A., 1997. Precision rotation measurements with an atom interferometer gyroscope. Physical Review Letters 78, 2046–2049. https://doi.org/10.1103/PhysRevLett.78.2046. https://link.aps.org/doi/10.1103/PhysRevLett.78.2046.

Hagley, E.W., Deng, L., Kozuma, M., Wen, J., Helmerson, K., Rolston, S.L., Phillips, W.D., 1999. A well-collimated quasi-continuous atom laser. Science 283 (5408), 1706–1709. https://doi.org/10.1126/science.283.5408.1706. https://www.science.org/doi/abs/10.1126/science.283.5408.1706.

Haine, S.A., Hope, J.J., Robins, N.P., Savage, C.M., 2002. Stability of continuously pumped atom lasers. Physical Review Letters 88, 170403. https://doi.org/10.1103/PhysRevLett.88.170403. https://link.aps.org/doi/10.1103/PhysRevLett.88.170403.

Hamann, S.E., Haycock, D.L., Klose, G., Pax, P.H., Deutsch, I.H., Jessen, P.S., 1998. Resolved-sideband Raman cooling to the ground state of an optical lattice. Physical Review Letters 80, 4149–4152. https://doi.org/10.1103/PhysRevLett.80.4149. https://link.aps.org/doi/10.1103/PhysRevLett.80.4149.

Han, D.-J., Wolf, S., Oliver, S., McCormick, C., DePue, M.T., Weiss, D.S., 2000. 3D Raman sideband cooling of cesium atoms at high density. Physical Review Letters 85, 724–727. https://doi.org/10.1103/PhysRevLett.85.724. https://link.aps.org/doi/10.1103/PhysRevLett.85.724.

Han, D.J., DePue, M.T., Weiss, D.S., 2001. Loading and compressing Cs atoms in a very far-off-resonant light trap. Physical Review A 63, 023405. https://doi.org/10.1103/PhysRevA.63.023405. https://link.aps.org/doi/10.1103/PhysRevA.63.023405.

Hardman, K.S., Kuhn, C.C.N., McDonald, G.D., Debs, J.E., Bennetts, S., Close, J.D., Robins, N.P., 2014. Role of source coherence in atom interferometry. Physical Review A 89, 023626. https://doi.org/10.1103/PhysRevA.89.023626. https://link.aps.org/doi/10.1103/PhysRevA.89.023626.

Hardman, K.S., Everitt, P.J., McDonald, G.D., Manju, P., Wigley, P.B., Sooriyabandara, M.A., Kuhn, C.C.N., Debs, J.E., Close, J.D., Robins, N.P., 2016. Simultaneous precision gravimetry and magnetic gradiometry with a Bose-Einstein Condensate: a high precision, quantum sensor. Physical Review Letters 117, 138501. https://doi.org/10.1103/PhysRevLett.117.138501. https://link.aps.org/doi/10.1103/PhysRevLett.117.138501.

Hartwig, J., Abend, S., Schubert, C., Schlippert, D., Ahlers, H., Posso-Trujillo, K., Gaaloul, N., Ertmer, W., Rasel, E.M., 2015. Testing the universality of free fall with rubidium and ytterbium in a very large baseline atom interferometer. New Journal of Physics 17 (3), 035011. https://doi.org/10.1088/1367-2630/17/3/035011.

He, L., Sieberer, L.M., Diehl, S., 2017. Space-time vortex driven crossover and vortex turbulence phase transition in one-dimensional driven open condensates. Physical Review Letters 118, 085301. https://doi.org/10.1103/PhysRevLett.118.085301. https://link.aps.org/doi/10.1103/PhysRevLett.118.085301.

Hobson, R., Bowden, W., Vianello, A., Hill, I.R., Gill, P., 2020. Midinfrared magneto-optical trap of metastable strontium for an optical lattice clock. Physical Review A 101, 013420. https://doi.org/10.1103/PhysRevA.101.013420. https://link.aps.org/doi/10.1103/PhysRevA.101.013420.

Holland, M., Burnett, K., Gardiner, C., Cirac, J.I., Zoller, P., 1996. Theory of an atom laser. Physical Review A 54, R1757–R1760. https://doi.org/10.1103/PhysRevA.54.R1757. https://link.aps.org/doi/10.1103/PhysRevA.54.R1757.

Hu, J., Urvoy, A., Vendeiro, Z., Crépel, V., Chen, W., Vuletiü, V., 2017. Creation of a Bose-condensed gas of ^{87}Rb by laser cooling. Science 358 (6366), 1078–1080. https://doi.org/10.1126/science.aan5614. https://www.science.org/doi/abs/10.1126/science.aan5614.

Huft, P., Song, Y., Graham, T.M., Jooya, K., Deshpande, S., Fang, C., Kats, M., Saffman, M., 2022. Simple, passive design for large optical trap arrays for single atoms. Physical Review A 105, 063111. https://doi.org/10.1103/PhysRevA.105.063111. https://link.aps.org/doi/10.1103/PhysRevA.105.063111.

Ido, T., Isoya, Y., Katori, H., 2000. Optical-dipole trapping of sr atoms at a high phase-space density. Physical Review A 61, 061403. https://doi.org/10.1103/PhysRevA.61.061403. https://link.aps.org/doi/10.1103/PhysRevA.61.061403.

Inouye, S., Chikkatur, A.P., Stamper-Kurn, D.M., Stenger, J., Pritchard, D.E., Ketterle, W., 1999a. Superradiant Rayleigh scattering from a Bose-Einstein Condensate. Science 285 (5427), 571–574. https://doi.org/10.1126/science.285.5427.571. https://www.science.org/doi/abs/10.1126/science.285.5427.571.

Inouye, S., Pfau, T., Gupta, S., Chikkatur, A.P., Görlitz, A., Pritchard, D.E., Ketterle, W., 1999b. Phase-coherent amplification of atomic matter waves. Nature (ISSN 1476-4687) 402 (6762), 641–644. https://doi.org/10.1038/45194.

Jenkins, A., Lis, J.W., Senoo, A., McGrew, W.F., Kaufman, A.M., 2022. Ytterbium nuclear-spin qubits in an optical tweezer array. Physical Review X 12, 021027. https://doi.org/10.1103/PhysRevX.12.021027. https://link.aps.org/doi/10.1103/PhysRevX.12.021027.

Jeppesen, M., Dugué, J., Dennis, G.R., Johnsson, M.T., Figl, C., Robins, N.P., Close, J.D., 2008. Approaching the Heisenberg limit in an atom laser. Physical Review A 77, 063618. https://doi.org/10.1103/PhysRevA.77.063618. https://link.aps.org/doi/10.1103/PhysRevA.77.063618.

Kasevich, M., Chu, S., 1992. Laser cooling below a photon recoil with three-level atoms. Physical Review Letters 69, 1741–1744. https://doi.org/10.1103/PhysRevLett.69.1741. https://link.aps.org/doi/10.1103/PhysRevLett.69.1741.

Katori, H., 2021. Longitudinal Ramsey spectroscopy of atoms for continuous operation of optical clocks. Applied Physics Express 14 (7), 072006. https://doi.org/10.35848/1882-0786/ac0e16.

Katori, H., Ido, T., Isoya, Y., Kuwata-Gonokami, M., 1999. Magneto-optical trapping and cooling of strontium atoms down to the photon recoil temperature. Physical Review Letters 82, 1116–1119. https://doi.org/10.1103/PhysRevLett.82.1116. https://link.aps.org/doi/10.1103/PhysRevLett.82.1116.

Katori, H., Ido, T., Isoya, Y., Kuwata-Gonokami, M., 2001. Laser cooling of strontium atoms toward quantum degeneracy. AIP Conference Proceedings 551 (1), 382–396. https://doi.org/10.1063/1.1354362. https://aip.scitation.org/doi/abs/10.1063/1.1354362.

Kaufman, A.M., Ni, K.-K., 2021. Quantum science with optical tweezer arrays of ultracold atoms and molecules. Nature Physics (ISSN 1745-2481) 17 (12), 1324–1333. https://doi.org/10.1038/s41567-021-01357-2.

Kawasaki, A., Braverman, B., Yu, Q., Vuletić, V., 2015. Two-color magneto-optical trap with small magnetic field for ytterbium. Journal of Physics. B, Atomic, Molecular and Optical Physics 48 (15), 155302. https://doi.org/10.1088/0953-4075/48/15/155302.

Keith, D.W., Ekstrom, C.R., Turchette, Q.A., Pritchard, D.E., 1991. An interferometer for atoms. Physical Review Letters 66, 2693–2696. https://doi.org/10.1103/PhysRevLett.66.2693. https://link.aps.org/doi/10.1103/PhysRevLett.66.2693.

Kerman, A.J., Vuletić, V., Chin, C., Chu, S., 2000. Beyond optical molasses: 3D Raman sideband cooling of atomic cesium to high phase-space density. Physical Review Letters 84, 439–442. https://doi.org/10.1103/PhysRevLett.84.439. https://link.aps.org/doi/10.1103/PhysRevLett.84.439.

Ketterle, W., 2002. Nobel lecture: when atoms behave as waves: Bose-Einstein condensation and the atom laser. Reviews of Modern Physics 74, 1131–1151. https://doi.org/10.1103/RevModPhys.74.1131. https://link.aps.org/doi/10.1103/RevModPhys.74.1131.

Ketterle, W., Inouye, S., 2001a. Collective enhancement and suppression in Bose–Einstein condensates. Comptes Rendus de l'Académie des Sciences - Series IV - Physics (ISSN 1296-2147) 2 (3), 339–380. https://doi.org/10.1016/S1296-2147(01)01180-5. https://www.sciencedirect.com/science/article/pii/S1296214701011805.

Ketterle, W., Inouye, S., 2001b. Does matter wave amplification work for fermions? Physical Review Letters 86, 4203–4206. https://doi.org/10.1103/PhysRevLett.86.4203. https://link.aps.org/doi/10.1103/PhysRevLett.86.4203.

Ketterle, W., Miesner, H.-J., 1997. Coherence properties of Bose-Einstein condensates and atom lasers. Physical Review A 56, 3291–3293. https://doi.org/10.1103/PhysRevA.56.3291. https://link.aps.org/doi/10.1103/PhysRevA.56.3291.

Ketterle, W., Davis, K.B., Joffe, M.A., Martin, A., Pritchard, D.E., 1993. High densities of cold atoms in a dark spontaneous-force optical trap. Physical Review Letters 70, 2253–2256. https://doi.org/10.1103/PhysRevLett.70.2253. https://link.aps.org/doi/10.1103/PhysRevLett.70.2253.

Ketterle, W., Durfee, D.S., Stamper-Kurn, D.M., 1999. Making, probing and understanding Bose-Einstein condensates. http://arxiv.org/abs/cond-mat/9904034.

Kindt, L., 2011. Shock wave loading of a magnetic guide. PhD thesis. University of Utrecht. https://dspace.library.uu.nl/bitstream/handle/1874/211584/kindt.pdf?sequence=1&isAllowed=y.

Kleppner, D., 1997. A beginner's guide to the atom laser. Physics Today 50 (8), 11–13. https://doi.org/10.1063/1.881877.

Klostermann, T., Cabrera, C.R., von Raven, H., Wienand, J.F., Schweizer, C., Bloch, I., Aidelsburger, M., 2022. Fast long-distance transport of cold cesium atoms. Physical Review A 105, 043319. https://doi.org/10.1103/PhysRevA.105.043319. https://link.aps.org/doi/10.1103/PhysRevA.105.043319.

Knight, P.L., Hinds, E.A., Plenio, M.B., Porto, J.V., Rolston, S., Laburthe Tolra, B., Williams, C.J., Phillips, W.D., 2003. Quantum information with neutral atoms as qubits. Philosophical Transactions of the Royal Society of London. Series A: Mathematical, Physical and Engineering Sciences 361 (1808), 1417–1427. https://doi.org/10.1098/rsta.2003.1211. https://royalsocietypublishing.org/doi/abs/10.1098/rsta.2003.1211.

Kocharovsky, V.V., Kocharovsky, V.V., Scully, M.O., 2000. Condensate statistics in interacting and ideal dilute Bose gases. Physical Review Letters 84, 2306–2309. https://doi.org/10.1103/PhysRevLett.84.2306. https://link.aps.org/doi/10.1103/PhysRevLett.84.2306.

Kozuma, M., Suzuki, Y., Torii, Y., Sugiura, T., Kuga, T., Hagley, E.W., Deng, L., 1999a. Phase-coherent amplification of matter waves. Science 286 (5448), 2309–2312. https://doi.org/10.1126/science.286.5448.2309. https://www.science.org/doi/abs/10.1126/science.286.5448.2309.

Kozuma, M., Deng, L., Hagley, E.W., Wen, J., Lutwak, R., Helmerson, K., Rolston, S.L., Phillips, W.D., 1999b. Coherent splitting of Bose-Einstein Condensed atoms with optically induced Bragg diffraction. Physical Review Letters 82, 871–875. https://doi.org/10.1103/PhysRevLett.82.871. https://link.aps.org/doi/10.1103/PhysRevLett.82.871.

Kristensen, M.A., Christensen, M.B., Gajdacz, M., Iglicki, M., Pawłowski, K., Klempt, C., Sherson, J.F., Rzążewski, K., Hilliard, A.J., Arlt, J.J., 2019. Observation of atom number fluctuations in a Bose-Einstein Condensate. Physical Review Letters 122, 163601. https://doi.org/10.1103/PhysRevLett.122.163601. https://link.aps.org/doi/10.1103/PhysRevLett.122.163601.

Kwolek, J., Fancher, C., Bashkansky, M., Black, A., 2020. Three-dimensional cooling of an atom-beam source for high-contrast atom interferometry. Physical Review Applied 13, 044057. https://doi.org/10.1103/PhysRevApplied.13.044057. https://link.aps.org/doi/10.1103/PhysRevApplied.13.044057.

Kwolek, J.M., Black, A.T., 2022. Continuous sub-Doppler-cooled atomic beam interferometer for inertial sensing. Physical Review Applied 17, 024061. https://doi.org/10.1103/PhysRevApplied.17.024061. https://link.aps.org/doi/10.1103/PhysRevApplied.17.024061.

Lachmann, M.D., Ahlers, H., Becker, D., Dinkelaker, A.N., Grosse, J., Hellmig, O., Müntinga, H., Schkolnik, V., Seidel, S.T., Wendrich, T., Wenzlawski, A., Carrick, B., Gaaloul, N., Lüdtke, D., Braxmaier, C., Ertmer, W., Krutzik, M., Lämmerzahl, C., Peters, A., Schleich, W.P., Sengstock, K., Wicht, A., Windpassinger, P., Rasel, E.M., 2021. Ultracold atom interferometry in space. Nature Communications (ISSN 2041-1723) 12 (1), 1317. https://doi.org/10.1038/s41467-021-21628-z.

Lahaye, T., Guéry-Odelin, D., 2005. Discrete-step evaporation of an atomic beam. The European Physical Journal. D, Atomic, Molecular, Optical and Plasma Physics (ISSN 1434-6079) 33 (1), 67–75. https://doi.org/10.1140/epjd/e2005-00007-y.

Lahaye, T., Guéry-Odelin, D., 2006. Kinetics of the evaporative cooling of an atomic beam. Physical Review A 73, 063622. https://doi.org/10.1103/PhysRevA.73.063622. https://link.aps.org/doi/10.1103/PhysRevA.73.063622.

Lahaye, T., Cren, P., Roos, C., Guéry-Odelin, D., 2003. Propagation of guided cold atoms. In: Chaotic Transport and Compexity in Classical and Quantum Dynamics. Communications in Nonlinear Science and Numerical Simulation (ISSN 1007-5704) 8 (3), 315–328. https://doi.org/10.1016/S1007-5704(03)00032-7. https://www.sciencedirect.com/science/article/pii/S1007570403000327.

Lahaye, T., Vogels, J.M., Günter, K.J., Wang, Z., Dalibard, J., Guéry-Odelin, D., 2004. Realization of a magnetically guided atomic beam in the collisional regime. Physical Review Letters 93, 093003. https://doi.org/10.1103/PhysRevLett.93.093003. https://link.aps.org/doi/10.1103/PhysRevLett.93.093003.

Lahaye, T., Wang, Z., Reinaudi, G., Rath, S.P., Dalibard, J., Guéry-Odelin, D., 2005. Evaporative cooling of a guided rubidium atomic beam. Physical Review A 72, 033411. https://doi.org/10.1103/PhysRevA.72.033411. https://link.aps.org/doi/10.1103/PhysRevA.72.033411.

Le Coq, Y., Thywissen, J.H., Rangwala, S.A., Gerbier, F., Richard, S., Delannoy, G., Bouyer, P., Aspect, A., 2001. Atom laser divergence. Physical Review Letters 87, 170403. https://doi.org/10.1103/PhysRevLett.87.170403. https://link.aps.org/doi/10.1103/PhysRevLett.87.170403.

Lee, H.J., Adams, C.S., Kasevich, M., Chu, S., 1996. Raman cooling of atoms in an optical dipole trap. Physical Review Letters 76, 2658–2661. https://doi.org/10.1103/PhysRevLett.76.2658. https://link.aps.org/doi/10.1103/PhysRevLett.76.2658.

Lee, J., Lee, J.H., Noh, J., Mun, J., 2015. Core-shell magneto-optical trap for alkaline-earth-metal-like atoms. Physical Review A 91, 053405. https://doi.org/10.1103/PhysRevA.91.053405. https://link.aps.org/doi/10.1103/PhysRevA.91.053405.

Lenz, G., Meystre, P., Wright, E.M., 1993. Nonlinear atom optics. Physical Review Letters 71, 3271–3274. https://doi.org/10.1103/PhysRevLett.71.3271. https://link.aps.org/doi/10.1103/PhysRevLett.71.3271.

Lester, B.J., Luick, N., Kaufman, A.M., Reynolds, C.M., Regal, C.A., 2015. Rapid production of uniformly filled arrays of neutral atoms. Physical Review Letters 115, 073003. https://doi.org/10.1103/PhysRevLett.115.073003. https://link.aps.org/doi/10.1103/PhysRevLett.115.073003.

Lett, P.D., Watts, R.N., Westbrook, C.I., Phillips, W.D., Gould, P.L., Metcalf, H.J., 1988. Observation of atoms laser cooled below the Doppler limit. Physical Review Letters 61, 169–172. https://doi.org/10.1103/PhysRevLett.61.169. https://link.aps.org/doi/10.1103/PhysRevLett.61.169.

Levine, H., Keesling, A., Semeghini, G., Omran, A., Wang, T.T., Ebadi, S., Bernien, H., Greiner, M., Vuletić, V., Pichler, H., Lukin, M.D., 2019. Parallel implementation of high-fidelity multiqubit gates with neutral atoms. Physical Review Letters 123, 170503. https://doi.org/10.1103/PhysRevLett.123.170503. https://link.aps.org/doi/10.1103/PhysRevLett.123.170503.

Lisdat, C., Grosche, G., Quintin, N., Shi, C., Raupach, S.M.F., Grebing, C., Nicolodi, D., Stefani, F., Al-Masoudi, A., Dörscher, S., Häfner, S., Robyr, J.-L., Chiodo, N., Bilicki, S., Bookjans, E., Koczwara, A., Koke, S., Kuhl, A., Wiotte, F., Meynadier, F., Camisard, E., Abgrall, M., Lours, M., Legero, T., Schnatz, H., Sterr, U., Denker, H., Chardonnet, C., Le Coq, Y., Santarelli, G., Amy-Klein, A., Le Targat, R., Lodewyck, J., Lopez, O., Pottie, P.-E., 2016. A clock network for geodesy and fundamental science. Nature Communications (ISSN 2041-1723) 7 (1), 12443. https://doi.org/10.1038/ncomms12443.

Liu, C., Mucci, M., Cao, X., Dutt, M.V.G., Hatridge, M., Pekker, D., 2021. Proposal for a continuous wave laser with linewidth well below the standard quantum limit. Nature Communications (ISSN 2041-1723) 12 (1), 5620. https://doi.org/10.1038/s41467-021-25879-8.

Liu, H., Jäger, S.B., Yu, X., Touzard, S., Shankar, A., Holland, M.J., Nicholson, T.L., 2020. Rugged mHz-linewidth superradiant laser driven by a hot atomic beam. Physical Review Letters 125, 253602. https://doi.org/10.1103/PhysRevLett.125.253602. https://link.aps.org/doi/10.1103/PhysRevLett.125.253602.

Ludlow, A.D., Boyd, M.M., Ye, J., Peik, E., Schmidt, P.O., 2015. Optical atomic clocks. Reviews of Modern Physics 87, 637–701. https://doi.org/10.1103/RevModPhys.87.637. https://link.aps.org/doi/10.1103/RevModPhys.87.637.

Madjarov, I.S., Covey, J.P., Shaw, A.L., Choi, J., Kale, A., Cooper, A., Pichler, H., Schkolnik, V., Williams, J.R., Endres, M., 2020. High-fidelity entanglement and detection of alkaline-earth Rydberg atoms. Nature Physics (ISSN 1745-2481) 16 (8), 857–861. https://doi.org/10.1038/s41567-020-0903-z.

Mahnke, J., Kruse, I., Hüper, A., Jöllenbeck, S., Ertmer, W., Arlt, J., Klempt, C., 2015. A continuously pumped reservoir of ultracold atoms. Journal of Physics. B, Atomic, Molecular and Optical Physics 48 (16), 165301. https://doi.org/10.1088/0953-4075/48/16/165301.

McDonald, G.D., Kuhn, C.C.N., Bennetts, S., Debs, J.E., Hardman, K.S., Johnsson, M., Close, J.D., Robins, N.P., 2013. $80\hbar k$ momentum separation with Bloch oscillations in an optically guided atom interferometer. Physical Review A 88, 053620. https://doi.org/10.1103/PhysRevA.88.053620. https://link.aps.org/doi/10.1103/PhysRevA.88.053620.

Meiser, D., Ye, J., Carlson, D.R., Holland, M.J., 2009. Prospects for a millihertz-linewidth laser. Physical Review Letters 102, 163601. https://doi.org/10.1103/PhysRevLett.102.163601. https://link.aps.org/doi/10.1103/PhysRevLett.102.163601.

Metcalf, H.J., van der Straten, P., 1999. Laser Cooling and Trapping. Springer, New York.

Mewes, M.-O., Andrews, M.R., Kurn, D.M., Durfee, D.S., Townsend, C.G., Ketterle, W., 1997. Output coupler for Bose-Einstein Condensed atoms. Physical Review Letters 78, 582–585. https://doi.org/10.1103/PhysRevLett.78.582. https://link.aps.org/doi/10.1103/PhysRevLett.78.582.

Meystre, P., 2001. Atom Optics. Springer-Verlag, New York.

Michel, F.C., Siegman, A.E., Kleppner, D., 1998. The 'Atom Laser' and the constructs of physicists—revisited. Physics Today 51 (1), 90–91. https://doi.org/10.1063/1.882121.

Miesner, H.-J., Stamper-Kurn, D.M., Andrews, M.R., Durfee, D.S., Inouye, S., Ketterle, W., 1998. Bosonic stimulation in the formation of a Bose-Einstein Condensate. Science 279 (5353), 1005–1007. https://doi.org/10.1126/science.279.5353.1005. https://www.science.org/doi/abs/10.1126/science.279.5353.1005.

Milton, J.S., Arnold, J.C., 2014. Introduction to Probability and Statistics, 5th edition. McGraw-Hill Education. Chapter 9.

Miossec, T., Barbé, R., Keller, J.-C., Gorceix, O., 2002. Pulsed magnetic lenses for producing intense and bright cold atom beams. Optics Communications (ISSN 0030-4018) 209 (4), 349–362. https://doi.org/10.1016/S0030-4018(02)01733-9. https://www.sciencedirect.com/science/article/pii/S0030401802017339.

Miyazawa, Y., Inoue, R., Matsui, H., Takanashi, K., Kozuma, M., 2021. Narrow-line magneto-optical trap for europium. Physical Review A 103, 053122. https://doi.org/10.1103/PhysRevA.103.053122. https://link.aps.org/doi/10.1103/PhysRevA.103.053122.

Moore, M.G., Meystre, P., 2001. Parametric amplification of coupled atomic and optical fields. In: Carmichael, H.J., Glauber, R.J., Scully, M.O. (Eds.), Directions in Quantum Optics. In: Lecture Notes in Physics, vol. 561. Springer, Berlin, Heidelberg. ISBN 978-3-540-41187-1, pp. 116–125.

Morigi, G., Cirac, J.I., Ellinger, K., Zoller, P., 1998. Laser cooling of trapped atoms to the ground state: a dark state in position space. Physical Review A 57, 2909–2914. https://doi.org/10.1103/PhysRevA.57.2909. https://link.aps.org/doi/10.1103/PhysRevA.57.2909.

Müller, H., Chiow, S.-w., Long, Q., Herrmann, S., Chu, S., 2008. Atom interferometry with up to 24-photon-momentum-transfer beam splitters. Physical Review Letters 100, 180405. https://doi.org/10.1103/PhysRevLett.100.180405. https://link.aps.org/doi/10.1103/PhysRevLett.100.180405.

Müntinga, H., Ahlers, H., Krutzik, M., Wenzlawski, A., Arnold, S., Becker, D., Bongs, K., Dittus, H., Duncker, H., Gaaloul, N., Gherasim, C., Giese, E., Grzeschik, C., Hänsch, T.W., Hellmig, O., Herr, W., Herrmann, S., Kajari, E., Kleinert, S., Lämmerzahl, C., Lewoczko-Adamczyk, W., Malcolm, J., Meyer, N., Nolte, R., Peters, A., Popp, M., Reichel, J., Roura, A., Rudolph, J., Schiemangk, M., Schneider, M., Seidel, S.T., Sengstock, K., Tamma, V., Valenzuela, T., Vogel, A., Walser, R., Wendrich, T., Windpassinger, P., Zeller, W., van Zoest, T., Ertmer, W., Schleich, W.P., Rasel, E.M., 2013. Interferometry with Bose-Einstein Condensates in microgravity. Physical Review Letters 110, 093602. https://doi.org/10.1103/PhysRevLett.110.093602. https://link.aps.org/doi/10.1103/PhysRevLett.110.093602.

Nelson, K.D., Fertig, C.D., Hamilton, P., Brown, J.M., Estey, B., Müller, H., Compton, R.L., 2020. Guided matter wave inertial sensing in a miniature physics package. Applied Physics Letters 116 (23), 234002. https://doi.org/10.1063/5.0010070.

Norcia, M.A., 2017. New tools for precision measurement and quantum science with narrow linewidth optical transitions. PhD thesis. University of Colorado. https://scholar.colorado.edu/concern/graduate_thesis_or_dissertations/t435gc985.

Norcia, M.A., Winchester, M.N., Cline, J.R.K., Thompson, J.K., 2016. Superradiance on the millihertz linewidth strontium clock transition. Science Advances 2 (10), e1601231. https://doi.org/10.1126/sciadv.1601231. https://www.science.org/doi/abs/10.1126/sciadv.1601231.

Oelker, E., Hutson, R.B., Kennedy, C.J., Sonderhouse, L., Bothwell, T., Goban, A., Kedar, D., Sanner, C., Robinson, J.M., Marti, G.E., Matei, D.G., Legero, T., Giunta, M., Holzwarth, R., Riehle, F., Sterr, U., Ye, J., 2019. Demonstration of 4.8×10^{-17} stability at 1 s for two independent optical clocks. Nature Photonics (ISSN 1749-4893) 13 (10), 714–719. https://doi.org/10.1038/s41566-019-0493-4.

Olson, J., Fox, R.W., Fortier, T.M., Sheerin, T.F., Brown, R.C., Leopardi, H., Stoner, R.E., Oates, C.W., Ludlow, A.D., 2019. Ramsey-Bordé matter-wave interferometry for laser frequency stabilization at 10^{-16} frequency instability and below. Physical Review Letters 123, 073202. https://doi.org/10.1103/PhysRevLett.123.073202. https://link.aps.org/doi/10.1103/PhysRevLett.123.073202.

Olson, S.E., Mhaskar, R.R., Raithel, G., 2006. Continuous propagation and energy filtering of a cold atomic beam in a long high-gradient magnetic atom guide. Physical Review A 73, 033622. https://doi.org/10.1103/PhysRevA.73.033622. https://link.aps.org/doi/10.1103/PhysRevA.73.033622.

Olson, S.E., Raithel, G., Christlieb, A.J., 2014. Pressure-driven evaporative cooling in atom guides. Physical Review A 90, 043612. https://doi.org/10.1103/PhysRevA.90.043612. https://link.aps.org/doi/10.1103/PhysRevA.90.043612.

Park, A.J., Trautmann, J., Šantić, N., Klüsener, V., Heinz, A., Bloch, I., Blatt, S., 2022. Cavity-enhanced optical lattices for scaling neutral atom quantum technologies to higher qubit numbers. PRX Quantum 3, 030314. https://doi.org/10.1103/PRXQuantum.3.030314. https://link.aps.org/doi/10.1103/PRXQuantum.3.030314.

Pause, L., Preuschoff, T., Schäffner, D., Schlosser, M., Birkl, G., 2023. Reservoir-based deterministic loading of single-atom tweezer array. http://arxiv.org/abs/2302.12730.

Peil, S., Porto, J.V., Tolra, B.L., Obrecht, J.M., King, B.E., Subbotin, M., Rolston, S.L., Phillips, W.D., 2003. Patterned loading of a Bose-Einstein condensate into an optical lattice. Physical Review A 67, 051603. https://doi.org/10.1103/PhysRevA.67.051603. https://link.aps.org/doi/10.1103/PhysRevA.67.051603.

Perrin, H., Kuhn, A., Bouchoule, I., Salomon, C., 1998. Sideband cooling of neutral atoms in a far-detuned optical lattice. Europhysics Letters 42 (4), 395. https://doi.org/10.1209/epl/i1998-00261-y.

Peters, A., Chung, K.Y., Chu, S., 1999. Measurement of gravitational acceleration by dropping atoms. Nature (ISSN 1476-4687) 400 (6747), 849–852. https://doi.org/10.1038/23655.

Phillips, W.D., Metcalf, H., 1982. Laser deceleration of an atomic beam. Physical Review Letters 48, 596–599. https://doi.org/10.1103/PhysRevLett.48.596. https://link.aps.org/doi/10.1103/PhysRevLett.48.596.

Pinkse, P.W.H., Mosk, A., Weidemüller, M., Reynolds, M.W., Hijmans, T.W., Walraven, J.T.M., 1997. Adiabatically changing the phase-space density of a trapped Bose gas. Physical Review Letters 78, 990–993. https://doi.org/10.1103/PhysRevLett.78.990. https://link.aps.org/doi/10.1103/PhysRevLett.78.990.

Power, E.P., George, L., Vanderelzen, B., Herrera-Fierro, P., Murphy, R., Yalisove, S.M., Raithel, G., 2012. Design and fabrication of a chip-based continuous-wave atom laser. https://doi.org/10.48550/arXiv.1202.0479. https://arxiv.org/abs/1202.0479.

Pritchard, D.E., 1983. Cooling neutral atoms in a magnetic trap for precision spectroscopy. Physical Review Letters 51, 1336–1339. https://doi.org/10.1103/PhysRevLett.51.1336. https://link.aps.org/doi/10.1103/PhysRevLett.51.1336.

Radwell, N., Walker, G., Franke-Arnold, S., 2013. Cold-atom densities of more than 10^{12} cm^{-3} in a holographically shaped dark spontaneous-force optical trap. Physical Review A 88, 043409. https://doi.org/10.1103/PhysRevA.88.043409. https://link.aps.org/doi/10.1103/PhysRevA.88.043409.

Reinaudi, G., Lahaye, T., Couvert, A., Wang, Z., Guéry-Odelin, D., 2006a. Evaporation of an atomic beam on a material surface. Physical Review A 73, 035402. https://doi.org/10.1103/PhysRevA.73.035402. https://link.aps.org/doi/10.1103/PhysRevA.73.035402.

Reinaudi, G., Wang, Z., Couvert, A., Lahaye, T., Guéry-Odelin, D., 2006b. A moving magnetic mirror to slow down a bunch of atoms. The European Physical Journal. D, Atomic, Molecular, Optical and Plasma Physics (ISSN 1434-6079) 40 (3), 405–410. https://doi.org/10.1140/epjd/e2006-00244-6.

Riedmann, M., Kelkar, H., Wübbena, T., Pape, A., Kulosa, A., Zipfel, K., Fim, D., Rühmann, S., Friebe, J., Ertmer, W., Rasel, E., 2012. Beating the density limit by continuously loading a dipole trap from millikelvin-hot magnesium atoms. Physical Review A 86, 043416. https://doi.org/10.1103/PhysRevA.86.043416. https://link.aps.org/doi/10.1103/PhysRevA.86.043416.

Riehle, F., Witte, A., Kisters, T., Helmcke, J., 1992. Interferometry with Ca atoms. Applied Physics B (ISSN 1432-0649) 54 (5), 333–340. https://doi.org/10.1007/BF00325376.

Riis, E., Weiss, D.S., Moler, K.A., Chu, S., 1990. Atom funnel for the production of a slow, high-density atomic beam. Physical Review Letters 64, 1658–1661. https://doi.org/10.1103/PhysRevLett.64.1658. https://link.aps.org/doi/10.1103/PhysRevLett.64.1658.

Riou, J.-F., Guerin, W., Coq, Y.L., Fauquembergue, M., Josse, V., Bouyer, P., Aspect, A., 2006. Beam quality of a nonideal atom laser. Physical Review Letters 96, 070404. https://doi.org/10.1103/PhysRevLett.96.070404. https://link.aps.org/doi/10.1103/PhysRevLett.96.070404.

Robins, N., Altin, P., Debs, J., Close, J., 2013. Atom lasers: production, properties and prospects for precision inertial measurement. Physics Reports (ISSN 0370-1573) 529 (3), 265–296. https://doi.org/10.1016/j.physrep.2013.03.006. https://www.sciencedirect.com/science/article/pii/S037015731300118X.

Robins, N.P., Figl, C., Haine, S.A., Morrison, A.K., Jeppesen, M., Hope, J.J., Close, J.D., 2006. Achieving peak brightness in an atom laser. Physical Review Letters 96, 140403. https://doi.org/10.1103/PhysRevLett.96.140403. https://link.aps.org/doi/10.1103/PhysRevLett.96.140403.

Robins, N.P., Figl, C., Jeppesen, M., Dennis, G.R., Close, J.D., 2008. A pumped atom laser. Nature Physics (ISSN 1745-2481) 4 (9), 731–736. https://doi.org/10.1038/nphys1027.

Roos, C.F., Cren, P., Lahaye, T., Dalibard, J., Guéry-Odelin, D., 2003a. Injection of a cold atomic beam into a magnetic guide. https://arxiv.org/abs/cond-mat/0212147.

Roos, C.F., Cren, P., Dalibard, J., Guéry-Odelin, D., 2003b. A source of cold atoms for a continuously loaded magnetic guide. Physica Scripta 2003 (T105), 19. https://doi.org/10.1238/Physica.Topical.105a00019.

Roos, C.F., Cren, P., Guéry-Odelin, D., Dalibard, J., 2003c. Continuous loading of a non-dissipative atom trap. Europhysics Letters 61 (2), 187. https://doi.org/10.1209/epl/i2003-00211-3.

Rührig, J., Bäuerle, T., Griesmaier, A., Pfau, T., 2015. High efficiency demagnetization cooling by suppression of light-assisted collisions. Optics Express 23 (5), 5596–5606. https://doi.org/10.1364/OE.23.005596. https://opg.optica.org/oe/abstract.cfm?URI=oe-23-5-5596.

Safronova, M.S., 2019. The search for variation of fundamental constants with clocks. Annalen der Physik 531 (5), 1800364. https://doi.org/10.1002/andp.201800364. https://onlinelibrary.wiley.com/doi/abs/10.1002/andp.201800364.

Safronova, M.S., Budker, D., DeMille, D., Kimball, D.F.J., Derevianko, A., Clark, C.W., 2018. Search for new physics with atoms and molecules. Reviews of Modern Physics 90, 025008. https://doi.org/10.1103/RevModPhys.90.025008. https://link.aps.org/doi/10.1103/RevModPhys.90.025008.

Salzburger, T., Ritsch, H., 2008. Twin stimulated amplification of light and matter waves in an atom-photon pair laser. Physical Review A 77, 063620. https://doi.org/10.1103/PhysRevA.77.063620. https://link.aps.org/doi/10.1103/PhysRevA.77.063620.

Santos, L., Floegel, F., Pfau, T., Lewenstein, M., 2001. Continuous optical loading of a Bose-Einstein condensate. Physical Review A 63, 063408. https://doi.org/10.1103/PhysRevA.63.063408. https://link.aps.org/doi/10.1103/PhysRevA.63.063408.

Savoie, D., Altorio, M., Fang, B., Sidorenkov, L.A., Geiger, R., Landragin, A., 2018. Interleaved atom interferometry for high-sensitivity inertial measurements. Science Advances 4 (12), eaau7948. https://doi.org/10.1126/sciadv.aau7948. https://www.science.org/doi/abs/10.1126/sciadv.aau7948.

Schawlow, A.L., Townes, C.H., 1958. Infrared and optical masers. Physical Review 112, 1940–1949. https://doi.org/10.1103/PhysRev.112.1940. https://link.aps.org/doi/10.1103/PhysRev.112.1940.

Schioppo, M., Brown, R.C., McGrew, W.F., Hinkley, N., Fasano, R.J., Beloy, K., Yoon, T.H., Milani, G., Nicolodi, D., Sherman, J.A., Phillips, N.B., Oates, C.W., Ludlow, A.D., 2017. Ultrastable optical clock with two cold-atom ensembles. Nature Photonics (ISSN 1749-4893) 11 (1), 48–52. https://doi.org/10.1038/nphoton.2016.231.

Schlosser, N., Reymond, G., Protsenko, I., Grangier, P., 2001. Sub-Poissonian loading of single atoms in a microscopic dipole trap. Nature (ISSN 1476-4687) 411 (6841), 1024–1027. https://doi.org/10.1038/35082512.

Schmid, S., Thalhammer, G., Winkler, K., Lang, F., Denschlag, J.H., 2006. Long distance transport of ultracold atoms using a 1D optical lattice. New Journal of Physics 8 (8), 159. https://doi.org/10.1088/1367-2630/8/8/159.

Schneble, D., Torii, Y., Boyd, M., Streed, E.W., Pritchard, D.E., Ketterle, W., 2003a. The onset of matter-wave amplification in a superradiant Bose-Einstein Condensate. Science 300 (5618), 475–478. https://doi.org/10.1126/science.1083171. https://www.science.org/doi/abs/10.1126/science.1083171.

Schneble, D., Hasuo, M., Anker, T., Pfau, T., Mlynek, J., 2003b. Integrated atom-optical circuit with continuous-wave operation. Journal of the Optical Society of America. B, Optical Physics 20 (4), 648–651. https://doi.org/10.1364/JOSAB.20.000648. https://opg.optica.org/josab/abstract.cfm?URI=josab-20-4-648.

Schneble, D., Campbell, G.K., Streed, E.W., Boyd, M., Pritchard, D.E., Ketterle, W., 2004. Raman amplification of matter waves. Physical Review A 69, 041601. https://doi.org/10.1103/PhysRevA.69.041601. https://link.aps.org/doi/10.1103/PhysRevA.69.041601.

Schreck, F., Druten, K.v., 2021. Laser cooling for quantum gases. Nature Physics (ISSN 1745-2481) 17 (12), 1296–1304. https://doi.org/10.1038/s41567-021-01379-w.

Schymik, K.-N., Pancaldi, S., Nogrette, F., Barredo, D., Paris, J., Browaeys, A., Lahaye, T., 2021. Single atoms with 6000-second trapping lifetimes in optical-tweezer arrays at cryogenic temperatures. Physical Review Applied 16, 034013. https://doi.org/10.1103/PhysRevApplied.16.034013. https://link.aps.org/doi/10.1103/PhysRevApplied.16.034013.

Scully, M.O., 1999. Condensation of *N* Bosons and the laser phase transition analogy. Physical Review Letters 82, 3927–3931. https://doi.org/10.1103/PhysRevLett.82.3927. https://link.aps.org/doi/10.1103/PhysRevLett.82.3927.

Sesko, D.W., Walker, T.G., Wieman, C.E., 1991. Behavior of neutral atoms in a spontaneous force trap. Journal of the Optical Society of America. B, Optical Physics 8 (5), 946–958. https://doi.org/10.1364/JOSAB.8.000946. https://opg.optica.org/josab/abstract.cfm?URI=josab-8-5-946.

Setija, I.D., Werij, H.G.C., Luiten, O.J., Reynolds, M.W., Hijmans, T.W., Walraven, J.T.M., 1993. Optical cooling of atomic hydrogen in a magnetic trap. Physical Review Letters 70, 2257–2260. https://doi.org/10.1103/PhysRevLett.70.2257. https://link.aps.org/doi/10.1103/PhysRevLett.70.2257.

Sieberer, L.M., Huber, S.D., Altman, E., Diehl, S., 2013. Dynamical critical phenomena in driven-dissipative systems. Physical Review Letters 110, 195301. https://doi.org/10.1103/PhysRevLett.110.195301. https://link.aps.org/doi/10.1103/PhysRevLett.110.195301.

Spreeuw, R.J.C., Pfau, T., Janicke, U., Wilkens, M., 1995. Laser-like scheme for atomic-matter waves. Europhysics Letters 32 (6), 469. https://doi.org/10.1209/0295-5075/32/6/002.

Stamper-Kurn, D.M., Miesner, H.-J., Chikkatur, A.P., Inouye, S., Stenger, J., Ketterle, W., 1998. Reversible formation of a Bose-Einstein Condensate. Physical Review Letters 81, 2194–2197. https://doi.org/10.1103/PhysRevLett.81.2194. https://link.aps.org/doi/10.1103/PhysRevLett.81.2194.

Stellmer, S., Pasquiou, B., Grimm, R., Schreck, F., 2013. Laser cooling to quantum degeneracy. Physical Review Letters 110, 263003. https://doi.org/10.1103/PhysRevLett.110.263003.

Stockton, J.K., Takase, K., Kasevich, M.A., 2011. Absolute geodetic rotation measurement using atom interferometry. Physical Review Letters 107, 133001. https://doi.org/10.1103/PhysRevLett.107.133001. https://link.aps.org/doi/10.1103/PhysRevLett.107.133001.

Stray, B., Lamb, A., Kaushik, A., Vovrosh, J., Rodgers, A., Winch, J., Hayati, F., Boddice, D., Stabrawa, A., Niggebaum, A., Langlois, M., Lien, Y.-H., Lellouch, S., Roshanmanesh, S., Ridley, K., de Villiers, G., Brown, G., Cross, T., Tuckwell, G., Faramarzi, A., Metje, N., Bongs, K., Holynski, M., 2022. Quantum sensing for gravity cartography. Nature (ISSN 1476-4687) 602 (7898), 590–594. https://doi.org/10.1038/s41586-021-04315-3.

Taïeb, R., Dum, R., Cirac, J.I., Marte, P., Zoller, P., 1994. Cooling and localization of atoms in laser-induced potential wells. Physical Review A 49, 4876–4887. https://doi.org/10.1103/PhysRevA.49.4876. https://link.aps.org/doi/10.1103/PhysRevA.49.4876.

Takamoto, M., Hong, F.-L., Higashi, R., Katori, H., 2005. An optical lattice clock. Nature (ISSN 1476-4687) 435 (7040), 321–324. https://doi.org/10.1038/nature03541.

Takamoto, M., Ushijima, I., Ohmae, N., Yahagi, T., Kokado, K., Shinkai, H., Katori, H., 2020. Test of general relativity by a pair of transportable optical lattice clocks. Nature Photonics (ISSN 1749-4893) 14 (7), 411–415. https://doi.org/10.1038/s41566-020-0619-8.

Teo, B.K., Raithel, G., 2001. Loading mechanism for atomic guides. Physical Review A 63, 031402. https://doi.org/10.1103/PhysRevA.63.031402. https://link.aps.org/doi/10.1103/PhysRevA.63.031402.

Thomsen, L.K., Wiseman, H.M., 2002. Atom-laser coherence and its control via feedback. Physical Review A 65, 063607. https://doi.org/10.1103/PhysRevA.65.063607. https://link.aps.org/doi/10.1103/PhysRevA.65.063607.

Treutlein, P., Chung, K.Y., Chu, S., 2001. High-brightness atom source for atomic fountains. Physical Review A 63, 051401. https://doi.org/10.1103/PhysRevA.63.051401. https://link.aps.org/doi/10.1103/PhysRevA.63.051401.

Urvoy, A., Vendeiro, Z., Ramette, J., Adiyatullin, A., Vuletić, V., 2019. Direct laser cooling to Bose-Einstein Condensation in a dipole trap. Physical Review Letters 122, 203202. https://doi.org/10.1103/PhysRevLett.122.203202. https://link.aps.org/doi/10.1103/PhysRevLett.122.203202.

Vendeiro, Z., Ramette, J., Rudelis, A., Chong, M., Sinclair, J., Stewart, L., Urvoy, A., Vuletić, V., 2022. Machine-learning-accelerated Bose-Einstein condensation. Physical Review Research 4, 043216. https://doi.org/10.1103/PhysRevResearch.4.043216. https://link.aps.org/doi/10.1103/PhysRevResearch.4.043216.

Vermersch, F., Fabre, C.M., Cheiney, P., Gattobigio, G.L., Mathevet, R., Guéry-Odelin, D., 2011. Guided-atom laser: transverse mode quality and longitudinal momentum distribution. Physical Review A 84, 043618. https://doi.org/10.1103/PhysRevA.84.043618. https://link.aps.org/doi/10.1103/PhysRevA.84.043618.

Villain, P., Öhberg, P., Santos, L., Sanpera, A., Lewenstein, M., 2001. Four-wave mixing in degenerate atomic gases. Physical Review A 64, 023606. https://doi.org/10.1103/PhysRevA.64.023606. https://link.aps.org/doi/10.1103/PhysRevA.64.023606.

Volchkov, V.V., Rührig, J., Pfau, T., Griesmaier, A., 2013. Sisyphus cooling in a continuously loaded trap. New Journal of Physics 15 (9), 093012. https://doi.org/10.1088/1367-2630/15/9/093012.

Vuletić, V., Chin, C., Kerman, A.J., Chu, S., 1998. Degenerate Raman sideband cooling of trapped cesium atoms at very high atomic densities. Physical Review Letters 81, 5768–5771. https://doi.org/10.1103/PhysRevLett.81.5768. https://link.aps.org/doi/10.1103/PhysRevLett.81.5768.

Wang, P., Deng, L., Hagley, E.W., Fu, Z., Chai, S., Zhang, J., 2011. Observation of collective atomic recoil motion in a degenerate fermion gas. Physical Review Letters 106, 210401. https://doi.org/10.1103/PhysRevLett.106.210401. https://link.aps.org/doi/10.1103/PhysRevLett.106.210401.

Wcisłlo, P., Ablewski, P., Beloy, K., Bilicki, S., Bober, M., Brown, R., Fasano, R., Ciuryłlo, R., Hachisu, H., Ido, T., Lodewyck, J., Ludlow, A., McGrew, W., Morzyński, P., Nicolodi, D., Schioppo, M., Sekido, M., Targat, R.L., Wolf, P., Zhang, X., Zjawin, B., Zawada, M., 2018. New bounds on dark matter coupling from a global network of optical atomic clocks. Science Advances 4 (12), eaau4869. https://doi.org/10.1126/sciadv.aau4869. https://www.science.org/doi/abs/10.1126/sciadv.aau4869.

Wilkason, T., Nantel, M., Rudolph, J., Jiang, Y., Garber, B.E., Swan, H., Carman, S.P., Abe, M., Hogan, J.M., 2022. Atom interferometry with Floquet atom optics. Phys-

ical Review Letters 129, 183202. https://doi.org/10.1103/PhysRevLett.129.183202. https://link.aps.org/doi/10.1103/PhysRevLett.129.183202.

Williams, J., Walser, R., Wieman, C., Cooper, J., Holland, M., 1998. Achieving steady-state Bose-Einstein condensation. Physical Review A 57, 2030–2036. https://doi.org/10.1103/PhysRevA.57.2030. https://link.aps.org/doi/10.1103/PhysRevA.57.2030.

Winoto, S.L., DePue, M.T., Bramall, N.E., Weiss, D.S., 1999. Laser cooling at high density in deep far-detuned optical lattices. Physical Review A 59, R19–R22. https://doi.org/10.1103/PhysRevA.59.R19. https://link.aps.org/doi/10.1103/PhysRevA.59.R19.

Wiseman, H.M., 1999. Light amplification without stimulated emission: beyond the standard quantum limit to the laser linewidth. Physical Review A 60, 4083–4093. https://doi.org/10.1103/PhysRevA.60.4083. https://link.aps.org/doi/10.1103/PhysRevA.60.4083.

Wolf, S., Oliver, S.J., Weiss, D.S., 2000. Suppression of recoil heating by an optical lattice. Physical Review Letters 85, 4249–4252. https://doi.org/10.1103/PhysRevLett.85.4249. https://link.aps.org/doi/10.1103/PhysRevLett.85.4249.

Xue, H., Feng, Y., Chen, S., Wang, X., Yan, X., Jiang, Z., Zhou, Z., 2015. A continuous cold atomic beam interferometer. Journal of Applied Physics 117 (9), 094901. https://doi.org/10.1063/1.4913711.

Yamamoto, R., Kobayashi, J., Kato, K., Kuno, T., Sakura, Y., Takahashi, Y., 2017. Site-resolved imaging of single atoms with a Faraday quantum gas microscope. Physical Review A 96, 033610. https://doi.org/10.1103/PhysRevA.96.033610. https://link.aps.org/doi/10.1103/PhysRevA.96.033610.

Yang, C.Y., Halder, P., Appel, O., Hansen, D., Hemmerich, A., 2007. Continuous loading of $^1S_0$ calcium atoms into an optical dipole trap. Physical Review A 76, 033418. https://doi.org/10.1103/PhysRevA.76.033418. https://link.aps.org/doi/10.1103/PhysRevA.76.033418.

Yoshikawa, Y., Sugiura, T., Torii, Y., Kuga, T., 2004. Observation of superradiant Raman scattering in a Bose-Einstein condensate. Physical Review A 69, 041603. https://doi.org/10.1103/PhysRevA.69.041603. https://link.aps.org/doi/10.1103/PhysRevA.69.041603.

Yu, N., Tinto, M., 2011. Gravitational wave detection with single-laser atom interferometers. General Relativity and Gravitation (ISSN 1572-9532) 43 (7), 1943–1952. https://doi.org/10.1007/s10714-010-1055-8.

Zhang, W., Walls, D.F., Sanders, B.C., 1994. Atomic soliton in a traveling wave laser beam. Physical Review Letters 72, 60–63. https://doi.org/10.1103/PhysRevLett.72.60. https://link.aps.org/doi/10.1103/PhysRevLett.72.60.

Zhang, X., Beloy, K., Hassan, Y.S., McGrew, W.F., Chen, C.-C., Siegel, J.L., Grogan, T., Ludlow, A.D., 2022. Subrecoil clock-transition laser cooling enabling shallow optical lattice clocks. Physical Review Letters 129, 113202. https://doi.org/10.1103/PhysRevLett.129.113202. https://link.aps.org/doi/10.1103/PhysRevLett.129.113202.

Zhu, M., Oates, C.W., Hall, J.L., 1991. Continuous high-flux monovelocity atomic beam based on a broadband laser-cooling technique. Physical Review Letters 67, 46–49. https://doi.org/10.1103/PhysRevLett.67.46. https://link.aps.org/doi/10.1103/PhysRevLett.67.46.

Zozulya, A.A., Anderson, D.Z., 2013. Principles of an atomtronic battery. Physical Review A 88, 043641. https://doi.org/10.1103/PhysRevA.88.043641. https://link.aps.org/doi/10.1103/PhysRevA.88.043641.